



METEOROLOGY HYDROLOGY
AND WATER MANAGEMENT

IMGW-PIB Science Journal since 2013

VOL. 10 | ISSUE 1 | 2022



The evaluation of weekly extended range river basin rainfall forecasts and a new bias correction mechanism for flood management in India

Pulak Guhathakurta, Ashwini Kumar Prasad, Rajib Chattopadhyay, Neha Sangwan, Nilesh Wagh, D.R. Pattanaik, D.S. Pai, M. Mohapatra

India Meteorological Department, Pune, India

Abstract

Operational extended range forecasts are being disseminated once every week by the India Meteorological Department (IMD) for several sectorial applications. These forecasts show a reduction in amplitude and variance as a function of lead-time. Such reductions in variance can be due to several physical factors: inherent forecast model bias, a problem relating to initial conditions, lead-dependent statistical biases, etc. A week-by-week analysis shows that such biases are not systematic. Rainfall forecasts are underestimated in some regions, while others overestimate rainfall amplitude. To correct the bias in the extended range weekly averaged forecast, a statistical post-processing method (normal ratio correction) is proposed to make the outlook more valuable at a longer lead-time. The correction method is based on the World Meteorological Organization (WMO) technical guidance on rainfall estimation and is also shown to be useful for rainfall forecasts. In this analysis, we evaluate the extended range forecast skill at the river sub-basin-scale and show that there are several river sub-basins over the central Indian region where the correction has improved the model forecast in the one to two-week range. Although this analysis was tailored toward making the river basins and sub-basins of India more readily realizable for flood forecasters, it can be used for any administrative boundaries such as block, district, or state-level requirements.

Keywords

Extended range prediction, rainfall bias correction, flood management.

Submitted 22 July 2021, revised 15 February 2022, accepted 17 February 2022

DOI: 10.26491/mhwm/146785

1. Introduction

One of the major purposes of the extended range forecast is to provide a high-resolution spatial-temporal forecast on a weekly scale, with up to 2-3 weeks lead time. The weekly outlooks can provide important input to the decision-making process of various stakeholders (Pattanaik, Das 2015; Chattopadhyay et al. 2018; Pattanaik et al. 2019; Sahai et al. 2019a-b). The extended range forecasts of the India Meteorological Department (IMD) are being generated at a spatial resolution of $1^{\circ}\times 1^{\circ}$ Grid. Forecasts of rainfall in different river basins have several important hydrometeorological applications, especially in flood forecasting based on rainfall variables (Ming et al. 2020; Webster, Hoyos 2004; Webster et al. 2010; Gilewski, Nawalany 2018; Sayama et al. 2020; Gilewski 2021). In this regard, the most critical application is the forecast of heavy rainfall (daily rainfall of 7 cm or more) in the river basins. This can lead to flooding and inundations, and a considerable loss of life and property. Hence, for flood forecasting and other hydrometeorological requirements, the precipitation forecast must be as quantitative as possible. However, it is occasionally found that there is a significant bias in amplitude and variance in the forecasted rainfall. This often leads to a severe underestimation of rainfall outlook, thereby adding additional input errors to hydrological models that use these quantitative rainfall forecasts.

The Ministry of Earth Sciences, the Government of India, and the IMD have the mandate to provide rainfall forecast and long-range outlooks in the S2S (seasonal to sub-seasonal) scale¹. Such predictions are required to be as accurate as possible. Bias in rainfall forecasts is a common problem in raw model forecast data, which can be problematic for quantitative precipitation forecast. Such amplitude biases in rainfall in longer lead times arise due to inefficient representation of model physics and dynamics, or due to systematic errors in the large-scale forcing. To make the forecast more useful, these biases should be reduced as much as possible. One crucial error in rainfall forecasts is the underrepresentation of rainfall amplitude after a forecast lead-time of a few days. The forecast often shows that the variance is severely underrepresented in the forecasted rainfall, as lead-time increases. Several statistical post-processing methods, using complex to simple approaches to correct the rainfall bias, exist to improve the rainfall forecast under such circumstances (Boé et al. 2007; Leander, Buishand 2007; Ghimire et al. 2019). These bias corrections are shown to improve hydrological forecasts (Teutschbein, Seibert 2012). The results show that a bias in rainfall arising due to improper amplitude attenuations as a function of lead-time, could be corrected under many circumstances – provided climatological or observed rainfall amplitude is known for any lead day. This shows promise for correcting amplitude bias arising in operational dynamical models (Singh et al. 2017; Jabbari, Bae 2020).

The presented study aimed to provide better basin-wise weekly rainfall forecasts for the river sub-basins of India, using a novel method to correct the forecast bias in the extended range weekly forecast. The forecast ability of extended range weekly rainfall forecasts, as well as bias-corrected extended range weekly rainfall forecasts, were satisfactory in both 1-week and 2-weeks lead time. These forecasts can thus be used as model inputs for flood forecasting. Although this study focused on basin-wise rainfall forecast, the method is general and can be applied to the average rainfall of any administrative boundaries or geographical locations like districts or states.

2. Data and methodology

2.1. Data

The current study uses the daily observed rainfall data from the IMD 0.25 Deg × 0.25 Deg gridded data (Pai et al. 2014) and daily 1Deg × 1Deg rainfall forecast data received from the IMD_IITM extended range forecast system [ERF]. Daily observed gridded rainfall data of 0.25 Deg × 0.25 Deg has been generated by the IMD from the quality controlled daily rainfall data of rain gauge stations². The dataset covers a geographical domain of 6.5°-38.5°N and 66.5°-100.0°E and contains only values from land regions. The extended range forecast models generate precipitation forecast data up to four weeks in advance, based on the conditions observed at any given time (Chattopadhyay et al. 2019; Pattanaik et al. 2019, Sahai et al. 2019b). Currently, an operationally extended range forecast is disseminated once every week. For every week's operational forecast, there is corresponding “on the fly” hindcasts for the same set of recorded

¹ <https://pib.gov.in/PressReleaseIframePage.aspx?PRID=1706073>

² https://imd pune.gov.in/Clim_Pred_LRF_New/Gridded_Data_Download.html

conditions since 2003. The data is generated for the global domain. In this analysis we have used the data for the river basins of India. The Central Water Commission divides the country into 25 major river basins and 101 river sub-basins (Fig. 1 and Table 1). River sub-basins shapefiles were obtained from the Central Water Commission. Using the shapefile, the gridded data (both observation and forecast data) was masked and basin averaged data was prepared for each of the 101 river basins.

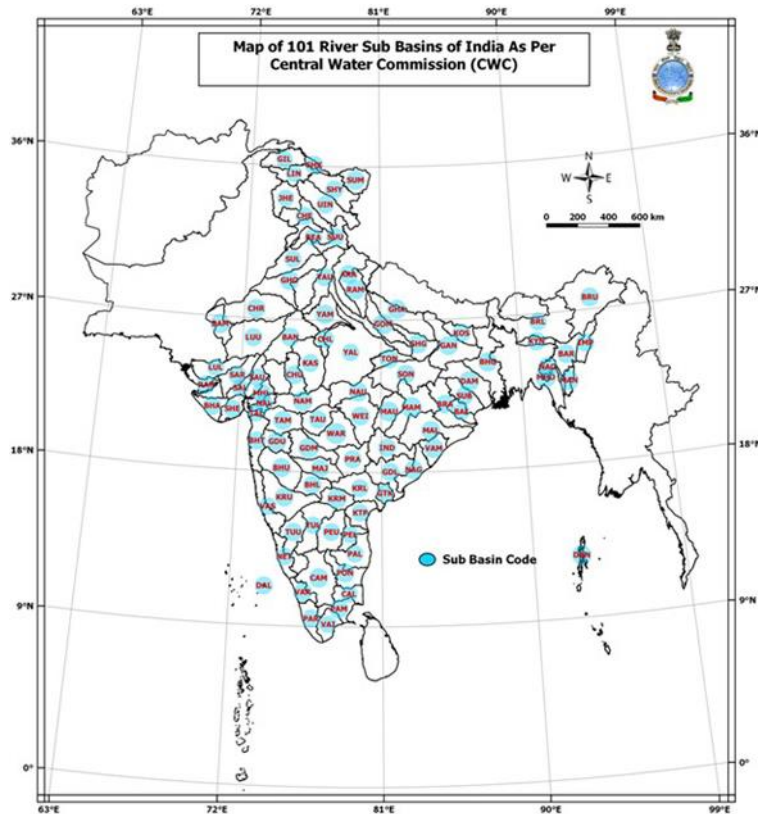


Fig. 1. Locations of the 101 river sub-basins of India.

Table 1. List of the 101 river sub-basins of India and their codes.

Sub Basin No.	SBCODE	Major Basin	SUB_BASIN
1	ARA	Ganga Basin	Above Ramganga Confluence
2	BAI	Brahmani and Baitarni Basin	Baitarni
3	BAM	Indus (Up to border) Basin	Barmer
4	BAN	Ganga Basin	Banas
5	BAR	Barak and others Basin	Barak
6	BEA	Indus (Up to border) Basin	Beas
7	BHA	West flowing rivers of Kutch and Saurashtra including Luni Basin	Bhadar and other west flowing rivers
8	BHG	Ganga Basin	Bhagirathi and others (Ganga Lower)
9	BHL	Krishna Basin	Bhima Lower
10	BHT	West flowing rivers South of Tapi Basin	Bhatsol and others
11	BHU	Krishna Basin	Bhima Upper
12	BRA	Brahmani and Baitarni Basin	Brahmani
13	BRL	Brahmaputra Basin	Brahmaputra Lower

14	BRU	Brahmaputra Basin	Brahmaputra Upper
15	CAL	Cauvery Basin	Cauvery Lower
16	CAM	Cauvery Basin	Cauvery Middle
17	CAU	Cauvery Basin	Cauvery Upper
18	CHA	Indus (Up to border) Basin	Chautang and others
19	CHE	Indus (Up to border) Basin	Chenab
20	CHL	Ganga Basin	Chambal Lower
21	CHR	Indus (Up to border) Basin	Churu
22	CHU	Ganga Basin	Chambal Upper
23	DAL	Drainage Area of Lakshadweep Islands Basin	Drainage Area of Lakshadweep Islands
24	DAM	Ganga Basin	Damodar
25	DAN	Drainage Area of Andaman and Nicobar Islands Basin	Drainage Area of Andaman and Nicobar Islands
26	GAN	Ganga Basin	Gandak and others
27	GDL	Godavari Basin	Godavari Lower
28	GDM	Godavari Basin	Godavari Middle
29	GDU	Godavari Basin	Godavari Upper
30	GHA	Ganga Basin	Ghaghara
31	GHG	Ganga Basin	Ghaghara Confluence to Gomti confluence
32	GHO	Indus (Up to border) Basin	Ghaghara and others
33	GIL	Indus (Up to border) Basin	Gilgit
34	GOM	Ganga Basin	Gomti
35	GTK	East flowing rivers between Godavari and Krishna Basin	East flowing rivers between Godavari and Krishna
36	IMP	Minor rivers draining into Myanmar Basin	Imphal and others
37	IND	Godavari Basin	Indravati
38	JHE	Indus (Up to border) Basin	Jhelum
39	KAS	Ganga Basin	Kali Sindh and others up to Confluence with Parbati
40	KOS	Ganga Basin	Kosi
41	KPO	Minor rivers draining into Bangladesh Basin	Karnaphuli and others
42	KRL	Krishna Basin	Krishna Lower
43	KRM	Krishna Basin	Krishna Middle
44	KRU	Krishna Basin	Krishna Upper
45	KTP	East flowing rivers between Krishna and Pennar Basin	East flowing rivers between Krishna and Pennar
46	KYN	Barak and others Basin	Kynchiang and other south flowing rivers
47	LIN	Indus (Up to border) Basin	Lower Indus
48	LUL	West flowing rivers of Kutch and Saurashtra including Luni Basin	Luni Lower
49	LUU	West flowing rivers of Kutch and Saurashtra including Luni Basin	Luni Upper
50	MAJ	Godavari Basin	Manjra
51	MAL	Mahanadi Basin	Mahanadi Lower
52	MAM	Mahanadi Basin	Mahanadi Middle
53	MAN	Minor rivers draining into Myanmar Basin	Mangpui Lui and others
54	MAU	Mahanadi Basin	Mahanadi Upper
55	MHO	Minor rivers draining into Bangladesh Basin	Muhury and others

56	MHU	Mahi Basin	Mahi Upper
57	NAG	East flowing rivers between Mahanadi and Godavari Basin	Nagvati and other
58	NAM	Narmada Basin	Narmada Middle
59	NAO	Barak and others Basin	Naoch chara and others
60	NAU	Narmada Basin	Narmada Upper
61	NET	West flowing rivers South of Tapi Basin	Netravati and others
62	PAL	East flowing rivers between Pennar and Cauvery Basin	Palar and other
63	PAM	East flowing rivers South of Cauvery Basin	Pamba and others
64	PAR	West flowing rivers South of Tapi Basin	Periyar and others
65	PEL	Pennar Basin	Pennar Lower
66	PEU	Pennar Basin	Pennar Upper
67	PON	East flowing rivers between Pennar and Cauvery Basin	Ponnaiyar and other
68	PRA	Godavari Basin	Pranhita and others
69	RAM	Ganga Basin	Ramganga
70	RAN	West flowing rivers of Kutch and Saurashtra including Luni Basin	Drainage of Rann
71	RAV	Indus (Up to border) Basin	Ravi
72	SAL	Sabarmati Basin	Sabarmati Lower
73	SAR	West flowing rivers of Kutch and Saurashtra including Luni Basin	Saraswati
74	SAU	Sabarmati Basin	Sabarmati Upper
75	SHE	West flowing rivers of Kutch and Saurashtra including Luni Basin	Shetranjuli and other east flowing rivers
76	SHK	Area of North Ladakha not draining into Indus Basin	Shaksgam
77	SHY	Indus (Up to border) Basin	Shyok
78	SON	Ganga Basin	Sone
79	SUB	Subernarekha Basin	Subernarekha
80	SUL	Indus (Up to border) Basin	Sutlaj Lower
81	SUM	Area of North Ladakha not draining into Indus Basin	Sulmar
82	SUU	Indus (Up to border) Basin	Sutlaj Upper
83	TAM	Tapi Basin	Tapi Middle
84	TAU	Tapi Basin	Tapi Upper
85	TON	Ganga Basin	Tons
86	TUL	Krishna Basin	Tungabhadra Lower
87	TUU	Krishna Basin	Tungabhadra Upper
88	UGO	Ganga Basin	Upstream of Gomti confluence to Muzaffarnagar
89	UIN	Indus (Up to border) Basin	Upper Indus
90	VAI	East flowing rivers South of Cauvery Basin	Vaippar and others
91	VAM	East flowing rivers between Mahanadi and Godavari Basin	Vamsadhara and other
92	VAR	West flowing rivers South of Tapi Basin	Varrar and others
93	VAS	West flowing rivers South of Tapi Basin	Vasishti and others
94	WAR	Godavari Basin	Wardha
95	WEI	Godavari Basin	Weinganga
96	YAL	Ganga Basin	Yamuna Lower

97	YAM	Ganga Basin	Yamuna Middle
98	YAU	Ganga Basin	Yamuna Upper
99	MHL	Mahi Basin	Mahi Lower
100	NAL	Narmada Basin	Narmada Lower
101	TAL	Tapi Basin	Tapi Lower

2.2. Methodology

Weekly grid point cumulative rainfall data for the years 2003-2019 were used. Average cumulative rainfall (in mm) in each sub-basin for every week was calculated using the Raster Statistics Method in the QGIS Software. More details on the operational extended-range forecast can be seen in a study by Sahai et al. (2019b). A diagram illustrating how the operational forecast is generated currently, is shown in Figure 2. The operational extended-range forecast is an ensembled mean of four dynamical models. Two of them are high resolution (denoted by suffix T382 or ~ 38 km), and two are low resolution models (indicated by suffix T126 or ~ 110 km). Two of the models have coupled models (CFS), and two are atmospheric models (GFS). Each model shares the same dynamic core but slightly different physics and resolutions. Each model has 4-member ensemble runs. Thus, we have a total of $4 \times 4 = 16$ ensemble members from the CFST126, CFST382, GFST126, and GFST382 models for runs from each set of condition. Atmospheric and oceanic initial conditions were generated by NCMRWF and INCOIS, respectively. The sea surface temperature boundary conditions for the GFS were derived from the CFS runs. Since the CFS sea surface temperature has a bias, a simple bias correction using observed climatology was applied to generate the final input boundary conditions for the GFS.

There are various metrics for evaluating rainfall forecasts (e.g., Barnston 1992; Huang, Zhao 2022). Several papers have used root mean square errors and correlation coefficients as a first order measure to evaluate the deterministic forecast ability of rainfall in the extended range (e.g., Joseph et al. 2019). Similarly, there are several methods to evaluate hydrological forecasts (e.g., Hoshin et al. 2009; Gilewski, Nawalany 2018). In this study, we computed and compared the "normalized root mean square error" (*NRMSE*) and "correlation coefficient" of raw extended range weekly forecast data (hereafter *ERF*) and bias-corrected forecast data (hereafter *BERF*). For basin averaged extended range forecast, it would be shown that the bias-corrected forecast improves the model performance.

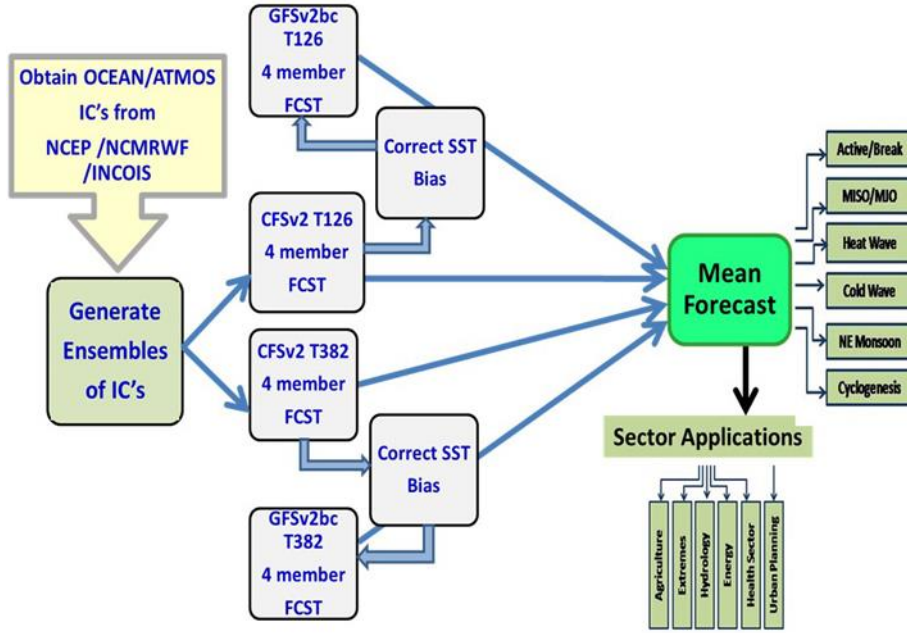


Fig. 2. Schematics of the end-to-end forecast and dissemination system implemented for Extended Range Prediction in India. Abbreviations: CFSv2: Coupled forecasting system version2; GFSv2: Global forecasting system; T382 and T126 suffixes specify the CFS and the GFS model horizontal spatial resolutions and different spectral truncations. T382 implies models CFS or GFS model run at ~ 38 km resolution. In comparison, T126 indicates the model to run at ~ 110 km spatial resolution. The suffix "bc" suggests that the GFS runs with bias-corrected sea surface temperature (SST) as boundary conditions. "FCST" indicates forecast runs, and ICs indicate initial conditions from which the model is run. INCOIS (Indian National Center for Ocean Information services) and NCMRWF (National Centre for Medium-Range Weather Forecasting) generate the ICs (i.e., initial conditions) for the operational forecasts. Models are an adapted version of models developed at the National Centre for Environmental Predictions (NCEP), USA, which also generates the ICs. MISO or MJO is the intra-seasonal monsoon oscillations and the Madden Julian Oscillations.

2.3. Bias correction with Normal Ratio Method

For the estimation of missing or unknown rainfall values, a normal ratio method is suggested by WMO (2018). We have adopted a similar approach to perform bias correction of the raw extended rainfall forecast (*ERF*) by multiplying the Bias correction ratio with the raw *ERF* rainfall. The normal ratio method is generally used for rainfall estimation, whereas difference correction is advised for temperature and other parameters.

According to the normal ratio method, the missing precipitation is given as:

$$P_x = \frac{1}{n} \sum_{i=1}^n \frac{N_x}{N_i} P_i \quad (1)$$

Where P_x is the missing precipitation for any storm at the interpolation station 'x', P_i is the precipitation for the same period for the same storm at the "ith" station of a group of index stations, N_x is the normal

precipitation value for the 'x' station and N_i the normal precipitation value for 'ith' station. In our bias correction method, P_i is the precipitation from raw *ERF*, N_i is the climatology of P_i , N_x is the observed climatology, and P_x is the bias corrected *ERF*.

Figure 3 shows the climatological differences between raw *ERF* rainfall and realized rainfall of 101 sub-basins of India for each of the 18 weeks of southwest monsoon. The first week of this period was from 30th May to 5th June and the last week was from 26th Sept to 2nd Oct (as 18th week). It can be seen that *ERF* has no systematic bias, as it is overestimating in some areas and underestimating in others. These differences also changed as the monsoon progresses. During the initial onset phase of the monsoon in June, the *ERF* climatology was higher than the observed climatology in most sub-basins. Still, during the peak monsoon period from July to August, *ERF* underestimated the rainfall for most sub-basins. Particularly during week number 8 (18th Jul to 25th July), *ERF* climatology was less significant for all the sub-basins of India – except one sub-basin in the extreme eastern parts of India. Another important finding in *ERF* was overestimation throughout the season, except one or two weeks for the sub-basins over Bihar, east UP, and adjacent areas. Thus, bias correction based on the normal ratio method has to be applied for all the weeks separately. This overcomes both the underestimating and overestimating of the raw *ERF* rainfall forecast and makes the prediction closer to the realized one. Thus, the bias correction ratio was different for each basin, as well as for each week during the monsoon onset, progress, and retreat phases.

The bias correction ratio for each of the 101 sub-basins and all the 18 weeks during the southwest monsoon season was estimated by the ratio of Actual Rainfall Climatology (for the same week in the period 2003-2019) and *ERF* Climatology (for the same week in the period 2003-2019). Here we have used the normal ratio in equation (1) for the estimation of missing rainfall, as the bias correction ratio in our bias correction method. This assists in improving the forecast value by giving weight to observed climatology.

Therefore, to improve the accuracy of the sub-basin rainfall forecast, we have adopted a new bias correction method given as follows:

The Bias Corrected Rainfall Forecast for each week and each basin = *ERF* (Rainfall) for that week X Bias correction ratio for the corresponding week of the same basin.

The correlation coefficient is one of the possible choices for forecast verification (Barnston 1992) and is given as:

$$r = \frac{\sum(x_i - \bar{x})(y_i - \bar{y})}{\sqrt{\sum(x_i - \bar{x})^2 \sum(y_i - \bar{y})^2}} \quad (2)$$

where: r – correlation coefficient; x_i – values of the x-variable in a sample; \bar{x} – mean of the values of the x-variable; y_i – values of the y-variable in a sample; \bar{y} – mean of the values of the y-variable.

In statistical modeling, another way of measuring the quality of the fit of the model, is the *RMSE* (also called Root Mean Square Deviation) (Barnston 1992) given by:

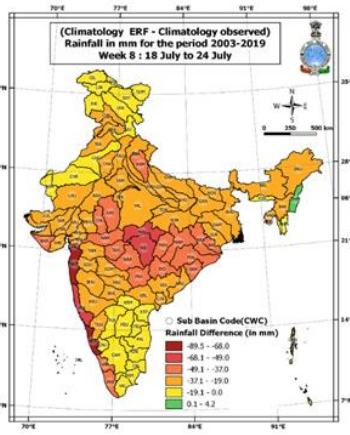
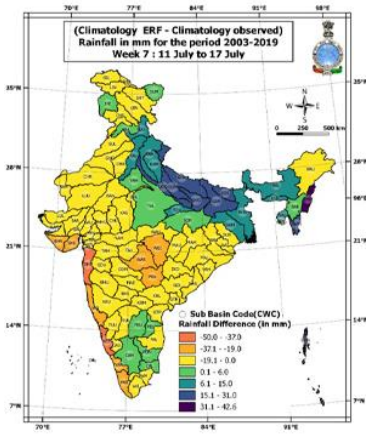
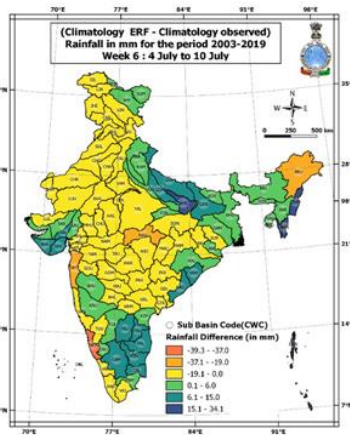
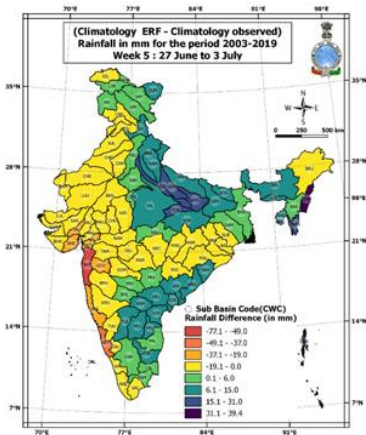
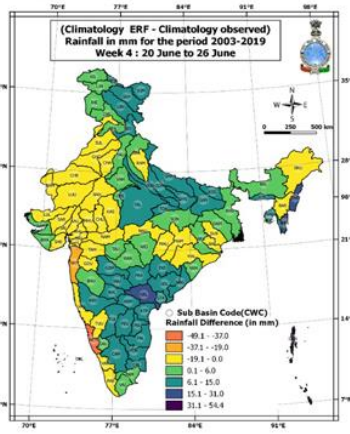
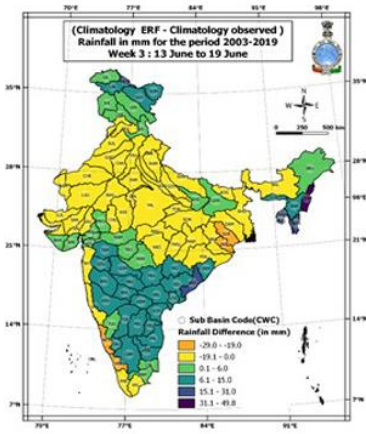
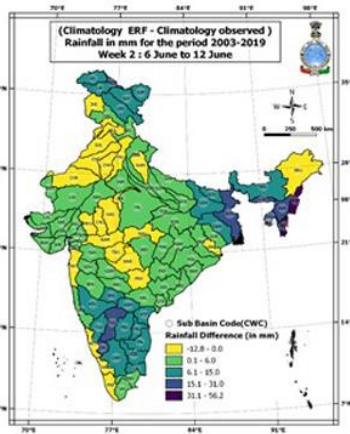
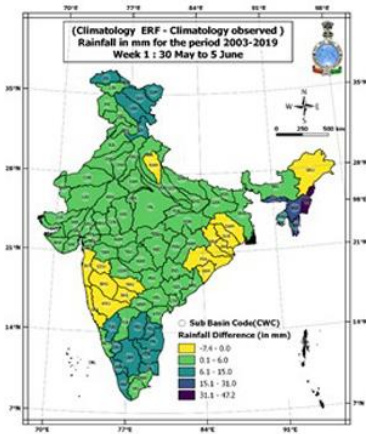
$$RMSE = \sqrt{\sum_{i=1}^n \frac{(\hat{y}_i - y_i)^2}{n}} \quad (3)$$

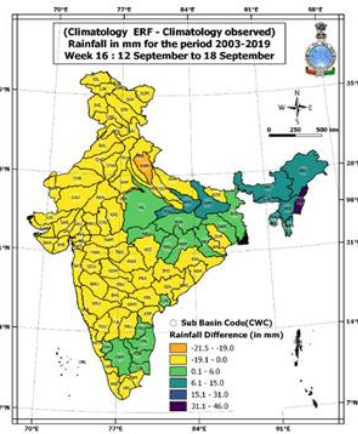
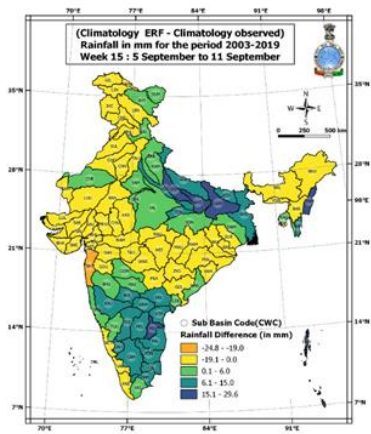
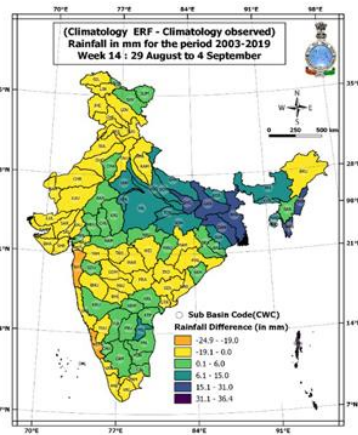
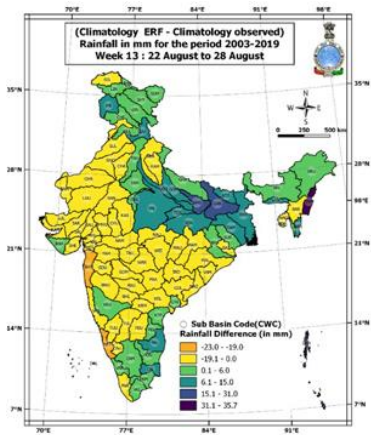
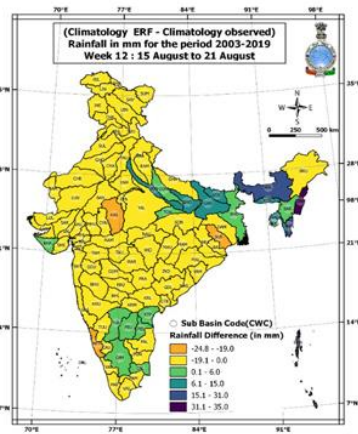
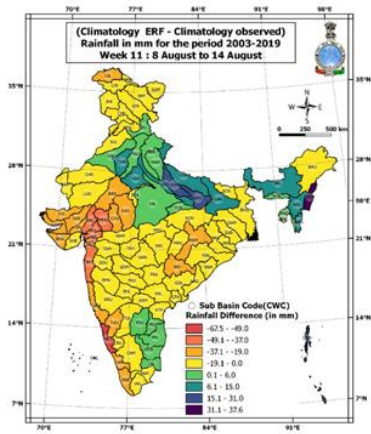
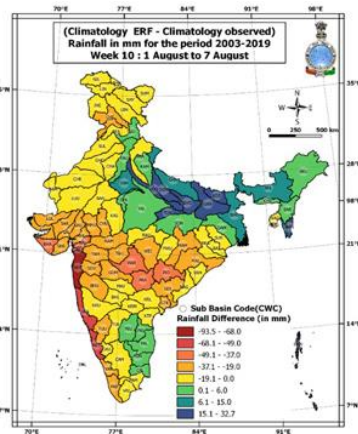
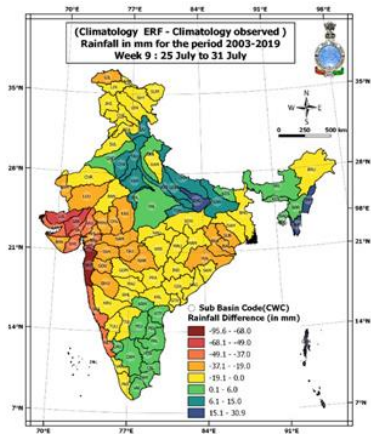
where y_i is the i^{th} observation of y and \hat{y}_i the predicted y value given the model. If the predicted responses are very close to the correct responses, the $RMSE$ will be small. If the predicted and true responses differ substantially – at least for some observations – the $RMSE$ will be large.

To compare $RMSE$ of rainfall forecast of the different river basins with different mean rainfall patterns, we have used Normalized Root Mean Square Error ($NRMSE$) as:

$$NRMSE = RMSE / \text{Mean (observed values)} \quad (4)$$

In the next sections, the $NRMSE$ and the correlation coefficient will be used as the standard skill score measures to evaluate the improvement in the rainfall forecast.





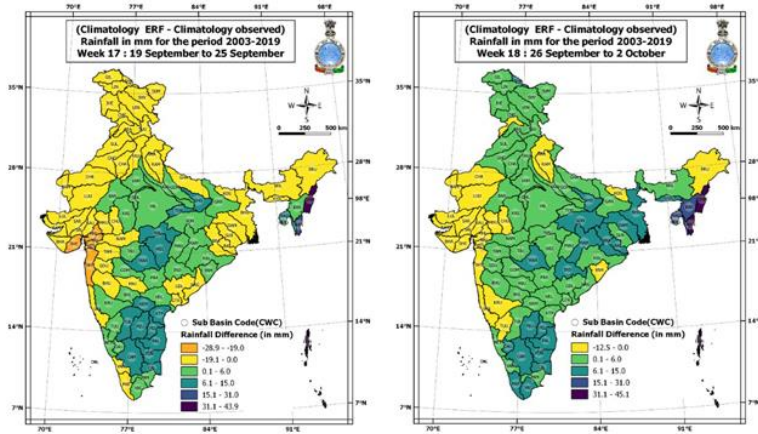


Fig. 3. Differences in climatology of raw *ERF* with realized rainfall climatology for the 18 weeks of the SW monsoon season (2003-2019).

3. Results and discussion

3.1. Performances of forecast

From a hydrological forecast perspective, the monsoon onset phase is perhaps the most important phenomenon. Every year, the onset over Kerala, and its subsequent propagation over the Indian Landmass, is monitored for agrometeorological predictions. The onset phase is often associated with a northward propagating rainfall pulse, providing rain over large regions of India and several river basins.

Rainfall during the onset phase of the monsoon is crucial for agricultural planning. Additionally, most flood events occur during July and August, when the monsoon is active. Week-by-week performances of the week 1 extended-range forecast, as well as the bias-corrected forecast, are shown for June (Fig. 4a), July (Fig. 4b), August (Fig. 4c), and September (Fig. 4d) of 2003-2019.

For all the weeks, the Normalized *RMSE* of bias-corrected *ERF* was less than 1 in most cases and for most sub-basins. In week 1 (Fig. 4a), due to bias correction, *NRMSE* of *ERF* has been reduced from 2.4 to 0.5 for the Drainage Area of Andaman and Nicobar Islands sub-basin, from 1.6 to 0.4 for the Drainage Area of Lakshadweep Islands sub-basin, from 1.7 to 1.4 for the Sulmar sub-basin, 1.0 to 0.7 for the Kynchiang sub-basin, and other south-flowing rivers of Barak basin during onset phases of the SW monsoon. For all four weeks of June (Fig. 4a), *NRMSE* of these sub-basins were high (more than 1.5) for raw *ERF*, whereas due to bias correction, *NRMSE* has come down by around 0.5. Furthermore, for all four weeks of June, *NRMSE* of bias-corrected *ERF* was less than the *NRMSE* of raw *ERF*. This was within 0.2 to 0.9 for all the sub-basins, except a few sub-basins in the first week and one sub-basin in the second and third weeks.

In the first week of July (27th Jun to 3rd July) (Fig. 4b), the bias corrections of several sub-basins have helped to improve the *NRMSE* by keeping it less than 0.8. In the following two weeks, though the *NRMSE* of bias-corrected *ERF* was less than the raw *ERF* for all the sub-basins, there was no significant improvement. However, in the last two weeks of July, significant improvement of the ability of bias-corrected *ERF* was seen for most of the sub-basins.

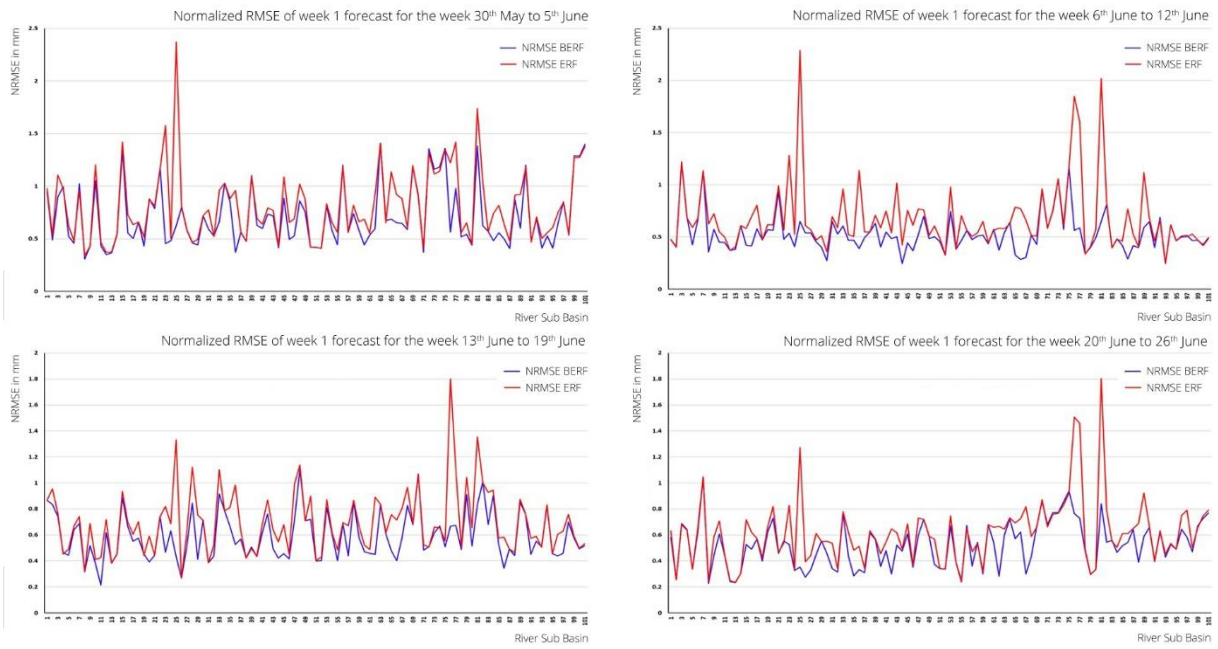


Fig. 4a. Normalized RMSE of Bias corrected *ERF* (*BERF*) and raw *ERF* of Week 1 rainfall during June.

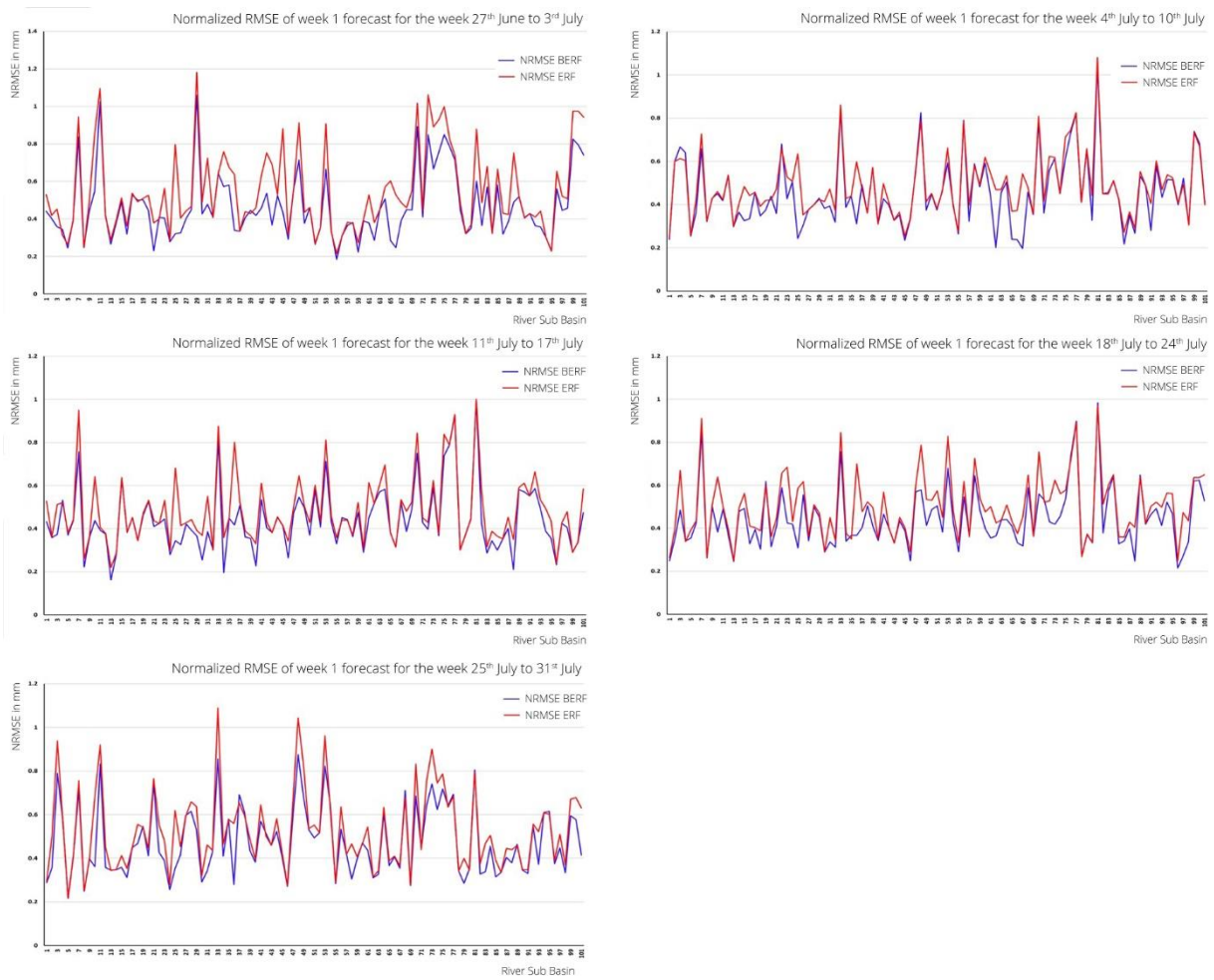


Fig. 4b. Normalized RMSE (*NRMSE*) of Bias corrected *ERF* (*BERF*) and raw *ERF* of Week 1 rainfall during July.

There is a remarkable improvement in the skill of bias-corrected *ERF* for the first two weeks of August (Fig. 4c), as *NRMSE* of bias-corrected *ERF* was between 0.2 to 0.6 in most of the sub-basins. Since most of the floods in India occur during July and August, bias correction can help improve flood forecasts and better flood management.

Even during all the weeks of September (Fig. 4d), bias correction reduced the *NRMSE* value to well below 1.0 of the *NRMSE* value and greater than 1 of raw *ERF*.

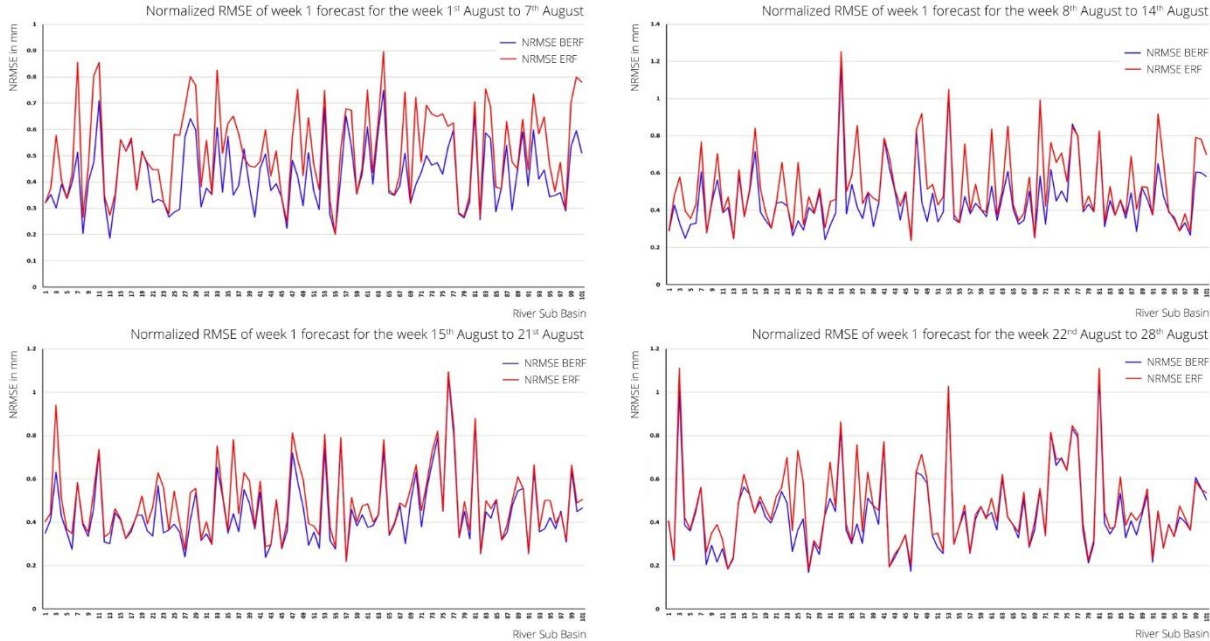


Fig. 4c. Normalized *RMSE* of Bias corrected *ERF* (*BERF*) and raw *ERF* of Week 1 rainfall during August.

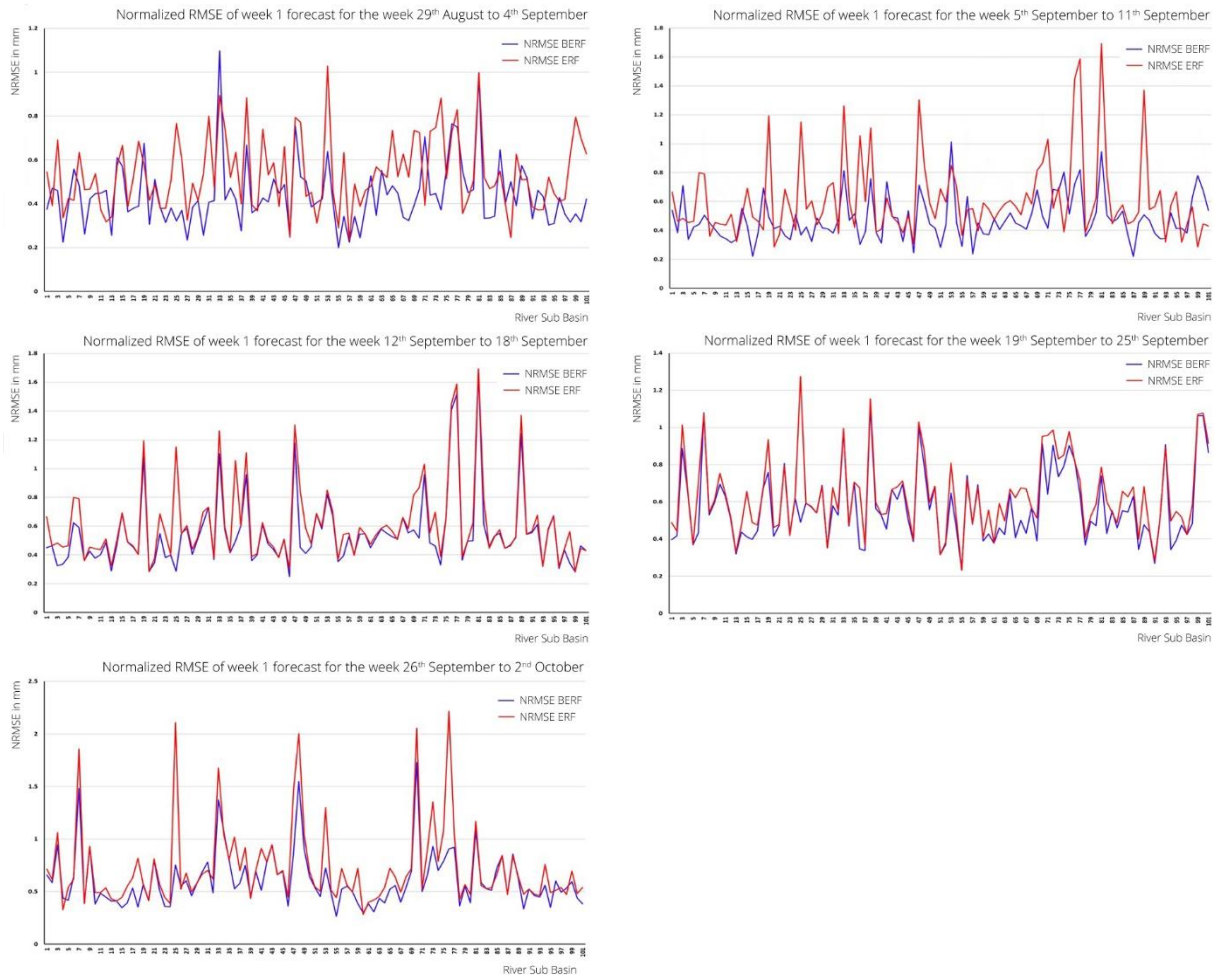


Fig. 4d. Normalized RMSE of Bias corrected *ERF* (*BERF*) and raw *ERF* of Week 1 rainfall during September.

3.2. The spatial pattern of Extended Range onset forecast skill for the period 2003-2019

To demonstrate the skill of the extended range forecast for the 1-week and 2-weeks lead-time during the monsoon season, we have computed the correlation coefficient and the normalized root mean square error (*NRMSE*) map between the *ERF* and observed rainfall for the years 2003-2019. The samples consisted of 18 weeks and 17 years ($18 \times 17 = 306$ samples) for each of the 101 sub-basins for the monsoon season. Figures 5a-b shows the basin-wise map of the correlation coefficients and normalized root mean square error for the raw *ERF* (left panels), respectively. The plot indicates relatively high correlations in the central and northern Indian basins and relatively low correlations in the southern peninsular basins. Furthermore, there were low correlations and higher *NRMSE* in the Jammu, Kashmir, and Ladakh regions. The root mean square error in Figure 5b shows that the model had the lowest error in central and northern India.

Similarly, Figures 5c-d show the same skill metrics for the bias-corrected forecast. The bias-corrected forecast shows some improvement in correlation skills in the Maharashtra sub-basins and some basins of peninsular India. There was also a significant decrease in *RMSE* over the basins of central to southern peninsular India.

Figure 6 shows the same skill plots but for the 2-week forecast.

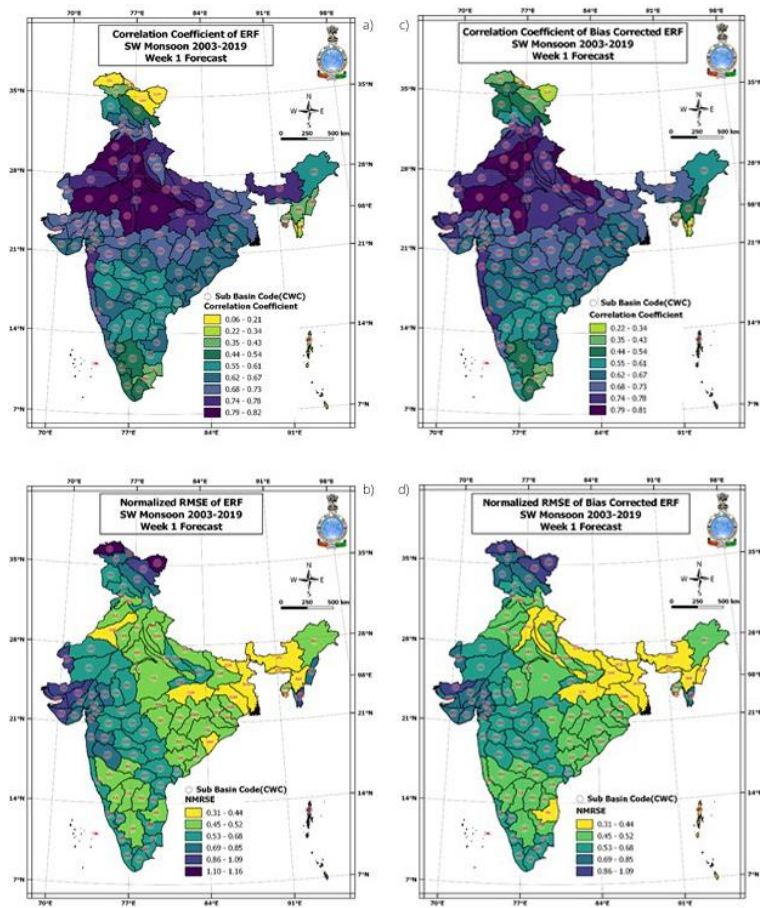


Fig. 5. (a) Correlation map of 1-week actual forecast, (b) RMSE of the actual forecast, (c) same as (a) but showing the cc map for bias-corrected forecast, (d) same as (b) but showing RMSE of bias-corrected forecast.

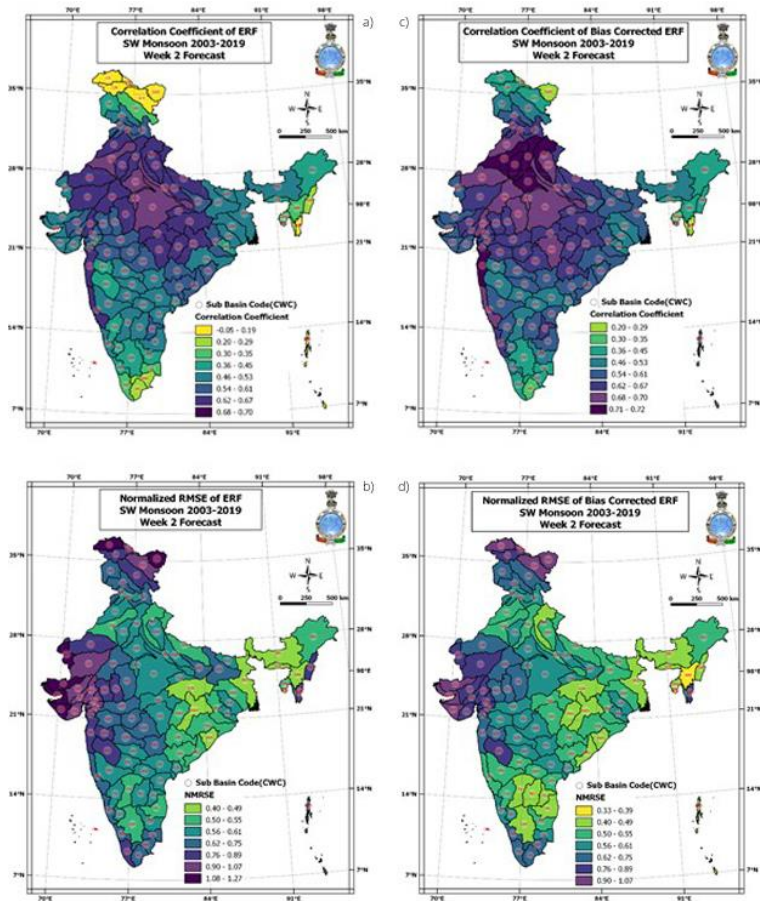


Fig. 6. Same as (5) but for the 2-week forecast.

3.4. Floods in Maharashtra and Bihar during 2019 and the evaluation of skill forecast for the year 2019

In 2019, several parts of the country had experienced severe floods affecting lakhs of people (Shagun 2019; Kambli 2020). During July and August 2019, heavy flooding occurred in Maharashtra due to intense rainfall. The Sangli and Kolhapur district in the Krishna sub-basin experienced severe floods of long durations. Substantial losses of life, property and crops were reported. At the beginning of the flood period, i.e., from 27th Jul to 3rd Aug, heavy rainfall events were localized in the northern part of the Konkan and adjoining North Madhya Maharashtra. Many stations in the Pune and Nasik districts recorded rainfall of more than 150 mm/day from 3rd to 5th August. Towards the latter part of the week, the rainfall belt shifted towards southern Madhya Maharashtra. Mahabaleshwar recorded the highest rainfall of 380 mm on 5th Aug 2019. It is also observed that the Kolhapur district continuously experienced heavy rain throughout this period, with the highest rainfall amounts on 6th Aug 2019. Gaganbawda recorded its highest rainfall of 340 mm on 6th Aug 2019. It is also seen that, though heavy rainfall occurred in the western part of the districts in Madhya Maharashtra, their eastern parts were devoid of rainfall. Furthermore, during the heavy rain spell of Aug 2019, many stations in the Kolhapur district and western parts of the Satara district have surpassed their previous record of 7 days rainfall. Compared to 2018, rainfall over the region was widespread and remained very intense for an extended period from 27th Jul to 13th Aug 2019

(Government of Maharashtra 2020). The expert committee of the Government of Maharashtra recommended that IMD 1-week and 2-week river sub-basin rainfall forecasts should be used in flood forecasting to improve the accuracy of the forecast. Another major affected state was Bihar, where around 306 lives were lost due to floods and heavy rain.

We have analyzed the 1-week forecasted rainfall of raw *ERF* compared to the actual rainfall for all the sub-basins of these two states, and showed how the bias-corrected forecast could have helped the flood management. The losses could have been minimized by using the bias-corrected forecast for these regions.

Figure 7 shows the realized, bias-corrected *ERF* and *ERF* rainfall for 18 weeks of SW Monsoon season of 2019. This includes the sub-basins viz. Godavari Upper, Godavari Middle, Wardha, Wainganga, Tapi Middle, Bhima Upper, Krishna Upper, Bhatsol and others, and Vasishti and other Flood-affected Maharashtra states. In the 9th and 10th weeks (25th Jul to 31st Jul and 1st Aug to 7th Aug), all nine of these sub-basins reported a significant increase in rainfall compared to previous weeks, which raw *ERF* was not able to predict in most of the cases. The sub-basins Weinganga, Vasishti, and others also reported increased rainfall activity in 11-weeks. The raw *ERF* underestimated the rainfall for all these basins. Applying the bias correction forecast to rainfall from these basins was almost comparable to that of the realized rainfall, indicating the usefulness of the bias-corrected Week 1 rainfall in improving flood management.



Fig. 7. Realized, Bias corrected *ERF* (*BERF*) and *ERF* rainfall for 18 weeks of the 2019 SW Monsoon season in 9 sub basins of the flood affected Maharashtra state.

For the Bihar flood, we have selected four sub-basins viz. Ghaghara, Ghaghara Confluence to Gomti confluence, Gandak and others, and Koshi. Figure 8 shows the realized, bias-corrected *ERF* and *ERF* rainfall for 18 weeks of the 2019 SW Monsoon season for sub-basins of Flood-affected Bihar. In the 6th and 7th weeks, all four sub-basins have reported increased rainfall activities causing devastating flooding over this region. The week 1 raw *ERF* rainfall has been overestimated in all these cases. The bias correction could help to minimize the differences between observed rainfall and forecast rainfall.

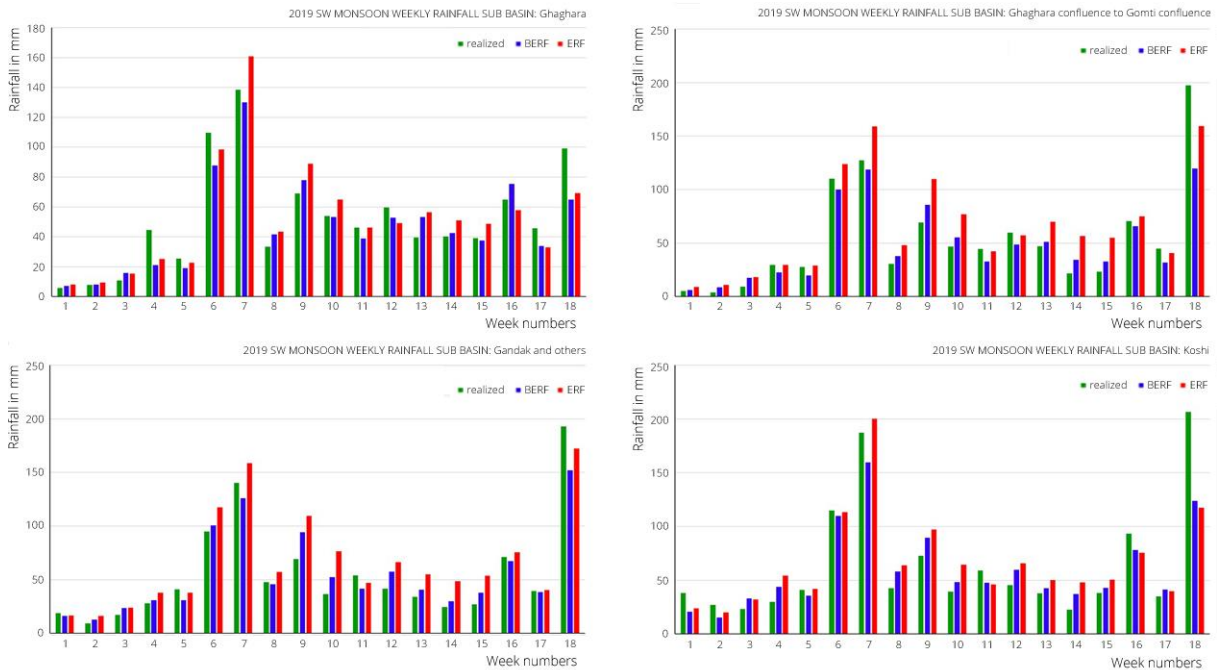


Fig. 8. Realized, Bias corrected *ERF* (*BERF*) and *ERF* rainfall for 18 weeks of SW Monsoon season 2019 of sub basins of flood-affected districts of the Bihar state.

To see the performance of raw *ERF* and bias-corrected *ERF* for the year 2019, the correlation coefficient between observed and forecast rainfall and normalized *RMSE* was calculated using 18 samples (all eighteen weeks of SW monsoon 2019) for both the 1-week and 2-week lead forecasts. Figure 9 shows the (a) correlation and (b) *RMSE* of the raw extended range forecast, calculated using the weekly data for the year 2019. (c) same as (a) but after using bias correction. (d) same as (b) but after using bias correction for the 1-week lead forecast.

The left column shows the raw extended range forecast, and the right column shows the corresponding bias-corrected forecast. There was a significant improvement in the correlation coefficient for most sub-basins, mainly over the northern and central parts of India. The normalized root means square error shows that there was a considerable improvement in the bias-corrected forecast, especially in the east and central parts of India, as normalized *RMSE* has been reduced to less than 0.3 due to bias correction over these parts. Additionally, in the western parts of Maharashtra, *NRMSE* has been reduced from near 1 in raw *ERF* to less than 0.5.

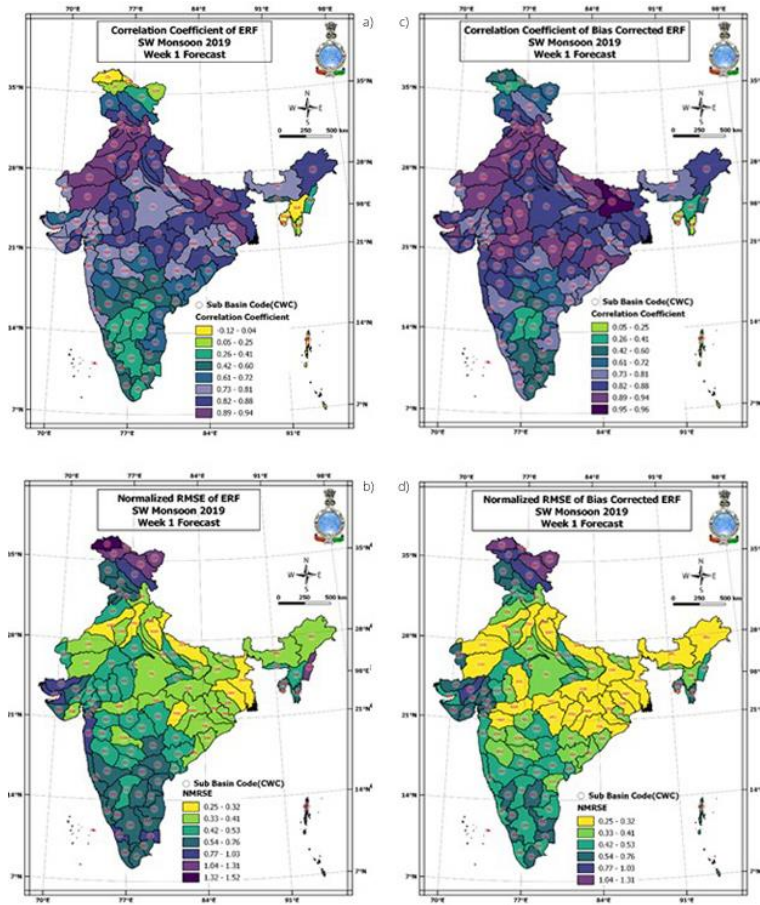


Fig. 9. (a) Correlation and (b) $RMSE$ of the raw extended range forecast calculated using the weekly data for the year 2019 of 1-week forecast. (c) same as (a) but after using bias correction. (d) same as (b) but after using bias correction.

Figure 10 shows the (a) correlation and (b) $RMSE$ of raw extended range forecast calculated using the weekly data for the year 2019. (c) same as (a) but after using bias correction. (d) same as (b) but after using bias correction for the 2-week lead forecast.

The left column shows the actual extended range forecast, and the right column shows the corresponding bias-corrected forecast. In the 2-week forecast, the correlation coefficient for the sub-basins of Maharashtra has been increased from around 0.7-0.8 in raw ERF to 0.93-0.97. The correlation coefficient is between 0.7-0.8 in most of the sub-basins of central India in the bias-corrected forecast. Normalized $RMSE$ is also less than 0.5 in the bias-corrected forecast for most of the sub-basins of India, with central India being less than 0.3.

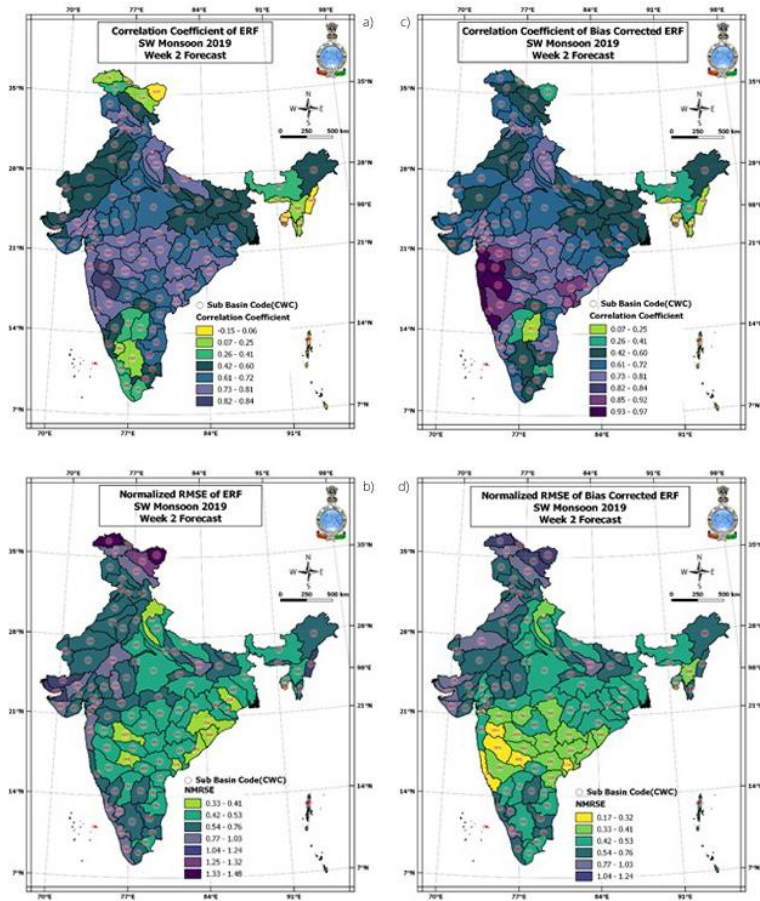


Fig. 10. (a) Correlation Coefficient and (b) *RMSE* of raw extended range forecast calculated using the weekly data for the year 2019 of the 2-week forecast (c) same as (a) but after using bias correction (d) same as (b) but after using bias correction.

4. Conclusions

For efficient flood and disaster management, an accurate rainfall forecast is essential to provide a quantitative prediction of precipitation during the June to September (monsoon) season over river basins of the Indian subcontinent. The weekly averaged extended range rainfall forecast of up to 2-weeks lead-time is important, as it provides a valuable input for generating flood forecast models in a time-scale that is crucial for water and dam management. A proper rainfall forecast with a longer lead time is always desirable to manage floods and their impact on disaster risk reduction. India's present operational flood forecasting models are primarily dependent on 1-3 days quantitative rainfall forecast and a forecast of up to 5 days generated by India Meteorological Department. In the extended range (i.e., 2-weeks lead time) the rainfall forecast is often not accurate, owing to the decrease in rainfall amplitude. In the current study, we have provided a comprehensive basin averaged rainfall skill analysis over different sub-basins of India, using the extended range retrospective forecast and proposing a bias correction method to improve the rainfall forecast in the extended range. We have found that the extended forecast has an unsystematic bias (i.e., overestimation and underestimation) for weekly averaged rainfall. The bias in precipitation is not systematic, and different sub-basins show the bias of different amplitude. Such amplitude biases would likely impact

forecast ability. Our bias corrected forecast has shown significant skill in predicting sub basin rainfall of 1-week as well as 2-weeks lead time.

We hypothesized that a part of the amplitude bias might be associated with systematic forecast model bias. Due to rainfall forecast error associated with model physics, dynamics, and several other factors, such biases can arise. Using an amplitude correction method based on the "Normal Ratio" correction method from the WMO manual, we devised an approach to see if the normal ratio correction would improve the first-order skill scores (root mean square error and correlation) for weekly extended range forecast over the Indian land region. The results show an encouraging improvement in statistical skill scores for several river basins over India. The long-term (2003-2019) skill analysis shows enough improvement in the weekly mean forecast. Similarly, case studies over the Maharashtra and Bihar river basins for 2019 show significant improvement in the weekly mean rainfall estimates. We also verified the week-by-week forecast from the onset to the withdrawal phase. The onset phase rainfall forecast over different sub-basins shows sufficient improvement. We propose that the analysis could be used as a background for operational forecast bias correction using the normal ratio method. This can be implemented for products based on extended range forecast and all forecast products in the sub-seasonal to seasonal (s2s) time-scale. Thus, these extended range basin rainfall forecasts of 1-week and 2-week lead times have shown good skill during the 2003-2019 period. In addition to existing flood forecasting systems of the central water commission of India, these findings can be used for generating flood forecasts with longer lead times to reduce disaster impacts.

Acknowledgment

Authors are grateful to the National Water Informatics Centre Ministry of Jalshakti for providing the river basin and sub-basin shapefiles that help initiate the weekly river subbasin wide rainfall forecast. We also acknowledge the India Meteorological department for making grid point rainfall data accessible to for observation and forecasting.

References

- Barnston A.G., 1992, Correspondence among the Correlation, RMSE, and Heidke Forecast Verification Measures; Refinement of the Heidke Score, *Weather and Forecasting*, 7 (4), 699-709, DOI: 10.1175/1520-0434(1992)007<0699:CATCRA>2.0.CO;2.
- Boé J., Terray L., Habets F., Martin E., 2007, Statistical and dynamical downscaling of the Seine basin climate for hydrometeorological studies, *International Journal of Climatology*, 27 (12), 1643-1655, DOI: 10.1002/joc.1602.
- Chattopadhyay R., Krishna R.P.M., Joseph S., Dey A., Mandal R., Sahai A.K., 2018, A comparison of extended-range prediction of monsoon in the IITM-CFSv2 with ECMWF S2S forecast system, IITM Research Report No. RR-139, available online <https://www.tropmet.res.in/~lip/Publication/RR-pdf/RR-139.pdf> (data access 28.02.2022).
- Chattopadhyay R., Susmitha J., Abhilash S., Mandal R., Dey A., Phani R., Saranya G., Kaur M., Pattanaik D.R., Sahai A.K., 2019, Understanding the intraseasonal variability over Indian region and development of an operational extended range prediction system, *Mausam*, 70 (1), 31-36, DOI: 10.54302/mausam.v70i1.166.
- Ghimire U., Srinivasan G., Agarwal A., 2019, Assessment of rainfall bias correction techniques for improved hydrological simulation, *International Journal of Climatology*, 39 (4), 2386-2399, DOI: 10.1002/joc.5959.

- Gilewski P., 2021, Impact of the grid resolution and deterministic interpolation of precipitation on rainfall-runoff modeling in a sparsely gauged mountainous catchment, *Water*, 13 (2), DOI: 10.3390/w13020230.
- Gilewski P., Nawalany M., 2018, Inter-comparison of rain-gauge, radar, and satellite (IMERG GPM) precipitation estimates performance for rainfall-runoff modeling in a mountainous catchment in Poland, *Water*, 10 (11), DOI: 10.3390/w10111665.
- Government of Maharashtra, 2020, A report on flood 2019 (Krishna Sub-basin), available online <https://wr.d.maharashtra.gov.in/Upload/PDF/Vol%201%20Main%20Report.pdf> (data access 28.02.2022).
- Gupta H.V, Kling H., Yilmaz K.K., Martinez G.F., 2009, Decomposition of the mean squared error and NSE performance criteria: Implications for improving hydrological modelling, *Journal of Hydrology*, 377 (1-2), 80-91, DOI: 10.1016/j.jhydrol.2009.08.003.
- Huang Z., Zhao T., 2022, Predictive performance of ensemble hydroclimatic forecasts: Verification metrics, diagnostic plots and forecast attributes, *WIREs Water*, e1580, DOI: 10.1002/wat2.1580.
- Jabbari A., Bae D.-H., 2020, Improving ensemble forecasting using total least squares and lead-time dependent bias correction, *Atmosphere*, 11 (3), DOI: 10.3390/atmos11030300.
- Joseph S., Sahai A.K., Phani R., Mandal R., Dey A., Chattopadhyay R., Abhilash S., 2019, Skill evaluation of extended-range forecasts of rainfall and temperature over the meteorological subdivisions of India, *Weather and Forecasting*, 34 (1), 81-101, DOI: 10.1175/WAF-D-18-0055.1.
- Kambli K., 2020, Top 5: Biggest floods to affect India in 2019, The Weather Channel, available online <https://weather.com/en-IN/india/news/news/2020-01-08-top-5-biggest-floods-affect-india-2019> (data access 28.02.2022).
- Leander R., Buishand T.A., 2007, Resampling of regional climate model output for the simulation of extreme river flows, *Journal of Hydrology*, 332 (3-4), 487-496, DOI: 10.1016/j.jhydrol.2006.08.006.
- Ming X., Liang Q., Xia X., Li D., Fowler H.J., 2020, Real-time flood forecasting based on a high-performance 2-D hydrodynamic model and numerical weather predictions, *Water Resources Research*, 56 (7), DOI: 10.1029/2019WR025583.
- Pai D.S., Rajeevan M., Sreejith O.P., Mukhopadhyay B., Satbhai N.S., 2014, Development of a new high spatial resolution (0.25°×0.25°) long period (1901-2010) daily gridded rainfall data set over India and its comparison with existing data sets over the region, *MAUSAM*, 65 (1), DOI: 10.54302/mausam.v65i1.851.
- Pattanaik D.R., Das A.K., 2015, Prospect of application of extended range forecast in water resource management: a case study over the Mahanadi River basin, *Natural Hazards*, 77, 575-595, DOI: 10.1007/s11069-015-1610-4.
- Pattanaik D.R., Sahai A.K., Mandal R., Muralikrishna R.P., Dey A., Chattopadhyay R., Joseph S., Tiwari A.D., Mishra V., 2019, Evolution of operational extended range forecast system of IMD: Prospects of its applications in different sectors, *MAUSAM*, 70 (2), DOI: 10.54302/mausam.v70i2.170.
- Sahai A.K., Chattopadhyay R., Joseph S., 2019a, Extended range forecast, *Geography and You*, 19, 16-21.
- Sahai A.K., Chattopadhyay R., Joseph S., Krishna P.M., Pattanaik D.R., Abhilash S., 2019b, Chapter 20 – Seamless prediction of monsoon onset and active/break phases, [in:] *Sub-Seasonal to Seasonal Prediction*, A.W. Robertson, F. Vitart (eds.), Elsevier, 421-438, DOI: 10.1016/B978-0-12-811714-9.00020-6.
- Sayama T., Yamada M., Sugawara Y., Yamazaki D., 2020, Ensemble flash flood predictions using a high-resolution nationwide distributed rainfall-runoff model: case study of the heavy rain event of July 2018 and Typhoon Hagibis in 2019, *Progress in Earth Planetary Science*, 7, 75, DOI: 10.1186/s40645-020-00391-7.
- Shagun K., 2019, Indian rivers crossed highest flood level 25 times in August 2019, *Down to Earth*, available online <https://www.downtoearth.org.in/news/natural-disasters/indian-rivers-crossed-highest-flood-level-25-times-in-august-2019-66818> (data access 28.02.2022).
- Singh A., Sahoo R.K., Nair A., Mohanty U.C., Rai R.K., 2017, Assessing the performance of bias correction approaches for correcting monthly precipitation over India through coupled models, *Meteorological Applications*, 24 (3), 326-337, DOI: 10.1002/met.1627.

- Teutschbein C., Seibert J., 2012, Bias correction of regional climate model simulations for hydrological climate-change impact studies: Review and evaluation of different methods, *Journal of Hydrology*, 456-457, 12-29, DOI: 10.1016/j.jhydrol.2012.05.052.
- Webster P.J., Hoyos C., 2004, Prediction of monsoon rainfall and river discharge on 15-30-day time scales, *Bulletin of the American Meteorological Society*, 85 (11), 1745-1765, DOI: 10.1175/BAMS-85-11-1745.
- Webster P.J., Jian J., Hopson T.M., Hoyos C.D., Agudelo P.A., Chang H., Curry J.A., Grossman R.L., Palmer T.N., Subbiah A.R., 2010, Extended-range probabilistic forecasts of Ganges and Brahmaputra floods in Bangladesh, *Bulletin of the American Meteorological Society*, 91 (11), 1493-1514, DOI: 10.1175/2010BAMS2911.1.
- WMO, 2018, *Guide to Climatological Practice*, WMO-No. 100, World Meteorological Organization, Geneva, 139 pp.

Digital Elevation Model resolution and its impact on the spatial pattern of rainfall-temperature prediction at the catchment scale: The case of the Mille catchment, Ethiopia

Hirpo Gudeta Bati 

Africa Center of Excellence for Water Management, Addis Ababa University, Ethiopia

Abstract

In a mountainous catchment, understanding the interaction between DEM resolution and climatic variables is essential for the accurate spatial interpolation of areal mean monthly and annual rainfall and temperature, which is required as an input for further applications such as hydrological and hydraulic modeling, agriculture, and environmental conservation. This case study applied the geostatistical interpolation technique, kriging with external drift (KED), with a digital elevation model (DEM) with various horizontal resolutions, which were used to assess the effects of the DEM horizontal resolutions on the spatial distributions of rainfall and temperature by focusing on interpolating the mean monthly and annual rainfall and temperature over a spatially diversified catchment. The assessment was undertaken using spatially and temporally complete sampled historical climatic datasets, and consequently, the spatial pattern of monthly and annual rainfall (temperature) from east to the west gradually increases or decreases following the DEM elevation increment along the same direction. As a result, the finer-resolution DEM (90-m SRTM-DEM) had a considerable impact on predicting the mean monthly minimum and maximum temperatures, whereas the resampled 500-m SRTM-DEM performed relatively better in mean monthly and annual rainfall and annual minimum temperature estimation values.

Keywords

KED, Mille catchment, mountainous catchment, rainfall, DEM resolution, temperature.

Submitted 26 December 2021, revised 18 March 2022, accepted 14 April 2022

DOI: 10.26491/mhwm/149231

1. Introduction

In mountain catchments, climatic variables such as rainfall and temperature play a key role in hydrological processes such as runoff, evapotranspiration, and water yield prediction (Chiew, McMahon 2002; Chen et al. 2020; Kim, Kim 2020). Flood early warning and forecasting as well as drought management for mitigating water-related problems significantly rely on the accuracy of predicted spatial rainfall data input (Bertini et al. 2020; Lu et al. 2020).

Several scholars have provided basic information on the impacts of the spatial distribution of climatic variable input on further hydrological analysis and related problems. However, in developing countries such as Ethiopia, the spatial array of input climatic variable stations is sparse, and the density of climatological stations is extremely low (Washington et al. 2006; Dinku 2019). Therefore, the spatial interpolation method has been used to predict spatial values for unsampled points (Kim et al. 2010; Adhikary et al. 2017; Aydin 2018). This crucial method helps solve the issue of the sparse and low hydroclimatic network density and is

widely used by governments and other sectors for planning water resource use and management at various spatiotemporal scales.

Spatial interpolation techniques require either ground-based observed climatic input data, radar rainfall, remote sensing-based satellite climatic input data, or blended data (Taesombat, Sriwongsitanon 2009; Verdin et al. 2015; Cantet 2017; Gebremedhin et al. 2021). The output of spatial interpolation is a map that shows the scale of the spatial climatic variable pattern of an area.

Digital elevation models (DEMs) are the main data commonly used as covariates in spatial interpolation techniques, specifically in geostatistics kriging. Several scholars have used topographic variables such as the elevation model as an explanatory variable and have confirmed that the covariate has a significant effect on the catchment's hydrological system and water balance (Novikov 1981; Hudson, Wackernagel 1994; Vaze et al. 2010; Meena, Nachappa 2019). For instance, the elevation with different spatial resolutions brings a valuable change to the catchment's spatial patterns of both rainfall and temperature (Hudson, Wackernagel 1994; Taesombat, Sriwongsitanon 2009). Research done by Taesombat and Sriwongsitanon (2009) revealed that the interpolation of point rainfall data using GLOBE-DEM (1000 m) and SRTM-DEM (90 m) elevation resolution as a predictor resulted in the coarser DEM resolution (GLOBE-DEM) performing slightly better in rainfall estimation than the finer one (SRTM-DEM). Vaze et al. (2010) investigated the effects of field survey DEM-derived elevation (25-m resolution) with finer-resolution light detection and ranging (LiDAR) DEM-derived elevation (1-m resolution) on the values of topographic indices, and the result showed that LiDAR DEM is a reasonably good representation of the real ground surface compared to DEMs derived from contour maps. Simanek and Holden (2020) suggest that DEM spatial resolution aggregated progressively to a coarser resolution, which resulted in decreased runoff and sediment.

Meena and Nachappa (2019) investigated the impacts of the DEM spatial resolution (12.5, 30, and 90 m) on landslide susceptibility mapping through a field survey, and the result depicted that the 30-m resolution is better suited for landslide susceptibility mapping. Numerous scholars have investigated the impacts of different spatial resolutions of DEM use on hydrological modeling (Schoorl et al. 2000; Wechsler 2007; Lin et al. 2010). For example, Lin et al. (2010) examined the effects of different DEM grid size resolutions on surface runoff and sedimentation using the SWAT model, and the results indicated that total phosphorous (TP) and total nitrogen (TN) decreased substantially with coarser resampled resolutions, whereas the predicted runoffs were not sensitive to resampled resolutions. The same result depicted the effect of grid size change on both the catchment landscape as well as the hydrological and geomorphic processes (Brown et al. 1993; Zhang, Montgomery 1994).

Although the Ethiopian landscape varies from flat to complex mountainous terrain, the impact of elevation horizontal resolution on rainfall and related climatological variable spatial distribution at the catchment scale

is rarely considered and has not been extensively investigated. The studied catchment, Mille, has large topographic differences, with highly variable climatic and agro-ecological zones. Based on this, the objective of this study is to examine the effect of the DEM resolution on the spatial prediction of the catchment's areal rainfall, maximum temperature, and minimum temperature, as well as to select the better and more reliable DEM resolution that serves as an auxiliary variable for future research work for the case of the Mille catchment in Ethiopia.

2. Study area

The studied catchment is located within the Awash River Basin (AwRB), which is the fourth largest basin in terms of area coverage and the seventh-largest basin in terms of surface water potential in Ethiopia (Berhanu et al. 2014). The Mille catchment area is nearly 5,599 km², situated to the east of the longest mountain chain of the western Awash River Basin escarpment encompassing the Mille River, which drains to the Awash River, between 11°17'-11°76'N latitude and 39°53'-40°94'E longitude. The topography of the Mille catchment ranges from steep mountainous terrain in the west to a gentle slope in the middle and undulating plains to the east (Fig. 1). The catchment elevations range from 412-755 m and 2,218-3,656 m above sea level for lowland plains and mountains, respectively. Land use/land cover is generally cultivated land, shrubland, woodland, forestland, grassland, bare land, and water bodies (MoWR 2009).

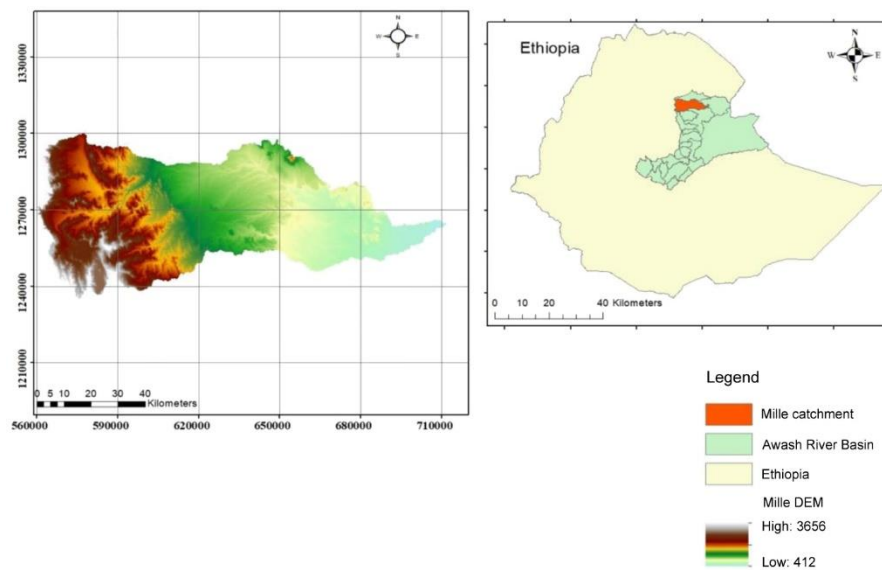


Fig. 1. Location of the Mille catchment in Ethiopia.

According to Berhanu et al. (2014), the catchment's climatic zone falls within five agroclimatic zones of Ethiopia, ranging from hot arid (<500 m) in the east to humid (>3,200 m) near the remotest of the upper catchment. The annual rainfall pattern is bimodal (Berhanu et al. 2016), with rain occurring between June and August (main rainy season) and between March and May (pre-rainy season). Based on long-term historic

climatic data (2000-2016), the estimated mean annual rainfall varies from approximately 465 mm on the easterly catchment to over 1,153 mm on the head of the drain catchment mountains, with a mean rainfall of 782 mm, and the estimated mean annual maximum and minimum temperatures vary between 29-43°C and 10-19°C, respectively.

2.1. Dataset

2.1.1. Rainfall and temperature data

The rainfall and temperature datasets used in this study were provided by the Ethiopia National Meteorological Agency (ENMA). These datasets encompass mean monthly and annual rainfall and mean minimum and maximum temperature, which have completed, reliable, and useful historical samples masked from the long-term daily (2000-2016) national-level historic climate grid-based pixel dataset, as shown in Figure 2. These daily pixel datasets were blended by the project Enhancing National Climate Services (ENACTS) at the national level, using combined satellite-based rainfall estimates and ground-based rainfall data for some African countries, such as Ethiopia; their consistency was checked using the double mass curve technique.

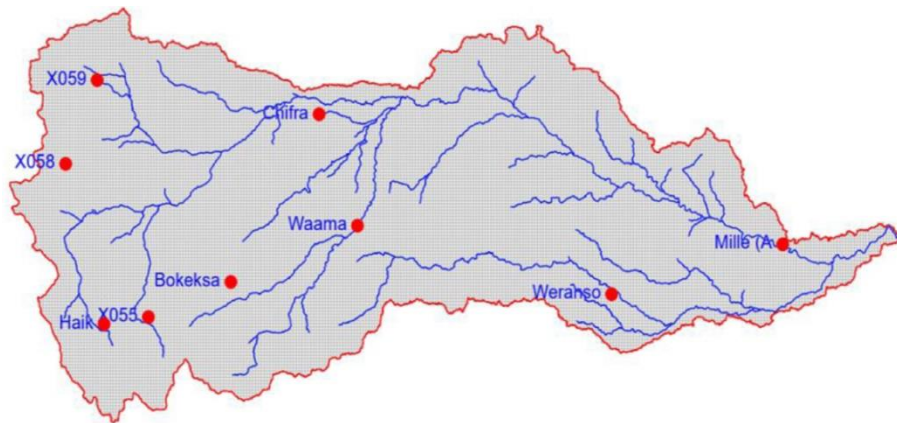


Fig. 2. Mille catchment in Ethiopia and locations of sampled climate stations.

2.1.2. Digital elevation model (DEM) data

The Shuttle Radar Topography Mission (SRTM 3 arc-Second Global) digital elevation model (DEM) data were downloaded from NASA (<https://urs.earthdata.nasa.gov>) and resampled in steps to generate 500-m and 1,000-m DEMs. Resampling was done using the Resampling Technique parameter, Bilinear in Data management tools in ArcGIS. The study site DEM was extracted from each DEM spatial resolution, and these DEM resolution data, such as SRTM 90 m, SRTM 500 m, and SRTM 1000 m DEM, were used as a covariate in the analysis to investigate whether the spatial resolution of DEM data would have any impact on the accuracy of areal climatic variable interpolation.

The spatial interpolation techniques were carried out by applying R programming used for the interpolation technique (Goovaerts 1997a) with the gstat package embedded within R (Pebesma, Wesseling 1998) to generate and evaluate the impacts of different resampled DEM spatial resolutions on climatological variable spatial prediction. The GIS tools (ArcGIS and QGIS) were used for processing DEM and preparing shapefiles.

2.2. Methods

Among the spatial interpolation techniques known as kriging (Matheron, Hasofer 1989), the geostatistical technique is considered the best unbiased linear predictor (BULP) for input data that satisfy the conditions of normality as the data are not skewed in any way (Isaaks, Srivastava 1994). However, climate data are often not symmetrical (skewness either to the right or to the left), which affects the spatial prediction of climate variables such as rainfall and temperature in that the few high values will overcome all the others. In experimental variogram prediction (Goovaerts 1997), nonsymmetric distributions are often transformed to conditions of normality using the natural logarithmic function and/or square root distance from the ocean/sea to minimize the skewness of input climate data and the influence of extreme values before variogram analysis and spatial interpolation (Goovaerts 1997). However, for small sampled data, such as our case, this can result in overprediction as well as empirical variograms that are difficult to model (Rossiter 2014). Therefore, the transformation was not applied because of the highly sparsely distributed climate data (see Fig. 2).

According to Goovaerts (1997), primary attributes of interest are usually accompanied by independent secondary information (auxiliary) that originates from continuous or random attributes, and the estimation generally improves when this information is taken into consideration, particularly in areas where the data are highly sparse or poorly correlated in space. Based on relevant literature reviews (e.g., Cantet 2017; Rata et al. 2020) and due to its high performance (in most cases) compared to other interpolation methods, kriging with external drift (KED) was selected to assess the effects of the catchment DEM spatial resolution on the spatial prediction of climatic variables. The methodological framework approaches used in this research article for the geostatistical interpolation technique were developed as follows (Fig. 3).

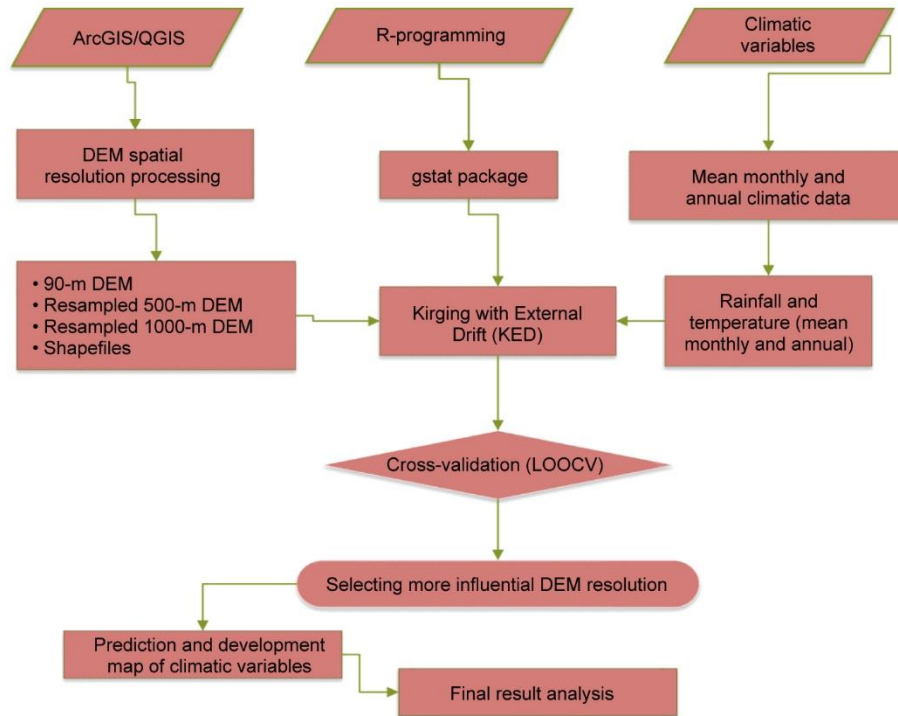


Fig. 3. Schematic flowchart showing the estimation of spatial climatic variables.

2.2.1. Experimental Variogram

Of the sampled data, $z(x_1), z(x_2) \dots z(x_n)$, where x_1, x_2, \dots, x_n represent the positions of the sampled in two-dimensional space, one can estimate both cloud and experimental variograms assuming those sampled data were unbiased.

The equation to compute the variogram is Matheron's method of moments (MoM) estimator (Oliver, Webster 2015):

$$\hat{\gamma}(h) = \frac{1}{2N(h)} \sum_i^{N(h)} \{z(x_i) - z(x_i + h)\}^2, \quad (1)$$

where $\hat{\gamma}(h)$ is the experimental variogram, which equals one-half the squared difference between points separated by a distance $x_i \pm (x_i + h)$ (assuming no direction preference), $z(x_i)$ and $z(x_i + h)$ are the observed values of sampled data z at places x_i and $x_i + h$, and $N(h) = \frac{N(N-1)}{2}$ is the number of paired values at lag h .

There are some methods to fit a variogram model to an experimental/empirical variogram, and this paper uses the exponential and spherical model (Eqs. 2 and 3) via a simple method called "automatic fitting variogram from the package automap.

$$\gamma(h) = \begin{cases} c_0 + c\{1 - \exp(-\frac{h}{a})\}, & \text{for } 0 < h \\ 0 & \text{for } h = 0 \end{cases} \quad (2)$$

where c_0 is a nugget, c is the sill of variance, h is the lag, and a is the practical range.

$$\gamma(h) = \begin{cases} c_0 + c \left[\frac{3h}{2a} - \frac{1}{2} \left(\frac{h}{a} \right)^3 \right] & \text{for } 0 < h \leq a \\ c_0 + c & \text{for } h > a \\ 0 & \text{for } h = 0 \end{cases} \quad (3)$$

2.2.2. Kriging with an external drift

Kriging with an external drift (KED)¹ is a widely applied geostatistics interpolation method that considers auxiliary variables as external or secondary variables in the estimation of a primary attribute (Goovaerts 1997). In KED, a linear weighted average from the N known points with the value Z_i is used to estimate the value at each unknown point Z_0 by using both the trend and local deviations (Rossiter 2019). The KED estimator is as follows:

$$\hat{Z}_{KED}(X_0) = \sum_{i=1}^n \lambda_i^{KED} Z(X_i) \quad (4)$$

Its expectation is as follows:

$$E[\hat{Z}_{KED}(X_0)] = \sum_{k=0}^K \sum_{i=1}^n \beta_k \lambda_i^{KED}(X_i) \quad (5)$$

The estimator is unbiased if:

$$\sum_{i=1}^n \lambda_i^{KED} Y_k(X_i) = Y_k(X_0) \quad (6)$$

2.3. Evaluation criteria for prediction performance

To evaluate the prediction accuracy, the measured data were compared with the estimated values in the same locations. The available data are usually split into two parts, namely the training and testing datasets. The training data were used to fit the model, whereas the testing dataset or validation dataset was used to validate prediction accuracy by estimating the prediction error. This procedure is called cross-validation, and they vary in type (Voltz, Webster 1990; Khorsandi et al. 2012). In this study, the author used the leave-one-out-cross-validation (LOOCV) type 1 because of the small observed dataset. In this method, the model was developed based on $N - 1$ observations and tested on the remaining observations. Next, this process was repeated for each observation in the dataset, and the average error for all trials was calculated.

¹ Confusingly, termed 'Universal Kriging' in gstat.

The predicted and measured datasets were compared by computing three statistical indices and graphically presenting the N sites belonging to the validation dataset.

Statistical indices:

The root mean square error ($RMSE$) measures the precision of the predictions and should be as small as possible.

$$RMSE = \sqrt{\frac{1}{n} \sum_{i=1}^n (\hat{Z}(X_i) - Z(X_i))^2} \quad (7)$$

The mean biased error (MBE) measures the bias of prediction and should be close to zero for unbiased methods.

$$MBE = \frac{1}{n} \sum_{i=1}^n [Z(X_i) - \hat{Z}(X_i)] \quad (8)$$

The coefficient of correlation (r) measures the strength of the relationship between the predicted and observed datasets. The value ranges between -1.0 and $+1.0$, and the equation is as follows:

$$r = \frac{\sum_{i=1}^n Z(X_i) \hat{Z}(X_i) - (\sum_{i=1}^n Z(X_i)) (\sum_{i=1}^n \hat{Z}(X_i))}{\sqrt{n(\sum_{i=1}^n (Z(X_i))^2) - (\sum_{i=1}^n Z(X_i))^2} \sqrt{n(\sum_{i=1}^n (\hat{Z}(X_i))^2) - (\sum_{i=1}^n \hat{Z}(X_i))^2}} \quad (9)$$

where $Z(x_i)$ is the measured value at x_i , and $\hat{Z}(x_i)$ is the predicted value.

3. Results

3.1. Effects of DEM spatial resolution on rainfall spatial prediction

The DEM elevations with various resolutions generated from the SRTM DEM covering the study area were between 490 and 2,088 m, 490.1 and 2,088.4 m, and 488.5 and 2,125.7 m above sea level (Table 1 and Fig. 4).

Table 1. Elevation values for the nine sampled climatic stations.

Stations name	DEM's Elevation (m.a.s.l.)		
	SRTM 90-m DEM	Resampled 500-m DEM	Resampled 1,000-m DEM
X055	2,088.0	2,088.4	2,125.7
X058	1,853.0	1,835.5	1,864.6
X059	1,574.0	1,566.0	1,559.0
Weranso	643.0	647.1	646.8
Waama	1,020.0	1,020.0	1,022.1
Mille (AVA)	490.0	490.1	488.5
Haik	2,003.0	1,996.9	2,012.8
Chifra	928.0	927.1	924.6
Bokeksa	1,768.0	1,733.3	1,747.2

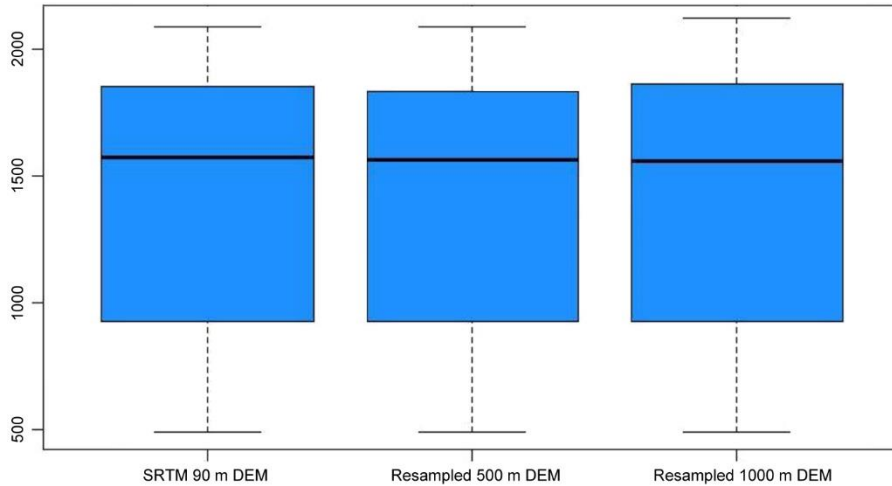


Fig. 4. Box plots of the descriptive statistical values of the elevations for nine sampled climatic stations.

Table 1 shows that the maximum elevation value increased from 2,088 to 2,125.7 with coarsening DEM resolutions, and the minimum elevation value decreased from 490 to 488.5 as the DEM coarsened from 90 to 1,000 m. This may be due to the loss of detailed topographic attributes at coarser resolution (Zhang et al. 2014; Reddy 2015).

The spatial pattern mapped for mean monthly and annual rainfall was detailed with less error at the 500-m DEM resolution and the 90-m resolution than at the 1,000-m DEM resolution (Fig. 5 and Table 2). Based on the performance of the predicted rainfall values depicted in Table 2, the monthly rainfall data at each point were removed, and the remaining point input data were used to estimate the missing data by using the LOOCV procedure. Taking the rainy season (June, July, and August) into consideration, the KED technique with 500-m DEM as a covariate produced relatively smaller (larger in r) values of RMSE and MBE than the KED techniques with 90-m and 1,000-m DEM as a covariate for the spatial prediction of catchment rainfall both at monthly and annual temporal scales, respectively.

On the other hand, the rainfall spatial distribution in two months, such as December and February, was less correlated with an auxiliary variable (elevation) and its resolution. Surprisingly, January's monthly spatial rainfall distribution was exceptional and was less negatively correlated with elevation itself and its resolution. The reasons were that supplements to local factors (e.g., topography), the spatial rainfall patterns were affected by different global and regional factors, such as the Inter-Tropical Convergence Zone (ITCZ), Tropical Easterlies, interseasonal variation, and latitudinal locations (Dawit 2010; Melesse et al. 2014). The results indicate that the KED with the 500-m DEM as a covariate was the most suitable for mean monthly and annual areal rainfall estimation compared to the other DEM resolutions.

In general, the point rainfall depths vary with spatial and temporal scales and tend to increase with increasing elevations because of the orographic effect, which results in a lifting of air vertically and forms clouds due to the adiabatic cooling effect.

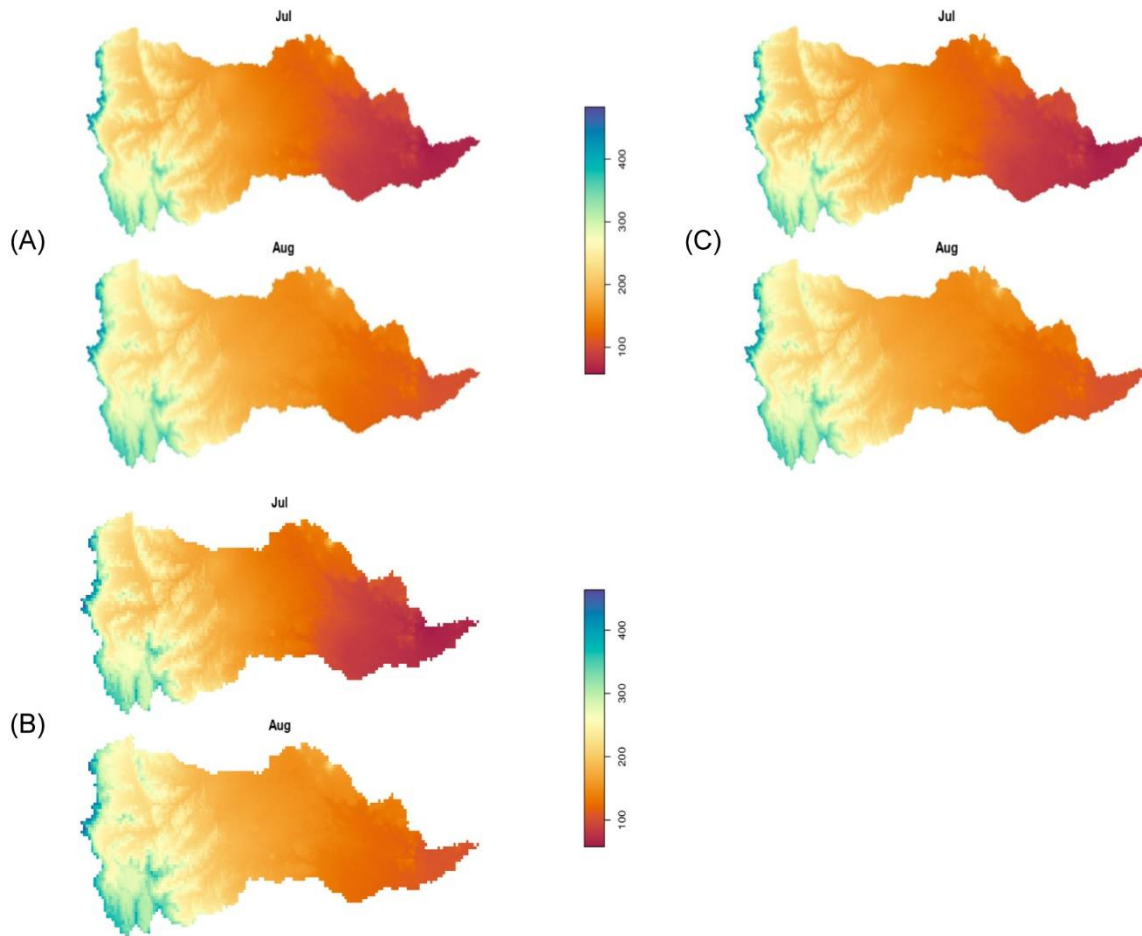


Fig. 5. July and August mean monthly rainfall map for 17 years at (A) 500-m DEM resolution, (B) 1,000-m DEM resolution, and (C) 90-m DEM resolution using KED.

Table 2. Statistical evaluation of the impact of DEM resolution on spatial rainfall prediction.

Month	R_o	90-m DEM and evaluation criteria				500-m DEM and evaluation criteria				1,000-m DEM and evaluation criteria			
		R_e	$RMSE$	MBE	r	R_e	$RMSE$	MBE	r	R_e	$RMSE$	MBE	r
Jan	11.42	11.79	5.72	-0.36	-0.015	11.82	5.77	-0.39	-0.047	11.83	5.81	-0.4	-0.067
Feb	6.799	6.752	3.17	0.05	0.570	6.748	3.14	0.05	0.578	6.758	3.16	0.04	0.572
Mar	37.92	38.33	9.05	-0.41	0.856	38.32	9.00	-0.41	0.858	38.36	9.27	-0.45	0.848
Apr	57.64	58.13	9.91	-0.49	0.863	58.15	10.00	-0.51	0.860	58.19	10.33	-0.55	0.850
May	43.40	43.95	9.26	-0.56	0.838	43.96	9.32	-0.57	0.835	44.01	9.63	-0.61	0.824
Jun	16.49	16.617	4.35	-0.13	0.878	16.616	4.32	-0.13	0.880	16.638	4.44	-0.15	0.873
Jul	192.76	194.87	35.96	-2.11	0.891	194.86	35.64	-2.10	0.893	194.92	36.08	-2.16	0.890
Aug	216.06	218.1	34.81	-2.05	0.878	218.1	34.24	-2.03	0.882	218.2	35.09	-2.13	0.875
Sep	64.03	64.69	13.45	-0.67	0.871	64.73	13.68	-0.70	0.866	64.79	14.12	-0.76	0.857
Oct	24.16	24.64	7.39	-0.48	0.746	24.66	7.46	-0.50	0.741	24.68	7.60	-0.52	0.730
Nov	16.08	16.25	2.76	-0.17	0.849	16.25	2.75	-0.17	0.851	16.26	2.81	-0.17	0.844
Dec	12.00	12.232	4.71	-0.24	0.500	12.243	4.74	-0.25	0.490	12.253	4.80	-0.26	0.475
Annual	698.8	706.4	123.96	-7.64	0.884	706.8	122.65	-7.52	0.894	706.8	127.35	-8.08	0.877

NB: R_o = observed mean rainfall (mm), R_e = estimated mean rainfall (mm).

3.2. Effects of DEM resolution on the spatial pattern of temperature

The spatial map of maximum temperature produced by KED using various DEM resolutions as a covariate showed more gradual and smoothing changes, with a regular distribution in the middle to the lower parts of the catchment. At the uppermost and escarpment parts of the catchment, the spatial map appeared irregularly distributed and with discontinuous borders, showing an abrupt change in spatial distribution (Fig. 6A-C).

Tables 3 and 4 show that the spatially predicted mean maximum and minimum temperature values were similar to the analyzed predicted rainfall in that they were significantly influenced by the DEM but less influenced by the DEM's horizontal resolution. Based on the statistical evaluation of three DEM resolutions in terms of RMSE, MBE, and r of the KED technique, the 90-m DEM resolution depicted the lowest error (highest r value) relative to the remaining DEM resolutions on maximum and minimum temperatures. As depicted in Figure 6A-C, the spatial pattern of maximum temperature gradually increases from west to the east following the elevation, which decreases progressively from west to east. Thus, based on the visual inspection of expert knowledge and statistical evaluations, it can be concluded that the spatial distributions of the mean minimum and maximum temperatures were presented in better detail at a 90-m DEM resolution than at the other DEM resolutions.

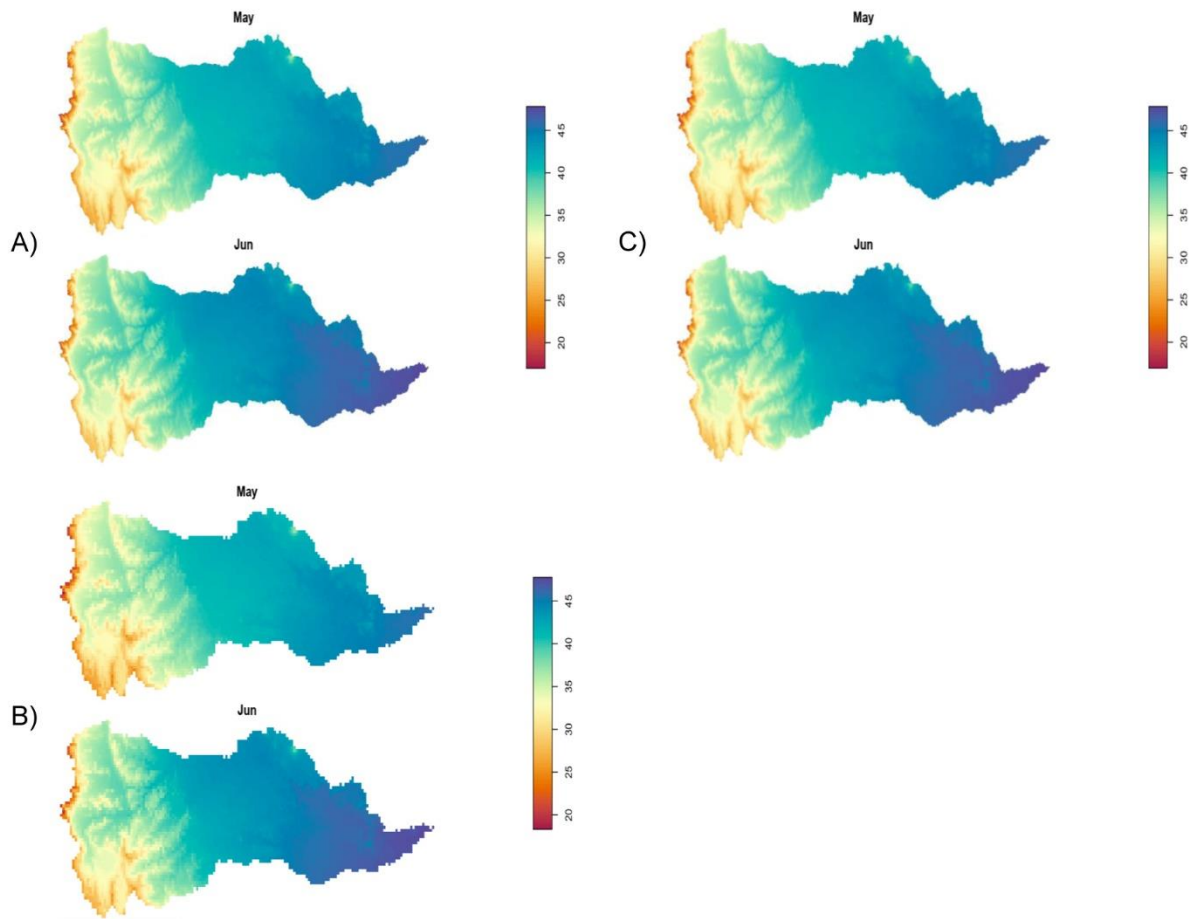


Fig. 6. May and June mean monthly maximum temperature map for 17 years at (A) SRTM 90-m DEM resolution, (B) SRTM 1,000-m DEM resolution, and (C) SRTM 500-m DEM resolution using KED.

Table 3. Mean monthly and annual maximum values observed and estimated temperature (°C) and covariates.

Month	$(T_{max})_o$	SRTM 90-m DEM and evaluation criteria				SRTM 500-m DEM and evaluation criteria				SRTM 1,000-m DEM and evaluation criteria			
		$(T_{max})_e$	<i>RMSE</i>	<i>MBE</i>	<i>r</i>	$(T_{max})_e$	<i>RMSE</i>	<i>MBE</i>	<i>r</i>	$(T_{max})_e$	<i>RMSE</i>	<i>MBE</i>	<i>r</i>
Jan	31.62	31.71	1.73	-0.09	0.897	31.70	1.77	-0.08	0.892	31.70	1.76	-0.07	0.893
Feb	33.47	31.71	0.68	0.02	0.984	33.45	0.73	0.02	0.981	33.45	0.76	0.03	0.980
Mar	36.06	36.11	1.69	-0.05	0.938	36.10	1.74	-0.04	0.935	36.10	1.71	-0.03	0.936
Apr	36.69	36.77	1.45	-0.08	0.966	36.76	1.52	-0.07	0.963	36.75	1.50	-0.07	0.964
May	37.36	37.38	0.90	-0.02	0.985	37.38	0.97	-0.02	0.983	37.37	0.98	-0.01	0.982
Jun	39.01	39.08	1.89	-0.07	0.941	39.07	1.97	-0.05	0.935	39.05	1.97	-0.04	0.935
Jul	38.86	38.99	2.20	-0.14	0.933	38.99	2.27	-0.13	0.929	38.98	2.27	-0.12	0.929
Aug	35.77	35.85	1.43	-0.08	0.974	35.84	1.49	-0.07	0.972	35.84	1.47	-0.06	0.973
Sep	34.38	34.32	1.64	0.06	0.960	34.31	1.68	0.06	0.958	34.31	1.70	0.07	0.957
Oct	34.33	34.36	1.16	-0.03	0.979	34.36	1.23	-0.03	0.976	34.35	1.24	-0.02	0.975
Nov	33.04	33.18	2.14	-0.14	0.916	33.17	2.20	-0.13	0.912	33.16	2.16	-0.12	0.914
Dec	30.42	30.43	0.62	-0.02	0.987	30.43	0.67	-0.02	0.985	30.43	0.68	-0.01	0.985
Annual	35.08	35.13	1.17	-0.05	0.974	35.13	1.23	-0.05	0.971	35.12	1.22	-0.04	0.971

NB: - $(T_{max})_o$ - observed mean maximum temperature, $(T_{max})_e$ - estimated mean maximum temperature.

Table 4. Mean monthly and annual minimum values observed and estimated temperature (°C) and covariates.

Month	$(T_{min})_o$	SRTM 90-m DEM and evaluation criteria				SRTM 500-m DEM and evaluation criteria				SRTM 1,000-m DEM and evaluation criteria			
		$(T_{min})_e$	<i>RMSE</i>	<i>MBE</i>	<i>r</i>	$(T_{min})_e$	<i>RMSE</i>	<i>MBE</i>	<i>r</i>	$(T_{min})_e$	<i>RMSE</i>	<i>MBE</i>	<i>r</i>
Jan	11.63	11.569	0.88	0.06	0.945	11.569	0.86	0.06	0.947	11.567	0.88	0.06	0.945
Feb	12.46	12.381	1.10	0.08	0.941	12.381	1.09	0.08	0.942	12.379	1.12	0.08	0.939
Mar	14.00	13.930	0.98	0.06	0.951	13.910	1.00	0.07	0.948	13.890	1.02	0.07	0.946
Apr	15.64	15.580	0.89	0.06	0.965	15.580	0.92	0.06	0.962	15.570	0.94	0.06	0.960
May	16.71	16.630	0.97	0.06	0.968	16.640	0.97	0.07	0.968	16.620	1.01	0.07	0.966
Jun	17.68	17.600	1.17	0.08	0.966	17.600	1.18	0.08	0.965	17.610	1.22	0.08	0.963
Jul	17.47	17.410	0.95	0.06	0.969	17.410	1.00	0.07	0.966	17.400	1.02	0.07	0.965
Aug	16.41	16.340	1.09	0.07	0.950	16.330	1.12	0.07	0.947	16.330	1.14	0.08	0.945
Sep	16.00	15.920	1.23	0.08	0.950	15.920	1.24	0.08	0.948	15.910	1.28	0.08	0.946
Oct	13.24	13.165	1.07	0.08	0.958	13.166	1.06	0.07	0.960	13.163	1.09	0.08	0.957
Nov	11.49	11.404	1.40	0.09	0.909	11.404	1.37	0.09	0.913	11.402	1.38	0.09	0.911
Dec	10.71	10.641	1.04	0.07	0.936	10.641	1.01	0.07	0.939	10.640	1.02	0.07	0.937
Annual	14.46	14.389	1.03	0.07	0.956	14.390	1.02	0.07	0.957	14.388	1.04	0.07	0.955

NB: – $(T_{min})_o$ – observed mean minimum temperature, $(T_{min})_e$ – estimated mean minimum temperature.

4. Discussion

As illustrated in Figures 7A and B, the relationships between the mean annual rainfall and the mean maximum annual temperature of each sampled climatic station between 2000 and 2016 and its elevation were plotted. The mean annual rainfall and mean maximum annual temperatures tended to increase/decrease with increasing observed elevations, with coefficients of determination of 0.86 and 0.97, respectively. However, the spatial resolution among the three DEMs had no significant effect on the spatial prediction of climatic variables (see Tables 2 and 3). The analysis indicates that the most important characteristics, such as the mean annual and mean monthly climatological variables, rainfall and temperature, were significantly correlated with DEM elevation but less correlated with DEM resolution.

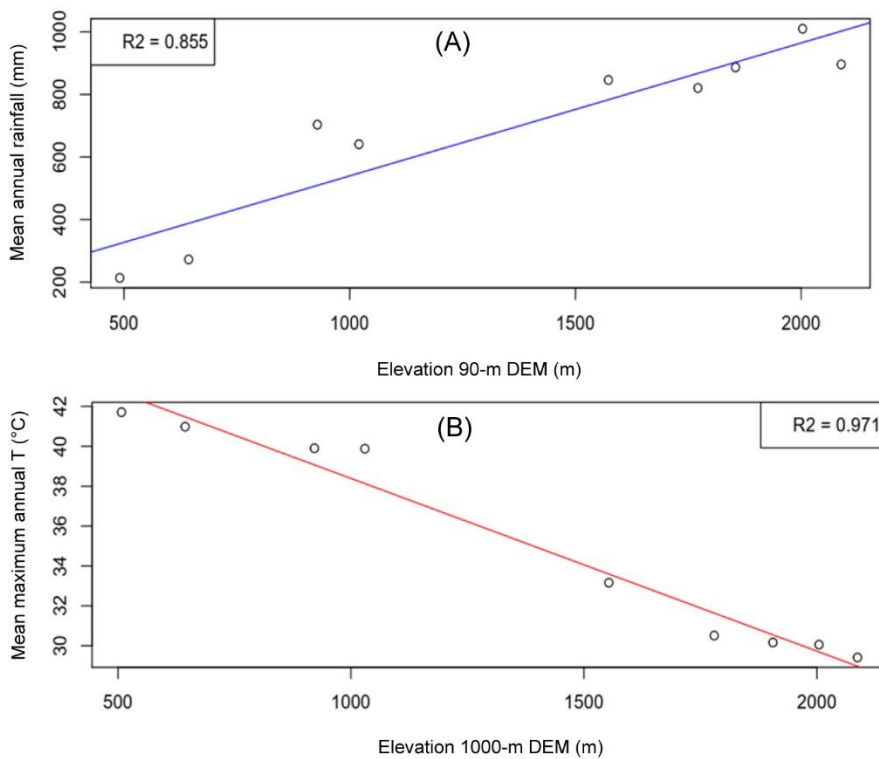


Fig. 7. Correlation diagram of annual mean predicted rainfall (A) and mean maximum predicted temperature (B) with elevation.

The predicted minimum and maximum temperatures were interpolated and extrapolated by KED to unsampled regions with a well-performing horizontal resolution DEM as a covariate (Figs. 8A, B). As seen in the developed maps, the highest amounts of spatial temperature were distributed in the catchment at the lowest elevations, which confirms that the spatial distribution of mean temperature is linearly correlated with the selected DEM (see Tables 3 and 4).

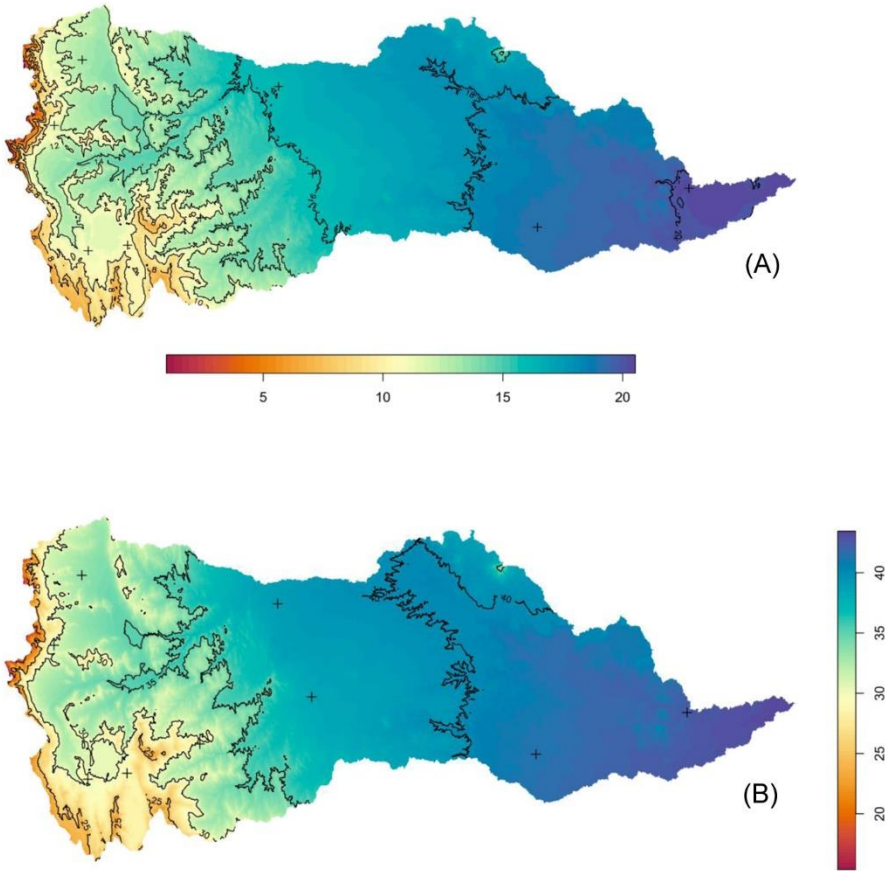


Fig. 8. Spatial map of the mean minimum and maximum annual temperatures with 90-m elevation as external drift, using the sampled stations.

The primary novelty of the study resides in the evaluation and selection of DEM with the spatial resolution which shows relatively good performance in the prediction of the spatial distribution of climatological variables based on cross-validation techniques and, to some extent, expert knowledge. According to the proposed techniques, selecting covariates slightly improves the predictive performance of KED. For instance, the mean annual rainfall predicted using elevation with spatial resolutions of 500 and 90 m showed a slightly good performance ($RMSE = 122.65$, $MBE = -7.52$, $r = 0.89$, and $RMSE = 123.96$, $MBE = -7.64$, $r = 0.88$) r compared to the 1,000-m resolution DEM ($RMSE = 127.35$, $MBE = -8.08$, $r = 0.877$).

The proposed procedure achieved good performance regarding the prediction of mean minimum and maximum annual and monthly temperature with elevation but showed lower performance on the prediction of both mean monthly and annual temperature with various DEM resolutions. Similar to a previous study (Taesombat, Sriwongsitanon 2009), the optimum coarser DEM (500-m SRTM-DEM) resolution seemed to outperform both the mean monthly and annual rainfall estimations compared to the finer DEM (90-m SRTM-DEM) and coarser (1,000-m SRTM-DEM) resolutions, whereas the fine resolution (90-m SRTM-DEM) showed relatively less error in the mean monthly minimum and maximum temperature estimations

than the remaining two DEM resolutions. This approach seems to be a great opportunity to perform and select the more advanced horizontal resolution of DEM, which is used as a predictor for geostatistical interpolation techniques in mountainous catchments with overly sparse and unrepresentative observational climatic data.

5. Conclusions

This study compared and examined the impacts of three DEM resolutions (SRTM 90-m DEM, SRTM 500-m DEM, and SRTM 1,000-m DEM) on the spatial prediction of rainfall and temperature in a topographic complex catchment by using the KED interpolation technique. Three different DEM resolutions were tested on a 5599-km² catchment. The minimum and maximum elevations in the catchment varied substantially due to DEM resolutions (see Table 1), and the results indicated that changes in DEM resolution somehow influenced the outcomes of the prediction performance for both rainfall and temperature. In general, there were two different effects of DEM resolution. The first was the overestimation of mean monthly and annual rainfall and maximum temperature, and the second was the underestimation of mean monthly and annual minimum temperature. The LOOCV procedure infers that for mean monthly and annual rainfall, the coarser DEM resolution (500-m SRTM-DEM) performed better in spatial prediction with less error, whereas for mean maximum and minimum temperature spatial estimation, the finer DEM resolution (SRTM 90-m DEM) performed slightly better than the remaining DEM spatial resolution. This type of interpolation technique plays a fundamental role in various applications by assessing the effects of climate on hydrology, the environment, agricultural activities, and water resource development. Overall, the findings in this paper confirm that, as the DEM resolutions vary, the impact on the spatial prediction of the climatic variable is less significant. However, a substantial difference in resolution brings a small elevation change (vertical height), and this may affect hydrologically important topographic attributes calculated from DEM, such as slope, aspects, and drainage networks, specifically in mountainous catchments (Wilson et al. 1998). There are important implications for those interested in using spatially distributed topographic attributes for further applications (Moore et al. 1991; Brown et al. 1993; Lin et al. 2010). Therefore, it is recommended to consider further application uses, specifically in mountainous catchments.

Acknowledgments

I would like to thank the Ethiopia National Meteorology Agency for providing climatological data and the Africa Center of Excellence for Water Management, University of Addis Ababa, Ethiopia, for financial support. The author is grateful to his supervisors, Prof. Tenalem Ayenew and Dr. Tena Alemirew, for valuable comments on the initial version of the paper. Additionally, the author sincerely thanks the Editor in Chief and the two anonymous reviewers for their constructive comments and suggestions on the 1st version of the paper.

Conflicts of Interest

The author declares no conflict of interest.

References

- Adhikary S.K., Muttil N., Yilmaz A.G., 2017, Cokriging for enhanced spatial interpolation of rainfall in two Australian catchments, *Hydrological Processes*, 31 (12), 2143-2161, DOI: 10.1002/hyp.11163.
- Aydin O., 2018, Evaluation of kriging with external drift method in spatial modelling of precipitation: a case of Aegean Region, Turkey, *Dumlupınar Üniversitesi Sosyal Bilimler Dergisi*, 56, 1-18.
- Berhanu B., Seleshi Y., Melesse A.M., 2014, Surface water and groundwater resources of Ethiopia: potentials and challenges of water resources development, [in:] Nile River Basin, A.M. Melesse, W. Abtew, S.G. Setegn (eds.), Springer International Publishing, Switzerland, 99-117, DOI: 10.1007/978-3-319-02720-3.
- Berhanu B., Seleshi Y., Demisse S.S., Melesse A.M., 2016, Bias correction and characterization of climate forecast system re-analysis daily precipitation in Ethiopia using fuzzy overlay, 23 (2), 230-243, DOI: 10.1002/met.1549.
- Bertini C., Buonora L., Ridolfi E., Russo F., Napolitano F., 2020, On the use of satellite rainfall data to design a dam in an ungauged site, *Water*, 12 (11), DOI: 10.3390/w12113028.
- Brown D.G., Bian L., Walsh S.J., 1993, Response of a distributed watershed erosion model to variations in input data aggregation levels, *Computers and Geosciences*, 19 (4), 499-509, DOI: 10.1016/0098-3004(93)90078-J.
- Cantet P., 2017, Mapping the mean monthly precipitation of a small island using kriging with external drifts, *Theoretical and Applied Climatology*, 127, 31-44, DOI: 10.1007/s00704-015-1610-z.
- Chen H.E., Chiu Y.Y., Tsai T.L., Yang J.C., 2020, Effect of rainfall, runoff and infiltration processes on the stability of footslopes, *Water*, 12 (5), DOI: 10.3390/w12051229.
- Chiew F.H.S., McMahon T.A., 2002, Modelling the impacts of climate change on Australian streamflow, *Hydrological Processes*, 16 (6), 1235-1245, DOI: 10.1002/hyp.1059.
- Dawit A., 2010, Future climate of Ethiopia from PRECIS Regional Climate Model Experimental Design, available online https://www.metoffice.gov.uk/binaries/content/assets/metofficegovuk/pdf/research/applied-science/precis/precis_experimental_design_dawit.pdf (data access 15.04.2022).
- Dinku T., 2019, Challenges with availability and quality of climate data in Africa, [in:] Extreme Hydrology and Climate Variability: Monitoring, Modelling, Adaptation and Mitigation, A.M. Melesse, W. Abtew, G. Senay (eds.), Elsevier, 71-80, DOI: 10.1016/B978-0-12-815998-9.00007-5.
- Gebremedhin M.A., Lubczynski M.W., Maathuis B.H.P., Teka D., 2021, Novel approach to integrate daily satellite rainfall with in-situ rainfall, Upper Tekeze Basin, Ethiopia, *Atmospheric Research*, 248, 105135, DOI: 10.1016/j.atmosres.2020.105135.
- Goovaerts P., 1997, *Geostatistics for Natural Resources Evaluation*, Oxford University Press, 496 pp.
- Hudson G., Wackernagel H., 1994, Mapping temperature using kriging with external drift: Theory and an example from Scotland, *International Journal of Climatology*, 14 (1), 77-91. DOI: 10.1002/joc.3370140107.
- Khorsandi N., Mahdian M.H., Pazira E., Nikkani D., Chamheidar H., 2012, Comparison of different interpolation methods for investigating spatial variability of rainfall erosivity index, *Polish Journal of Environmental Studies*, 21 (6), 1659-1666.
- Kim C., Kim D.H., 2020, Effects of rainfall spatial distribution on the relationship between rainfall spatiotemporal resolution and runoff prediction accuracy, *Water*, 12 (3), DOI: 10.3390/w12030846.
- Kim S.-N., Lee W.-K., Shin K.-I., Kafatos M., Seo D.J., Kwak H.-B., 2010, Comparison of spatial interpolation techniques for predicting climate factors in Korea, *Forest Science and Technology*, 6 (2), 97-109, DOI: 10.1080/21580103.2010.9671977.

- Lin S., Jing C., Chaplot V., Yu X., Zhang Z., Moore N., Wu J., 2010, Effect of DEM resolution on SWAT outputs of runoff, sediment and nutrients, *Hydrology and Earth System Sciences Discussions*, 7 (4), 4411-4435, DOI: 10.5194/hessd-7-4411-2010.
- Lu S., ten Veldhuis M.C., van Giesen N., 2020, A methodology for multiobjective evaluation of precipitation products for extreme weather (in a data-scarce environment), *Journal of Hydrometeorology*, 21 (6), 1223-1244, DOI: 10.1175/JHM-D-19-0157.1.
- Matheron G., Hasofer A.M., 1990, Estimating and choosing: an essay on probability in practice, *Journal of the American Statistical Association*, 85 (412), 1167-1168, DOI: 10.2307/2289620.
- Meena S.R., Nachappa T.G., 2019, Impact of spatial resolution of digital elevation model on landslide susceptibility mapping: A case study in Kullu Valley, Himalayas, *Geosciences*, 9 (8), DOI: 10.3390/geosciences9080360.
- Melesse A.M., Abteu W., Setegn S.G. (eds.), 2014, Nile River Basin, Springer International Publishing, Switzerland, 718 pp., DOI: 10.1007/978-3-319-02720-3.
- Moore I.D., Gessler P.E., Nielsen G.A., Peterson G.A., 1991, Soil attribute prediction using terrain analysis, *Soil Science Society of America Journal*, 57 (2), 443-453, DOI: 10.2136/sssaj1993.03615995005700020026x.
- Novikov S.L., 1981, Elevation: A major influence on the hydrology of New Hampshire and Vermont, USA, *Hydrological Sciences Bulletin*, 26 (4), 399-413, DOI: 10.1080/02626668109490904.
- Pebesma E.J., Wesseling C.G., 1998, Gstat: a program for geostatistical modelling, prediction and simulation, *Computers and Geosciences*, 24 (1), 17-31, DOI: 10.1016/S0098-3004(97)00082-4.
- Rata M., Douaoui A., Larid M., Douaik A., 2020, Comparison of geostatistical interpolation methods to map annual rainfall in the Chélif watershed, Algeria, *Theoretical and Applied Climatology*, 141 (3-4), 1009-1024, DOI: 10.1007/s00704-020-03218-z.
- Reddy A.S., Reddy M.J., 2015, Evaluating the influence of spatial resolutions of DEM on watershed runoff and sediment yield using SWAT, *Journal of Earth System Science*, 7, 1517-1529, DOI: 10.1007/s12040-015-0617-2.
- MoWR, 2009, Mille and Dirma integrated sub-watershed management study project, Federal Democratic Republic Of Ethiopia Ministry Of Water Resources.
- Rossiter D.G., 2014, Applied Geostatistics, Exercise 5b: Predicting from point samples (Part 4) Lognormal Kriging. Part 4.
- Rossiter D.G., 2019, Applied Geostatistics Tutorial : Regional mapping of climate variables from point samples, Cornell University, Section of Soil & Crop Sciences, ISRIC-World Soil Information.
- Schoorl J.M., Sonneveld M.P.W., Veldkamp A., 2000, Three-dimensional landscape process modelling: the effect of DEM resolution, *Earth Surface Processes and Landforms*, 25 (9), 1025-1034, DOI: 10.1002/1096-9837(200008)25:9<1025::AID-ESP116>3.0.CO;2-Z.
- Simanek D.E., Holden J., 2020, Environmental sciences, [in:] Science Askew, D.E. Simanek, J. Holden (eds.), CRC Press, 76-88, DOI: 10.1201/9781420033564-12.
- Isaaks E.H., Srivastava R.M., 1994, An introduction to Applied Geostatistics, *Geographical Analysis*, 26 (3), 282-283, DOI: 10.1111/j.1538-4632.1994.tb00325.x.
- Taesombat W., Sriwongsitanon N., 2009, Areal rainfall estimation using spatial interpolation techniques, *Science Asia*, 35 (3), 268-275, DOI: 10.2306/scienceasia1513-1874.2009.35.268.
- Vaze J., Teng J., Spencer G., 2010, Impact of DEM accuracy and resolution on topographic indices, *Environmental Modelling and Software*, 25 (10), 1086-1098, DOI: 10.1016/j.envsoft.2010.03.014.
- Verdin A., Rajagopalan B., Kleiber W., Funk C., 2015, A Bayesian kriging approach for blending satellite and ground precipitation observations, *Water Resources Research*, 51 (2), 908-921, DOI: 10.1002/2014WR015963.
- Voltz M., Webster R., 1990, A comparison of kriging, cubic splines and classification for predicting soil properties from sample information, *Journal of Soil Science*, 41 (3), 473-490, DOI: 10.1111/j.1365-2389.1990.tb00080.x.

- Washington R., Harrison M., Conway D., Black E., Challinor A., Grimes D., Jones R., Morse A., Kay G., Todd M., 2006, African climate change: Taking the shorter route, *Bulletin of the American Meteorological Society*, 87 (10), 1355-1366, DOI: 10.1175/BAMS-87-10-1355.
- Oliver M.W., Webster R., 2015, *Basic Steps in Geostatistics: The Variogram and Kriging*, Springer, Cham, 100 pp.
- Wechsler S.P., 2007, Uncertainties associated with digital elevation models for hydrologic applications: A review, *Hydrology and Earth System Sciences*, 11 (4), 1481-1500, DOI: 10.5194/hess-11-1481-2007.
- Wilson J.P., Spangrud D.J., Nielsen G.A., Jacobsen J.S., Tyler D.A., 1998, Global positioning system sampling intensity and pattern effects on computed topographic attributes, *Soil Science Society of America Journal*, 62 (5), 1410-1417, DOI: 10.2136/sssaj1998.03615995006200050038x.
- Zhang P., Liu R., Bao Y., Wang J., Yu W., Shen Z., 2014, ScienceDirect Uncertainty of SWAT model at different DEM resolutions in a large mountainous watershed, *Water Research*, 53, 132-144, DOI: 10.1016/j.watres.2014.01.018.
- Zhang W., Montgomery D.R., 1994, Digital elevation model grid size, landscape representation, and hydrologic simulation, *Water Resources Research*, 30 (4), 1019-1028, DOI: 10.1029/93WR03553.

Evaluation of Water Storage Changes in Southeastern Anatolia, Turkey, using GRACE and GLDAS

Emel Zeray Öztürk

Konya Technical University, Department of Geomatics Engineering, Konya, Turkey

Abstract

With climatic changes, access to freshwater resources becomes more limited. Correspondingly, water monitoring methods in sensitive or critical areas in terms of groundwater amount are becoming increasingly important. The monitoring of the water levels in these regions, using appropriate methods and data sets, is highly effective in preventing possible future water crises. This paper aims estimated water storage changes with available tools and data in southeastern Anatolia, Turkey, where hydro-climatological studies are scarce due to limited observations. Data obtained from the Gravity Recovery and Climate Experiment satellite mission and the Global Land Data Assimilation System were used for the analysis of water storage changes in the study area. The results demonstrate that water storage shows a downward trend in all subareas, particularly in high-elevation regions. In addition, climatic changes have both short- and long-term impacts on water storage. Climatic variables (increasing temperature and decreasing precipitation) showed the highest correlation with water storage at 2-month lags. The monitoring of water storage is crucial for the region, and our results confirm the major role of such monitoring in decision-making processes and water resource management.

Keywords

GRACE, GLDAS, Groundwater management, Climate change, Turkey, Water storage changes.

Submitted 31 January 2022, revised 8 April 2022, accepted 5 May 2022

DOI: 10.26491/mhwm/149849

1. Introduction

Water is an indispensable element in human life. Freshwater is of great importance in terms of agricultural productivity, human health, and the economic activities of a growing population. Nevertheless, many regions in the world face water shortages triggered by climate change and anthropogenic factors.

Freshwater accounts for less than 3% of the total amount of water on Earth and is mainly stored in polar glaciers or underground (Chao et al. 2018). For the sustainable management of water, it is essential to assess variations in groundwater storage (Famiglietti et al. 2011; Jiao et al. 2015; Yin et al. 2020).

In many regions of the world, especially in developing countries, valuable water resources tend to decrease due to reasons such as overconsumption of groundwater or inadequate water management (Salem et al. 2017; Moghim 2020). This is also an issue in the Middle East, which is facing severe water scarcity (Voss et al. 2013; Madani 2014; Al-Zyoud et al. 2015; Forootan et al. 2016). Consequently, one of the vital problems for countries of the Middle East is how they can most efficiently use their water resources (FAO 2021). Southeastern Anatolia, through which the rivers Euphrates and Tigris flow, has a strategic importance for the Middle East region, and these rivers have always been a crucial water resource for Middle East countries. In this context, the GAP (Southeastern Anatolia Project) has been running since the beginning of the 1990s, with the aim to optimize the exploitation of the water resources of the region

for hydropower and irrigation (Yılmaz et al. 2019). Water storage changes in Southeastern Anatolia will affect not only the region but also the surrounding countries.

Quantitative models and estimations regarding the temporal-spatial variations of water storage are required for an effective sustainable water resources management in this region (Joodaki et al. 2014). In this context, the Gravity Recovery and Climate Experiment (GRACE) mission can provide valuable gravity data for monitoring global/regional water resource changes (Tapley et al. 2004a; Wouters et al. 2014; Godah et al. 2018; Öztürk et al. 2018, 2020; Öztürk 2020). Trustworthy large-scale values can be obtained from GRACE, and many extensive studies about groundwater changes, using GRACE data, have been carried out in several parts of the world (Rodell et al. 2009; Tiwari et al. 2009; Voss et al. 2013; Nie et al. 2018; Hussain et al. 2021; Massoud et al. 2021; Akhtar et al. 2022; Ali et al. 2022; Wang et al. 2022; Zhang et al. 2022). Tiwari et al. (2011) stated that hydrological variations have strong effects on GRACE measurements. Also, Scanlon et al. (2012) indicated that GRACE has the unique ability to provide gravity data for the assessment of groundwater changes; the authors demonstrated the 2006-2010 drought in the California Central Valley, USA, which showed a decreasing trend in groundwater storage.

The Global Land Data Assimilation System (GLDAS) has also been widely employed for the estimation of groundwater changes (Feng et al. 2013; Huang et al. 2015; Long et al. 2016; Sahoo et al. 2021; Zhang et al. 2021; Dubey et al. 2022; Öztürk 2022; Zheng et al. 2022); it provides the hydrological status of the Earth at a 0.25° resolution (Rodell et al. 2004). In 2008, Syed et al. (2008) combined GRACE and GLDAS data to evaluate terrestrial water storage (*TWS*) and stated that they are consistent with each other. All these studies have shown that the *TWS* dataset obtained from GRACE and GLDAS can be useful for the evaluation and analysis of variations in water resources.

This study was carried out in the southeastern region of Turkey, where hydrology models and satellite gravimetry data from GRACE had not been used before for the analysis of water resource changes. The aim was to investigate the temporal and spatial features of water storage changes as well as the effects of climate change in the region. Additionally, the performances of *TWS*, estimated from the GLDAS, and liquid water equivalent (*LWE*) measurements, estimated from GRACE, were evaluated. Since insufficient observations limit hydro-climatological studies in the region, the results of this study are important in terms of the future of the resources and the influence of climatic changes.

2. Materials and methods

2.1. Study area

The study was performed in the southeastern region of Turkey, over latitude 36.5°N–38.5°N and longitude 36.3°E–44.5°E. The region comprises fertile plains and rugged mountains, of which the Cilo Mountain is the highest part of the study area, with a peak elevation of 4,135 m above sea level. The climate is diverse; the western parts receive more precipitation and have milder temperatures compared to the eastern parts. The eastern region is covered with a layer of snow in winter; the number of days with

snow cover exceeds 80 in the provinces of Van and Hakkari in Subarea 6 (Günel 2013). The research area was divided into nine equal sub-areas, considering the centers of the mass concentrations (mascons) provided by the Goddard Space Flight Center (GSFC), as shown in Figure 1.

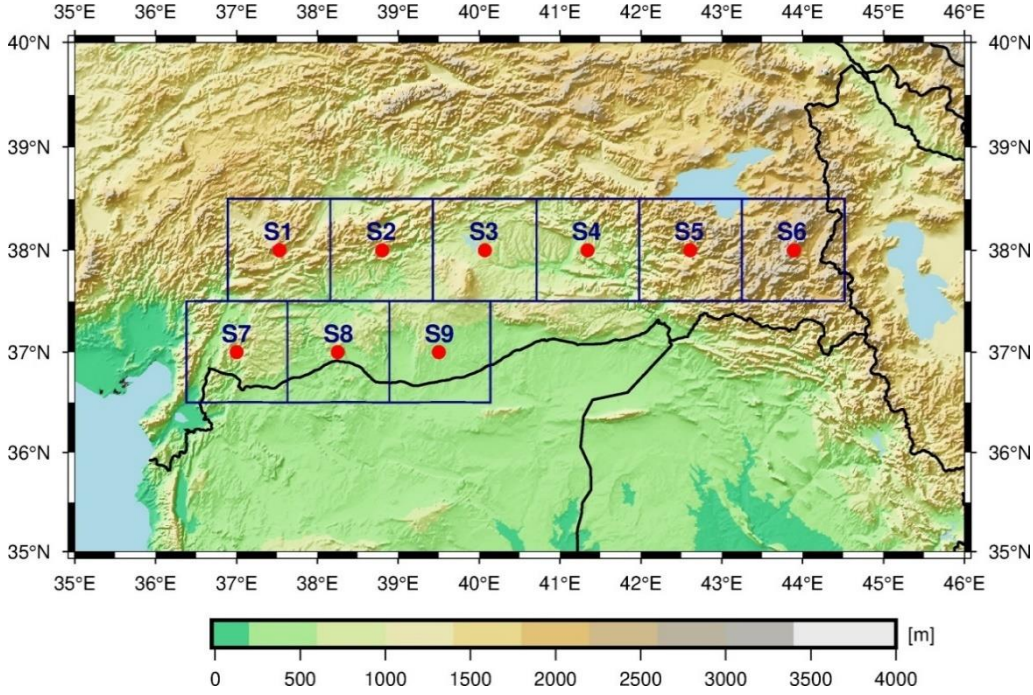


Fig. 1. Map showing the study area with the nine subareas (S1, S2, ..., S9).

2.2. Data and methodology

The terrestrial water budget consists of four major components, shown in Equation 1 (Zhang et al. 2018; Moghim 2020):

$$P - R - G - ET = \Delta TWS, \quad (1)$$

Where P , G , R , ET , and ΔTWS symbolize precipitation, groundwater, runoff, evapotranspiration, and total water storage changes, respectively. We used satellite data and a hydrological model to analyze water storage changes in southeastern Anatolia. To define the relationship between LWE and climate change more clearly, time-lagged cross-correlations between LWE and climatic variables were estimated as follows:

$$\rho_l = \frac{cov(LWE_{t+l}, V_t)}{\sigma_{LWE} \sigma_V}, \quad (2)$$

where V shows the climatic variables (precipitation and temperature) and l is the time lag, varying from 0 to 3 months.

2.2.1. GRACE Mascon products

The GRACE satellite mission is a joint project of NASA (National Aeronautics and Space Administration) and DLR (German Aerospace Center) (Tapley et al. 2004b). The GRACE satellite mission, launched in 2002, measures the time-variable gravity field. These measured variations are exploited for the estimation of mass changes, thus water storage changes; the monthly equivalent water thickness values in a region reveal water storage variation. This research spans 156 months, from January 2003 to December 2015. The equivalent water thickness (liquid water equivalent, *LWE*) from GRACE mascon solutions, provided by the GSFC, consists of soil moisture, plant canopy surface water, accumulated snow, and surface and groundwater (Moghim 2020). The GSFC mascons with a 1×1 spatial resolution can capture all signals from GRACE and can be employed without further processing; they are available at GSFC (2022). Gaps in the data were filled by means of linear interpolation. Since the *TWS* is used for the total water storage changes obtained with the GLDAS, the total water storage changes obtained with GRACE is shown as *LWE* to avoid confusion.

2.2.2. GLDAS Noah Land Surface Model

The GLDAS has been jointly produced by the National Oceanic and Atmospheric Administration (NOAA) and NASA (Rodell et al. 2004). It provides 3-hourly and monthly global data, including hydrological components, heat fluxes, meteorological variables, and radiation, from 1948 onward. In this study, GLDAS-2 0.25-degree products (GLDAS_NOAH025_M) were used. Compared to previous versions, some improvements have been carried out in GLDAS-2. This version has a model version upgrade, uses modified MODIS 20-category vegetation, GTOPO30 for elevation, and Hybrid STATSGO/FAO for soil texture. In this study, GLDAS products of monthly precipitation, temperature, and terrestrial water storage, including plant canopy surface water, snow water equivalent, and soil moisture from January 2003 to December 2015, were employed. The GLDAS datasets are available at GES DISC (2022).

Terrestrial hydro-climatology data obtained from the GLDAS can be used to conveniently assess water storage variations. Terrestrial water storage (*TWS*) consists of all surface and groundwater; it is derived from the GLDAS can be defined as follows (Moghim 2020; Zhang et al. 2021):

$$TWS = SWE + SM + PCSW, \quad (3)$$

where *SWE* is the snow water equivalent, *SM* is the soil moisture composed of four layers which have different depths (0-10 cm, 10-40 cm, 40-100 cm, 100-200 cm; 0-200 cm were used in this study), and *PCSW* represents plant canopy surface water. To assess the relationship between the *LWE* from GRACE and the *TWS* from the GLDAS, monthly anomalies (Δ_{anom}) were estimated with the following equation:

$$\Delta_{anom} = P_{monthly} - P_{mean}, \quad (4)$$

where $P_{monthly}$ reflects monthly the GLDAS and GRACE variables and P_{mean} is the mean value of the variables in the study period (2003-2016).

3. Results and discussion

3.1. LWE from GRACE

When the monthly *LWE* data were analyzed, the maximum change in the water storage in the region was observed for September 2014. Figure 2 illustrates the spatial variations in water storage in the southeastern region of Turkey in September 2014. The maximum decrease in water storage was recorded in Subareas 3, 4, and 5. The same subareas experienced both the most increase and decrease in mass variations in 2004 and 2014, respectively. The time series of the *LWE* average value for all subareas is shown in Figure 3.

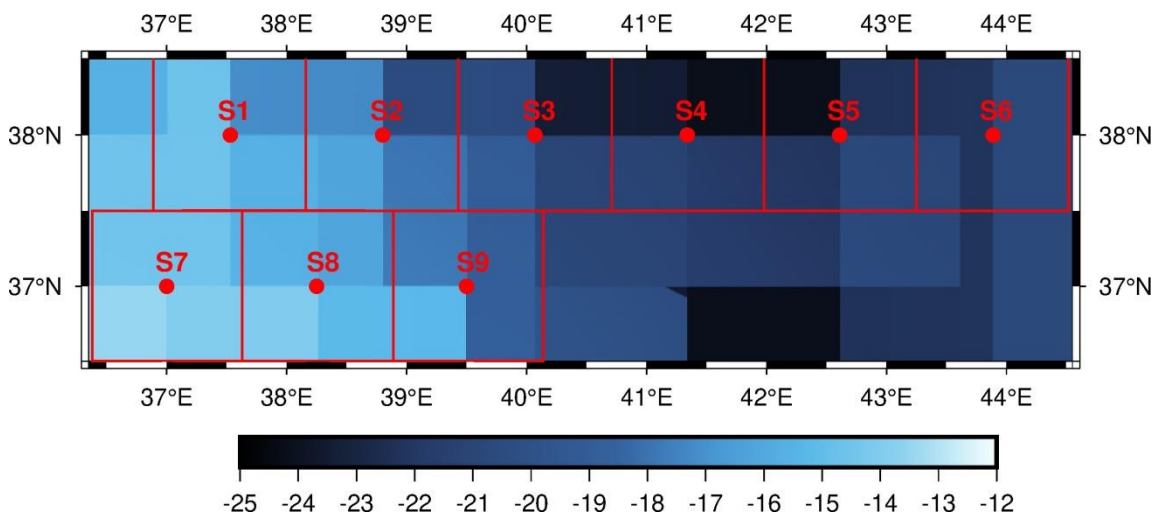


Fig. 2. Water storage changes in September 2014, *LWE* (cm).

Based on Figure 3, the seasonal pattern dominated the *LWE* time series for the study period. Between 2004 and 2014, the maximum increase in the *LWE* was observed in February 2004, and the maximum decrease was observed in September 2014. This result can be attributed to the precipitation over the region (Kayhan, Alan 2012). The average *LWE* showed a remarkable downward trend, with a decrease of ~ 1 cm per year. The decreasing trend in some subareas was more considerable. Particularly, Subareas 5 and 6 showed decreases of approximately 2 cm per year, revealing that in these regions, the discharge amounts are larger than the recharge amounts. The results also indicate that peak points of *LWE* changes for all subareas occurred in spring and autumn and are related to the precipitation pattern. These variations might be a result of the dry and rainy seasons.

The average of the liquid water equivalent for the region was estimated for all months (Fig. 4); all months showed a downward trend, albeit at different degrees. The *LWE* variations showed negative values, especially in the months after July. The month with the maximum reduction ratio was February. The multi-year trend values illustrated in Figures 3 and 4 were estimated via linear regression.

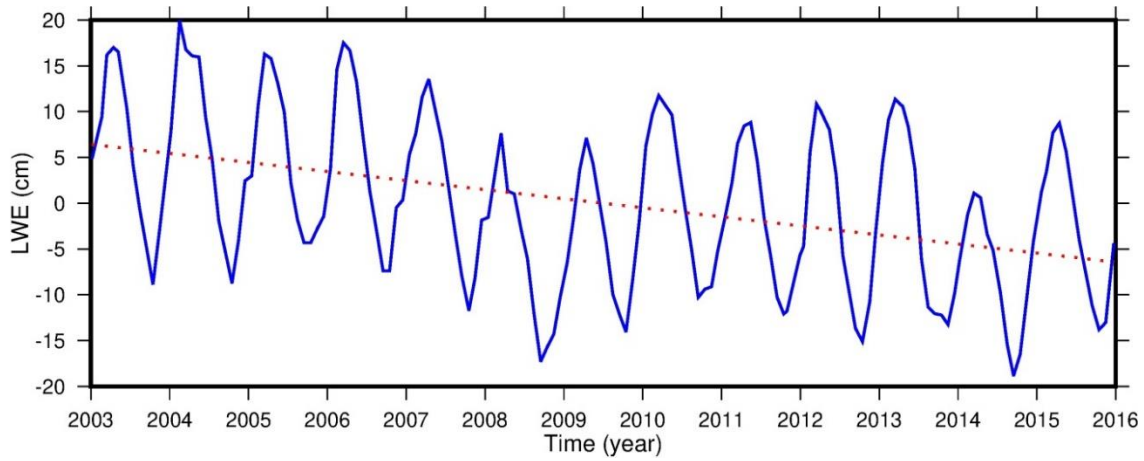


Fig. 3. Spatial average of the liquid water equivalent (LWE) in the study area (blue line) and trend of the LWE (red dots).

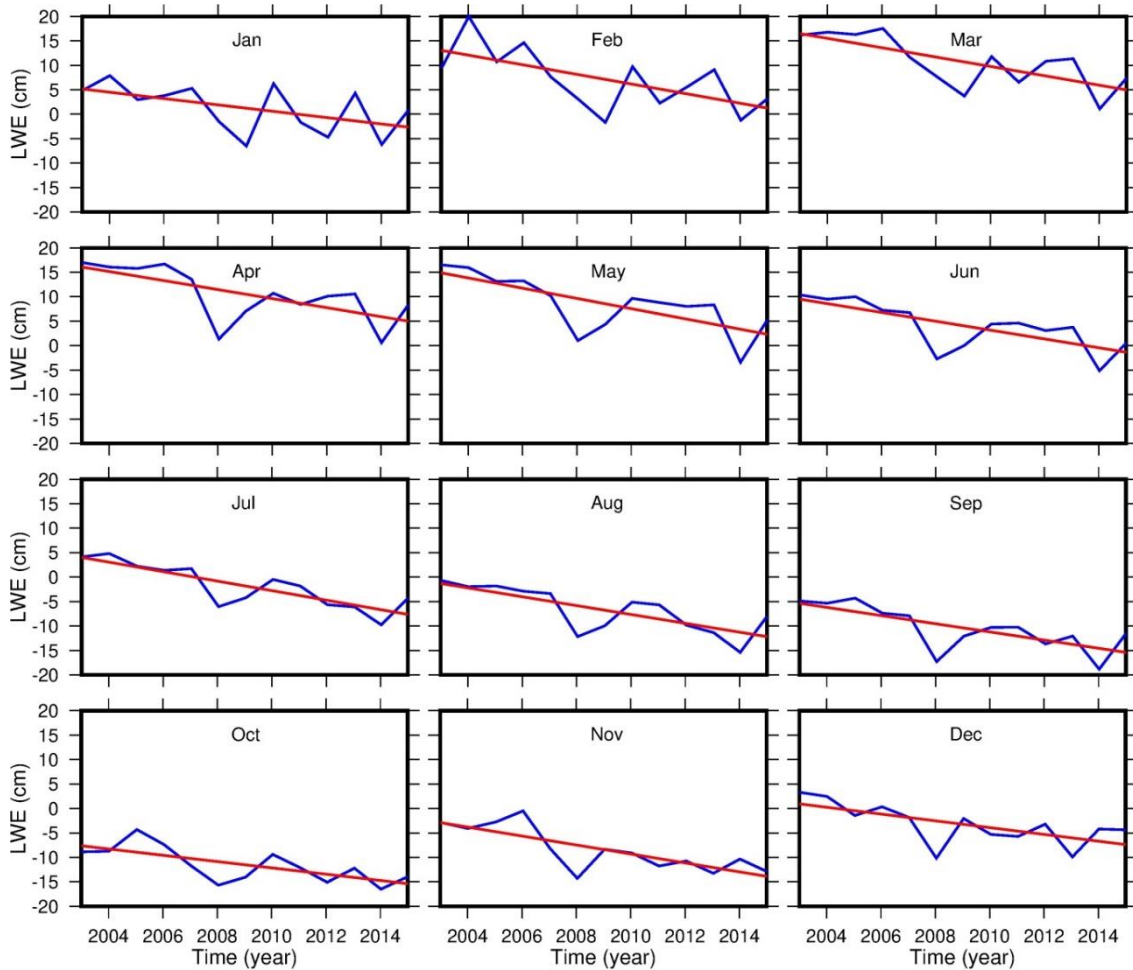


Fig. 4. Average of the liquid water equivalent (LWE) for individual months from 2003 to 2016.

3.2 TWS from GLDAS

To evaluate the TWS trend, the time series of the TWS average value for all subareas is demonstrated in Figure 5. The amounts of snow water equivalent, soil moisture, and plant canopy surface water decreased from 2003 onward. Soil moisture, affected by climate change through variations in temperature and

rainfall, showed a decrease of ~ 15 mm per decade. High temperatures over long periods can result in increased evaporation and, consequently, decreased soil moisture. Furthermore, climate change affects precipitation types as well as the amount and frequency of precipitation, and increasing temperatures cause precipitation to fall as rain rather than snow. In the last decades, the temperature has increased, and the precipitation patterns and types have been affected, especially in growing cities (Tayanç, Toros 1997; Tayanç et al. 2009). As seen in Figure 5, the amount of the *SWE* showed a decrease of approximately 17 mm per decade.

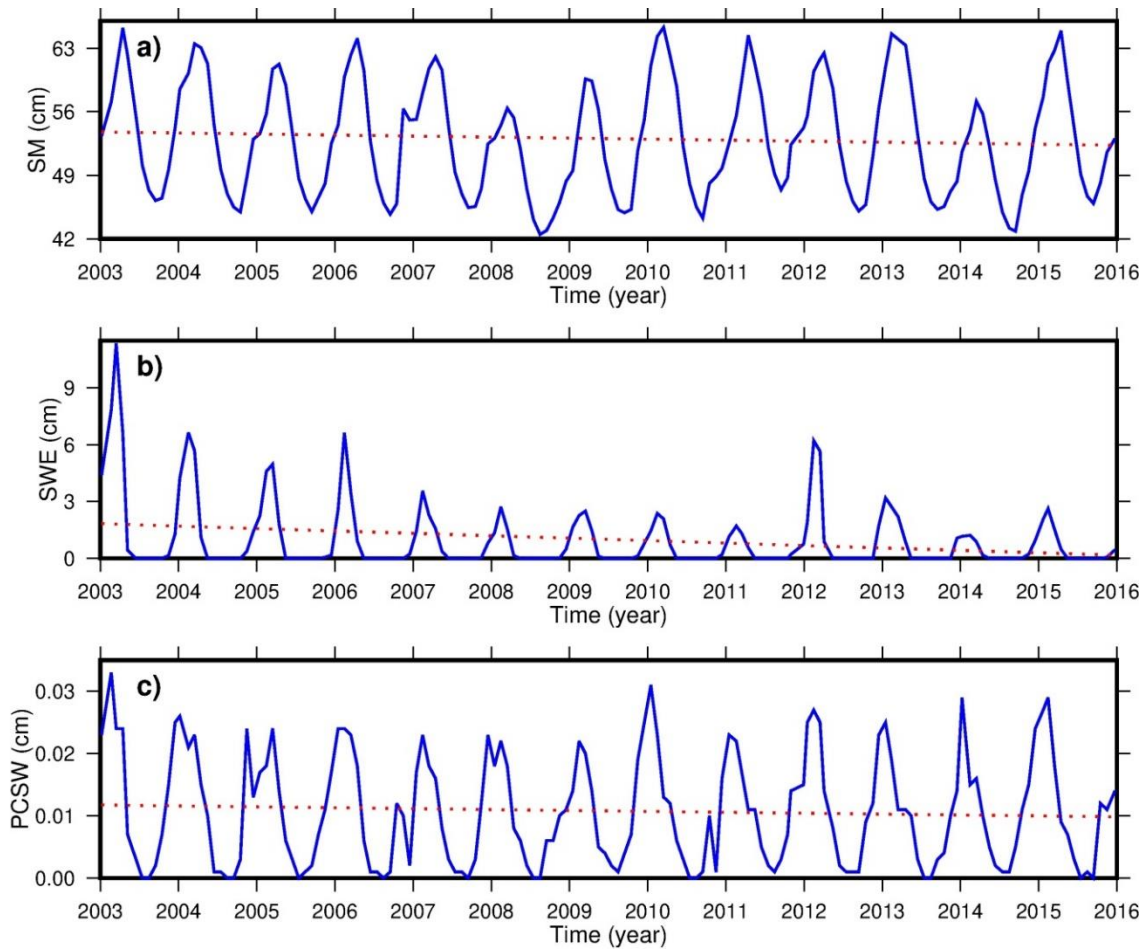


Fig. 5. Domain average of the *TWS* involving soil moisture (a), snow water equivalent (b), and plant canopy surface water (c).

Figure 6 shows the mean *LWE* and *TWS* anomalies based on GRACE and GLDAS. The obtained results provide evidence that both data sets are consistent and highly correlated with each other ($\rho = 0.87$). This consistency indicates that groundwater and surface water in the region are parallel with accumulated snow, soil moisture, and plant canopy surface water during the study period. The relationship between *TWS* and *LWE* anomalies was evaluated spatially, and their cross-correlation values are given in Table 1.

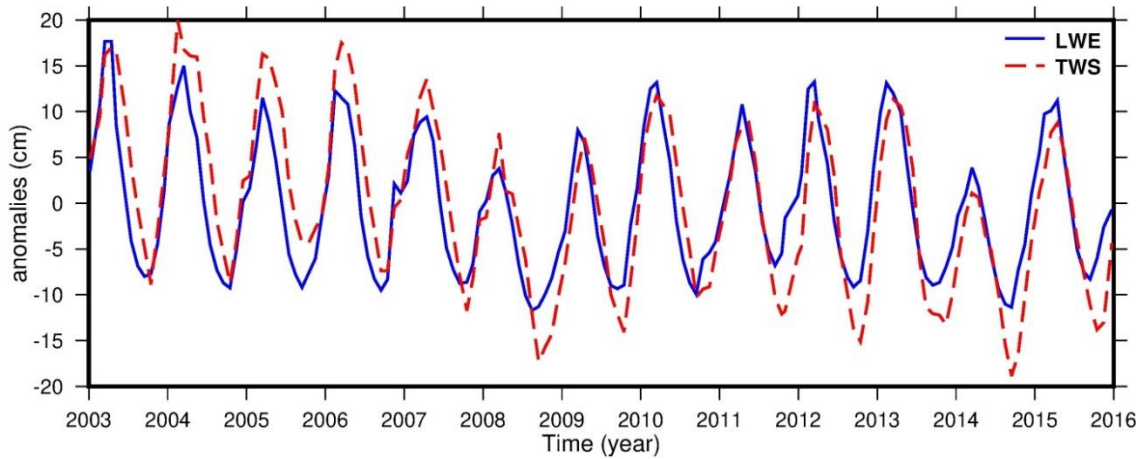


Fig. 6. Anomalies of the liquid water equivalent (*LWE*, blue line) and terrestrial water storage (*TWS*, red dashed line).

Table 1. Correlation between terrestrial water storage (*TWS*) and liquid water equivalent (*LWE*) anomalies for all subareas.

Subareas	Correlation value
1	0.93
2	0.93
3	0.98
4	0.99
5	0.98
6	0.93
7	0.93
8	0.93
9	0.93

According to Table 1, both *LWE* and *TWS* anomalies were highly and positively related in all subareas, which indicates that the *SM*, *SWE*, and *PCSW* components of the terrestrial water storage coincide with the *LWE* trend and that the other components (e.g., surface and groundwater) of the *LWE* do not exhibit a distinct trend during the study period.

3.3. Analysis of water storage changes

Increased temperature and evaporation are results of climate change and have a direct effect on water storage. To evaluate the short- and long-term impacts of climate change, initially, the correlation between climatic variables (temperature and precipitation) and the *LWE* was estimated (Table 2). The anomalies of these climatic variables used in the study were obtained by subtracting the average value from each month.

As seen in the 0 lag column in Table 2, increasing temperatures go along with a reduction in water storage in all subareas, with a negative correlation. In addition, increasing temperatures had the largest negative effect on water storage at the end of 2 months almost in all subareas. Regarding the precipitation results in Table 3, the highest relation was observed again at 2-month lags almost in all subareas. It should be mentioned that the ranges of correlation at 2-month lags was almost twice as much as that of the 0-month lag (without lag). Climatic changes affect some variables immediately and some after a certain period. For

example, soil moisture can increase instantly with precipitation, whereas groundwater resources can only increase when they receive sufficient precipitation. In addition, it is crucial that precipitation accumulates as snowpack, in addition to the amount of precipitation.

Table 2. Correlation between the liquid water equivalent (*LWE*) and anomalies of temperature at 0 lag, 1-month, 2-month and 3-month lags for all subareas.

Subareas	Correlation for time lag			
	0 lag	1-month lag	2-month lag	3-month lag
Subarea 1	-0.32	-0.64	-0.79	-0.74
Subarea 2	-0.18	-0.55	-0.79	-0.83
Subarea 3	-0.25	-0.62	-0.83	-0.83
Subarea 4	-0.30	-0.67	-0.86	-0.83
Subarea 5	-0.34	-0.70	-0.87	-0.82
Subarea 6	-0.33	-0.68	-0.86	-0.81
Subarea 7	-0.28	-0.59	-0.74	-0.72
Subarea 8	-0.29	-0.68	-0.88	-0.85
Subarea 9	-0.34	-0.69	-0.85	-0.80

Table 3. Correlation between the liquid water equivalent (*LWE*) and anomalies of precipitation at 0 lag, 1-month, 2-month, and 3-month lags for all subareas.

Subareas	Correlation for time lag			
	0 lag	1-month lag	2-month lag	3-month lag
Subarea 1	0.32	0.56	0.62	0.54
Subarea 2	0.19	0.48	0.60	0.59
Subarea 3	0.30	0.56	0.63	0.55
Subarea 4	0.35	0.57	0.60	0.50
Subarea 5	0.40	0.60	0.59	0.46
Subarea 6	0.42	0.57	0.52	0.37
Subarea 7	0.17	0.43	0.54	0.52
Subarea 8	0.31	0.62	0.73	0.67
Subarea 9	0.33	0.62	0.66	0.59

In the research area, the highest decrease in *LWE* occurred in Subarea 2, which was located at the highest elevation. The two subareas with the least decrease in *LWE* were Subareas 8 and 9, at lower elevations (Fig. 1). These results indicate that a prolonged snow line in subareas at high elevations decreases against the background of a changing climate. Alternatively, the results verified that climate change (a downward trend in snowpack/precipitation and an upward trend in temperature) has a notable impact on water storage in the region. Besides, anthropogenic activities, mainly agriculture, urbanization, and dam construction, can also influence water storage. At the beginning of 2016, 19 dams were completed in the study region, in the framework of the GAP project. In addition, the area opened to irrigation in 2002 was 198,854 ha and increased to 474,528 ha in 2016 (GAP Administration 2016). The reverse migration and meticulous water management in the region reduced the negative consequences of human activities. However, the negative water budget in the *LWE* and *TWS* results (Figs. 2 and 6) in the region emphasizes the requirement for groundwater monitoring to achieve sustainable water management.

4. Conclusions

Today, many regions of the world are concerned about their available water supply. Human activities, growing populations, and inadequate management make access to clean water increasingly more difficult. The lack of effective and sufficient observations in countries (especially developing countries) results in improper management. In this sense, the major tasks of the satellite and hydrology model in the analysis of water storage in areas with limited observations are emphasized.

The aim of the paper is to investigate the temporal and spatial features of water storage changes along with the effects of climate change in the southeastern region of Turkey. Additionally, terrestrial water storage estimated via the GLDAS and the liquid water equivalent estimated via GRACE were evaluated. Based on these results, water storage shows a downward trend in all subareas, especially in high-elevation regions. The spatial pattern of the *LWE* decline follows the patterns of accumulated snow and soil moisture, which have the largest reductions from the *TWS* components.

Climate change and anthropogenic activities remarkably affect water resources. The results obtained here show that water storage is easily influenced by climatic variables (precipitation and temperature), both directly and indirectly. For example, increasing temperature and decreasing precipitation showed the highest correlations with water storage after 2-month lags, which indicates that the long-term effects of climatic changes need to be well defined and the time delays between the related signals need to be determined. In addition to climate change, there are notable human activities in the study region, such as irrigation, canal establishment, and construction, affecting water resources. The GAP project, which has been ongoing in the region for years, aims for sustainable development with conserving natural resources. This study provides evidence that the GRACE satellite pair provides users with valid data even in regions where observations are limited. In addition, simulated models, such as GLDAS, provide supporting data. The obtained results also show that long-term monitoring of water storage is necessary to prevent possible water shortages in the future and to conserve natural resources. Continuous monitoring, which is a requirement of sustainable water management, is also of vital importance in terms of saving freshwater and delivering it to future generations.

Acknowledgments

The author would like to thank NASA and GSFC for publicly available data.

Availability of data and material

The datasets generated and analyzed during the current study are available in the GRACE and GLDAS repository (<https://ccar.colorado.edu/grace/gsfsc.html>, <https://hydro1.gesdisc.eosdis.nasa.gov/data/GLDAS>).

References

Akhtar F., Nawaz R.A., Hafeez M., Awan U.K., Borgemeister C., Tischbein B., 2022, Evaluation of GRACE derived groundwater storage changes in different agro-ecological zones of the Indus Basin, *Journal of Hydrology*, 605, DOI: 10.1016/j.jhydrol.2021.127369.

- Ali S., Wang Q., Liu D., Fu Q., Rahaman M.M., Faiz M.A., Cheema M.J.M., 2022, Estimation of spatio-temporal groundwater storage variations in the Lower Transboundary Indus Basin using GRACE satellite, *Journal of Hydrology*, 605, DOI: 10.1016/j.jhydrol.2021.127315.
- Al-Zyoud S., Rühaak W., Forootan E., Sass I., 2015, Over exploitation of groundwater in the centre of Amman Zarqa Basin – Jordan: evaluation of well data and GRACE satellite observations, *Resources*, 4 (4), 819-830, DOI: 10.3390/resources4040819.
- Chao N., Luo Z., Wang Z., Jin, T., 2018, Retrieving groundwater depletion and drought in the Tigris-Euphrates Basin between 2003 and 2015, *Groundwater*, 56 (5), 770-782, DOI: 10.1111/gwat.12611.
- Dubey S.K., Lal P., Choudhari P., Sharma A., Dubey A.K., 2022, Assessment of long-term groundwater variation in India using GLDAS reanalysis, [in:] *Advances in Remediation Techniques for Polluted Soils and Groundwater*, P.K. Gupta, B. Yadav, S.K. Himanshu (es.), Elsevier, 219-232, DO: 10.1016/B978-0-12-823830-1.00018-3.
- Famiglietti J.S., Lo M., Ho S.L., Bethune J., Anderson K.J., Syed T.H., Swenson S.C., de Linage C.R., Rodell M., 2011, Satellites measure recent rates of groundwater depletion in California's Central Valley, *Geophysical Research Letters*, 38 (3), DOI: 10.1029/2010GL046442.
- FAO, 2021, Irrigation, Water Development and Management Unit, Food and Agriculture Organization, available online <https://www.fao.org/3/cb7654en/cb7654en.pdf> (data access 06.05.2022).
- Feng W., Zhong M., Lemoine J.-M., Biancale R., Hsu H.-T., Xia J., 2013, Evaluation of groundwater depletion in North China using the gravity recovery and climate experiment (GRACE) data and ground-based measurements, *Water Resources Research*, 49 (4), 2110-2118, DOI: 10.1002/wrcr.20192.
- Forootan E., Khandu K., Awange J.L., Schumacher M., Anyah R.O., van Dijk A.I.J.M., Kusche J., 2016, Quantifying the impacts of ENSO and IOD on rain gauge and remotely sensed precipitation products over Australia, *Remote Sensing of Environment*, 172, 50-66, DOI: 10.1016/j.rse.2015.10.027.
- GAP Administration, 2016, GAP Status Report, Republic Of Turkey Ministry of Industry and Technology, in Turkish, Ankara.
- GES DISC, 2022, Global LDAS, available online <https://hydro1.gesdisc.eosdis.nasa.gov/data/GLDAS> (data access 06.05.2022).
- Godah W., Szelachowska M., Öztürk E.Z., Krynski J., 2018, On the contribution of physical height changes estimated with the use of GRACE satellite mission data to the modernization of a national vertical system, [in:] *American Geophysical Union, Fall Meeting: Abstracts*, G13B-0525.
- GSFC, 2022, Mascon Solutions, available online <https://ccar.colorado.edu/grace/gsfsc.html> (data access 06.05.2022).
- Günel N., 2013, Snowfall, snow cover duration and snow line elevation in Turkey, (in Turkish), *Acta Turcica*, 5, 1-13.
- Huang Z., Pan Y., Gong H., Yeh P.J.-F., Li X., Zhou D., Zhao W., 2015, Subregional-scale groundwater depletion detected by GRACE for both shallow and deep aquifers in North China Plain, *Geophysical Research Letters*, 42 (6), 1791-1799, DOI: 10.1002/2014gl062498.
- Hussain D., Khan A.A., Hassan S.N.U., Naqvi S.A.A., Jamil A., 2021, A time series assessment of terrestrial water storage and its relationship with hydro-meteorological factors in Gilgit-Baltistan region using GRACE observation and GLDAS-Noah model, *SN Applied Sciences*, 3 (5), 1-11, DOI: 10.1007/s42452-021-04525-4.
- Jiao J.J., Zhang X., Liu Y., Kuang X., 2015, Increased water storage in the Qaidam Basin, the North Tibet plateau from GRACE gravity data, *Plos One*, 10 (10), DOI: 10.1371/journal.pone.0141442.
- Joodaki G., Wahr J., Swenson S., 2014, Estimating the human contribution to groundwater depletion in the Middle East, from GRACE data, land surface models, and well observations, *Water Resources Research*, 50 (3), 2679-2692, DOI: 10.1002/2013WR014633.
- Kayhan M., Alan İ., 2012, The spatial precipitation analysis of Turkey in 1971-2010, General Directorate of Meteorology Publications, Ankara, 98 pp.
- Long D., Chen X., Scanlon B., Wada Y., Hong Y., Singh V., Yaning C., Wang C., Han Z., Yang W., 2016, Have GRACE satellites overestimated groundwater storage depletion in the Northwest India aquifers?, *Scientific Reports*, 6 (1), 24398, DOI: 10.1038/srep24398.

- Madani K., 2014, Water management in Iran: what is causing the looming crisis?, *Journal of Environmental Studies and Sciences*, 4, 315-328, DOI: 10.1007/s13412-014-0182-z.
- Massoud E.C., Liu Z., Shaban A., Hage M.E., 2021, Groundwater depletion signals in the Beqaa Plain, Lebanon: evidence from GRACE and sentinel-1 data, *Remote Sensing*, 13 (5), 915, DOI: 10.3390/rs13050915.
- Moghim S., 2020, Assessment of Water Storage Changes Using GRACE and GLDAS, *Water Resources Management*, 34 (2), 685-697, DOI: 10.1007/s11269-019-02468-5.
- Nie N., Zhang W., Chen H., Guo H., 2018, A global hydrological drought index dataset based on gravity recovery and climate experiment (GRACE) data, *Water Resources Management*, 32, 1275-1290, DOI: 10.1007/s11269-017-1869-1.
- Öztürk E.Z., 2020, Estimation and analysis of physical height changes using satellite gravimetry: case studies in Turkey and Greenland, PhD thesis, Konya Technical University Institute of Graduate Studies, Konya.
- Öztürk E.Z., 2022, Monitoring total water storage changes with GRACE mission and GLDAS model and effect of climatic factors on these changes: case study in Konya Basin, (in Turkish), *Doğal Afetler ve Çevre Dergisi*, 8 (1), 103-110, DOI: 10.21324/dacd.971834.
- Öztürk E.Z., Godah W., Abbak R.A., 2018, Analysis of De-correlation filters performance for estimating temporal mass variations determined from GRACE-based GGMs over Konya basin, [in:] FIG Congress 2018, Embracing our smart world where the continents connect: enhancing the geospatial maturity of societies, May 6-11, İstanbul, Turkey.
- Öztürk E.Z., Godah W., Abbak R.A., 2020, Estimation of physical height changes from GRACE satellite mission data and WGHM over Turkey, *Acta Geodaetica et Geophysica*, 55 (2), 301-317, DOI: 10.1007/s40328-020-00294-5.
- Rodell M., Houser P.R., Jambor U., Gottschalck J., Mitchell K., Meng C.-J., Arsenault K., Cosgrove B., Radakovich J., Bosilovich M., Entin J.K., Walker J.P., Lohmann D., Toll D., 2004, The global land data assimilation system, *Bulletin of the American Meteorological Society*, 85 (3), 381-394, DOI: 10.1175/BAMS-85-3-381.
- Rodell M., Velicogna I., Famiglietti J.S., 2009, Satellite-based estimates of groundwater depletion in India, *Nature*, 460, 999-1002, DOI: 10.1038/nature08238.
- Sahoo S., Chakraborty S., Pham Q.B., Sharifi E., Sammen S.S., Vojtek M., Vojtekova J., Elkhachy I., Costache R., Linh N.T.T., 2021, Recognition of district-wise groundwater stress zones using the GLDAS-2 catchment land surface model during lean season in the Indian state of West Bengal, *Acta Geophysica*, 69 (1), 175-198, DOI: 10.1007/s11600-020-00509-x.
- Salem G.S.A., Kazama S., Komori D., Shahid S., Dey N.C., 2017, Optimum abstraction of groundwater for sustaining groundwater level and reducing irrigation cost, *Water Resources Management*, 31, 1947-1959, DOI: 10.1007/s11269-017-1623-8.
- Scanlon B.R., Longuevergne L., Long D., 2012, Ground referencing GRACE satellite estimates of groundwater storage changes in the California Central Valley, USA, *Water Resources Research*, 48 (4), DOI: 10.1029/2011WR011312.
- Syed T.H., Famiglietti J.S., Rodell M., Chen J., Wilson C.R., 2008, Analysis of terrestrial water storage changes from GRACE and GLDAS, *Water Resources Research*, 44 (2), DOI: 10.1029/2006WR005779.
- Tapley B.D., Bettadpur S., Ries J.C., Thompson P.F., Watkins M.M., 2004a, GRACE measurements of mass variability in the Earth system, *Science*, 305 (5683), 503-505, DOI: 10.1126/science.1099192.
- Tapley B.D., Bettadpur S., Watkins M.M., Reigber C., 2004b, The gravity recovery and climate experiment: mission overview and early results, *Geophysical Research Letters*, 31 (9), DOI: 10.1029/2004GL019920.
- Tayanç M., İm U., Doğruel M., Karaca M., 2009, Climate change in Turkey for the last half century, *Climatic Change*, 94 (3), 483-502, DOI: 10.1007/s10584-008-9511-0.
- Tayanç M., Toros H., 1997, Urbanization effects on regional climate change in the case of four large cities of Turkey, *Climatic Change*, 35 (4), 501-524, DOI: 10.1023/A:1005357915441.
- Tiwari V.M., Wahr J., Swenson S., 2009, Dwindling groundwater resources in northern India, from satellite gravity observations, *Geophysical Research Letters*, 36 (18), DOI: 10.1029/2009GL039401.
- Tiwari V.M., Wahr J.M., Swenson S., Singh B., 2011, Land water storage variation over southern India from space gravimetry, *Current Science*, 111 (4), 536-541.

- Voss K.A., Famiglietti J.S., Lo M., de Linage C., Rodell M., Swenson S.C., 2013, Ground water depletion in the Middle East from GRACE with implications for transboundary water management in the Tigris – Euphrates – Western Iran region, *Water Resources Research*, 49 (2), 904-914, DOI: 10.1002/wrcr.20078.
- Wang H., Xiang L., Steffen H., Wu P., Jiang L., Shen Q., Li Z., Hayashi M., 2022, GRACE-based estimates of groundwater variations over North America from 2002 to 2017, *Geodesy and Geodynamics*, 13 (1), 11-23, DOI: 10.1016/j.geog.2021.10.003.
- Wouters B., Bonin J.A., Chambers D.P., Riva R.E.M., Sasgen I., Wahr J., 2014, GRACE, time-varying gravity, earth system dynamics and climate change, *Reports on Progress in Physics*, 77 (11), DOI: 10.1088/0034-4885/77/11/116801.
- Yilmaz Y.A., Sen O.L., Turuncoglu U.U., 2019, Modeling the hydroclimatic effects of local land use and land cover changes on the water budget in the upper Euphrates – Tigris basin, *Journal of Hydrology*, 576, 596-609, DOI: 10.1016/j.jhydrol.2019.06.074.
- Yin W., Li T., Zheng W., Hu L., Han S.-C., Tangdamrongsub N., Splrak M., Huang Z., 2020, Improving regional groundwater storage estimates from GRACE and global hydrological models over Tasmania, Australia, *Hydrogeology Journal*, 28, 1809-1825, DOI: 10.1007/s10040-020-02157-3.
- Zhang J., Liu K., Wang M., 2021, Downscaling groundwater storage data in China to a 1-km resolution using machine learning methods, *Remote Sensing*, 13 (3), 523, DOI: 10.3390/rs13030523.
- Zhang X., Ren L., Feng W., 2022, Comparison of the shallow groundwater storage change estimated by a distributed hydrological model and GRACE satellite gravimetry in a well-irrigated plain of the Haihe River basin, China, *Journal of Hydrology*, 610, DOI: 10.1016/j.jhydrol.2022.127799.
- Zhang Y., Pan M., Sheffield J., Siemann A.L., Fisher C.K., Liang M., Beck H.E., Wanders N., MacCracken R.F., Houser P.R., Zhou T., Lettenmaier D.P., Pinker R.T., Bytheway J., Kummerow C.D., Wood E.F., 2018, A Climate Data Record (CDR) for the global terrestrial water budget: 1984-2010, *Hydrology and Earth System Sciences*, 22 (1), 241-263, DOI: 10.5194/hess-22-241-2018.
- Zheng Z., Ning L., Dai D., Chen L., Wang Y., Ma Z., Yang Z.-L., Zhan C., 2022, Water budget variation, groundwater depletion, and water resource vulnerability in the Haihe River Basin during the new millennium, *Physics and Chemistry of the Earth, Parts A/B/C*, DOI: 10.1016/j.pce.2022.103141.

Convective environment and development of a tornadic supercell in the Czech Republic on 24 June 2021

Slawomir Sulik 

Nicolaus Copernicus University, Faculty of Earth Sciences and Spatial Management

Abstract

This study documents the atmospheric conditions and the development of a tornadic supercell in the Czech Republic, which occurred on the early evening on 24 June 2021. I used the data from the ERA5-reanalysis, vertical atmospheric sounding, synoptic map, and a Sentinel-2 satellite image to determinate the tornado route. As a result of the analysis, it can be concluded that the development of this tornadic supercell was caused by high CAPE values, amounting to around $5,000 \text{ J} \cdot \text{kg}^{-1}$, 0-6 km AGL wind shear $30 \text{ m} \cdot \text{s}^{-1}$, storm-relative helicity with values of $150 \text{ m}^2 \cdot \text{s}^{-2}$ and a wavy atmospheric front. The tornado occurred around 19:30 local time (1730 UTC) in the town Hrušky and moved north-east, reaching the town Hodonín. Based on satellite image derived from Sentinel-2, the widest point of the tornado reached 70 meters; it traveled a distance of about 20 kilometers and had a force of EF3/T5 on the Fujita/TORRO scale. As a result of this event, 6 people lost their lives, 200 people were seriously injured, and hundreds of buildings and cars were destroyed. Further studies on strong thunderstorm incidents in Europe are necessary for their better understanding and prediction.

Key words

Tornado, supercell, severe weather, Czech Republic.

Submitted 22 February 2022, revised 25 April 2022, accepted 12 May 2022

DOI: 10.26491/mhwm/150023

1. Introduction

Dangerous weather phenomena, related to atmospheric convection, are observed in Central Europe mostly in the summer season. Recently, tornadoes, large hailstones, or high lightning activity of the atmosphere during thunderstorms have frequently been observed (Taszarek et al. 2021a-b). In Europe, tornadoes are a rare phenomenon due to a number of complex and non-linear factors in the atmosphere that cause a tornado to form. According to the AMS *Glossary of Meteorology*, a tornado is defined as "rotating column of air, in contact with the surface, pendant from cumuliform cloud, and often visible as a funnel cloud and/or circulating debris/dust at the ground" (Glickman 2000, term updated 8 October 2013). Tornadoes occur in a small area for a short time, causing significant material damage and threatening human health or life, making it necessary to precisely forecast them. Forecasting tornadoes in relation to the spatial area, probability of occurrence or time is extremely difficult, and independent climatological studies on tornadoes have been prepared for various areas of Europe (Meaden 1976; Groenemeijer, Kühne 2014; Taszarek, Brooks 2015; Antonescu et al. 2016; Brázdil et al. 2020; Grieser, Haines 2020).

The most severe tornado in Europe in modern era struck on August 19, 1845, in Montville, France, where 80 people were injured. As a result of the reconstruction of the damage caused by the tornado in 1091 in London, it can be stated that over 600 wooden houses were damaged (Meaden 1976). It is assumed that if a tornado of similar strength appeared in "today's" London, the material losses would amount to several million pounds, in addition to the huge threat to the local population. In the 20th century, tornadoes in

Europe were usually regarded as strong but rare phenomena, as has been and is happening in the USA (Fujita 1973; Meaden 1976; Peterson 1982). Research covering the area of Europe has confirmed that these phenomena most often form in the June-August period. Comparing the intensity of tornadoes in Europe to those occurring in the United States, tornadoes in the east and west of Europe are more likely to be supercell tornadoes (Antonescu et al. 2016).

The creation of the European Severe Weather Database (ESWD; Groenemeijer et al. 2004; Dotzek et al. 2009), managed by the European Severe Storms Laboratory (ESSL), has led to an increased detection of severe weather events. Mass media now play an important role in documenting phenomena such as hailstorms or damage caused by strong winds. Antonescu et al. (2016) showed that, in the period of 1800-1850, approximately eight tornadoes were reported per year. In contrast, from 2000-2014, 242 tornadoes per year were reported.

Because of the difficulties in data collection, climatological results will always be somehow unreliable. Usually, when information about a destructive tornado or windstorm that passed through an area appears in the media, the event is only memorable until the next similar event. However, because of the ESWD database and other studies documenting particularly dangerous cases of tornadoes or thunderstorms, such events can be more reliably forecasted. In Europe, tornadoes are not a new phenomenon and will continue to appear in the future. However, the ongoing warming and increase in low-level moisture over central Europe might result in the formation of tornadoes with a higher intensity. On the other hand, lower relative humidity levels and a stronger inhibition of convection may mean that thunderstorms in a warming climate, despite increasing atmospheric instability, may not be that severe (Taszarek et al. 2021a).

Brázdil and co-authors (2020) confirmed that in the Czech Republic, tornadoes reach an intensity of F3 on the Fujita scale. They usually occur in the summer (June, July, August) in the afternoon and early evening hours, when the air temperatures reach their maximums, and the atmosphere is the most unstable. Tornadoes in the Czech Republic can occur in a wide range of Convective Available Potential Energy (CAPE) and with moderate and strong vertical wind shear. More than half of the tornadoes in the Czech Republic occurred under the conditions of MixedLayer CAPE and MostUnstable CAPE under 500 and 900 J·kg⁻¹. A median wind shear value of 20.8 m·s⁻¹ is associated with a well-organized super-cellular convection (Brázdil et al. 2020). Similar studies were carried out for Poland, where the authors found the highest number of tornadoes with force F0 or F1, with similar durations as those in the Czech Republic (Taszarek, Brooks 2015). This study documents the weather conditions that led to the tornado in the Czech Republic on June 24, 2021. Analysis of the convective environment was provided based on ERA5-reanalyses.

2. Area of interest, dataset and methodology

The research area covers mainly the territory of the Czech Republic, but to better visualize the parameters, the test area was extended to the neighboring countries. The Czech Republic is a country with a varied topography, dominated by upland and mountainous landscapes. The lowland depressions are mainly river

valleys and depressions, which cover about 24% of the total area of the country (Fig. 1A). The main land use cover types are typical European forests as well as meadows and pastures with arable land (Fig. 1B).

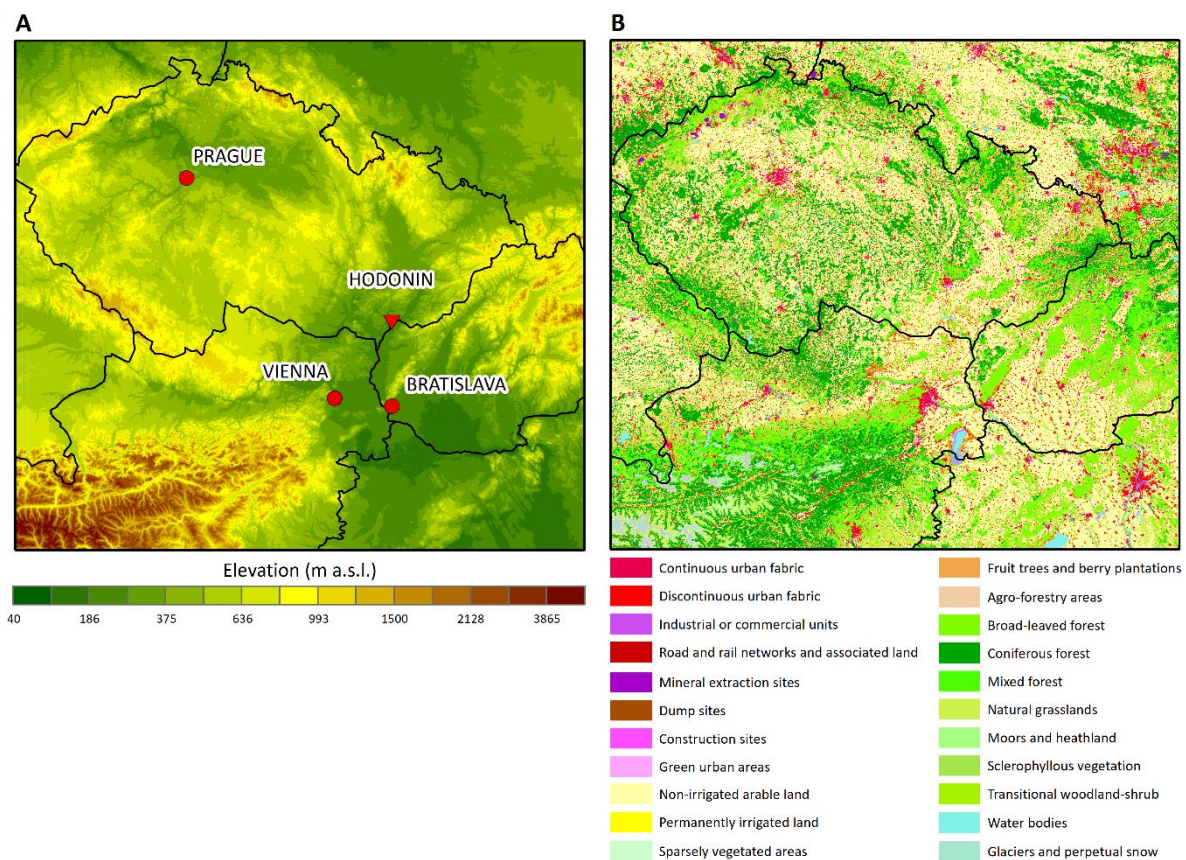


Fig. 1. A – Hypsometric map of the Czech Republic and neighboring countries based on the Shuttle Radar Topography Mission Global Coverage (SRTM3). B – Land use map of the Czech Republic and neighboring countries based on Corine Land Cover 2018 data.

Data from the European Center for Medium-Range Weather Forecast (ECMWF) ERA5 (Hersbach et al. 2018) model were used to determine the specific weather conditions on June 24, 2021. Reanalysis combines model data with observations from across the world into a globally complete and consistent dataset, using the laws of physics. This principle, called “data assimilation”, is based on the method generally used by weather prediction centers, where every 12 hours (at ECMWF), a previous forecast is combined with newly available observations to produce a new, best estimate of the state of the atmosphere; based on this analysis, an updated, improved forecast is issued. Data has been re-gridded to a regular lat-lon grid of 0.25 degrees for the reanalysis and 0.5 degrees for the uncertainty estimate. There were four main subsets: hourly and monthly products, both on pressure levels (upper air fields) and single levels (atmospheric, ocean-wave, and land surface quantities). Based on the ERA5 resources, values such as atmospheric pressure, air temperature, and dew point at various heights, geopotential, convective available potential energy, total cloud cover, or wind direction and speed were obtained. For this research, among others, data obtained from vertical atmospheric profiles were used; to obtain better results, data from outside the Czech

Republic were also included. Parameters such as surface-based Convective Available Potential Energy (CAPE), Lifted Condensation Level (LCL), 0-6-km AGL wind shear, 0-3-km AGL Storm-Relative Helicity (SRH), temperature on multiple levels, or geopotential height were calculated. The hours 1200, 1400, 1600, 1800 were selected to most accurately present the evolution of the atmospheric conditions that contributed to the tornado at 1740 UTC.

Vertical atmospheric soundings are performed in the Czech Republic at two stations (Prague and Prostejov) twice a day, at 0000 and 1200 UTC. The data were obtained from archives of the University of Wyoming. Rawinsonde data also served as reference data for reanalysis (Taszarek et al. 2021b). Data from 1200 UTC from the Prostejov station were selected for the study to most accurately describe the atmospheric parameters.

The synoptic map used to determine the meteorological conditions was generated independently, based on the standardization of various European sources. Designations of the types of air masses were used as described elsewhere (Mishra 2017). However, ERA5 data were used to determine the spatial distribution of atmospheric pressure. To visualize the course and damage caused by the tornado, POLRAD radar data, reports on dangerous weather phenomena from the ESWD database, and Sentinel-2 satellite data were used to assess the route covered by the tornado. Spatial analyses in the form of maps were performed in the ESRI ArcMap 10.8.1 computer software and R programming language (R Core Team 2014).

3. Results

From June 21 to 24, 2021, hot and unstable air of tropical origin flowed across Europe. The development of such a situation was accompanied by a quasi-stationary (wavy) atmospheric front located above the territory of Poland, along with a moving center of low pressure. On Thursday, June 24, the hot air mass over the Czech Republic and Poland was displaced (Fig. 2). According to the latest research, similar synoptic conditions accompanied the formation of high electrically active thunderstorms over Poland (Sulik 2021).

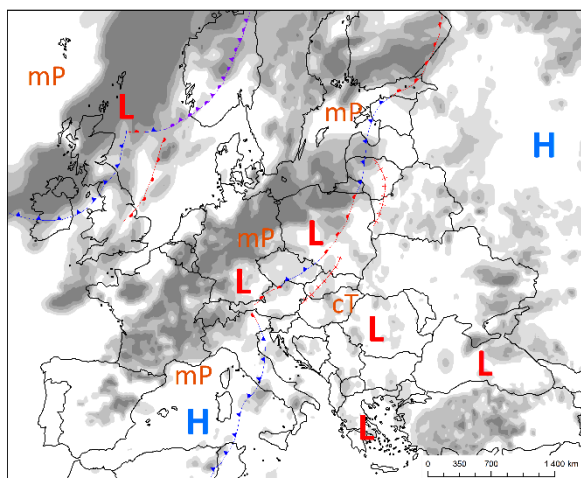


Fig. 2. Synoptic map at 1200 UTC; cloudiness (shaded), H – high pressure, L – low pressure, cT – continental tropical air mass, mP – maritime polar air mass, warm front – red line, cold front – blue line, occluded front – purple line, convergence zone – red line (based on Polish Institute of Meteorology and Water Management and ERA5 data).

The air of tropical origin reaching Europe for several days from over Africa, the Middle East, and the Atlantic Ocean led to an unstable atmosphere (Fig. 3A). Unstable equilibrium occurs when the current thermal vertical gradient is greater than the adiabatic dry gradient ($1^{\circ}\text{C}/100\text{ m}$), i.e., the temperature drop is, e.g., $1.2^{\circ}\text{C}/100\text{ m}$. Each parcel of air in this state of the atmosphere will constantly rise because it will always be warmer and lighter than the surrounding environment. This atmospheric state most frequently occurs in the layer near the earth's surface on a hot and sunny day. The accumulated convective energy (CAPE), indicating a favorable thunderstorm environment, is shown in the orange field (Fig. 3B).

According to the observations on days with strong storms for the area of Europe, CAPE takes values above $1,000\text{ J}\cdot\text{kg}^{-1}$, but in rare cases, the values may exceed $5,000\text{ J}\cdot\text{kg}^{-1}$ (Taszarek et al. 2018). Atmospheric soundings performed at 1200 UTC at the Prostejov station (Czech Republic) showed measured CAPE values around $1,990\text{ J}\cdot\text{kg}^{-1}$ (Fig. 3B). However, even low CAPE values can have a significant impact on the formation of severe storms, especially when in combination with other indicators. The CAPE value depends not only on a sufficiently large vertical temperature gradient but also on the air temperature and humidity in the lower troposphere. As a result of the CAPE analysis carried out between 1200 and 1800 UTC, a significant volatility of the atmosphere, reaching $5,000\text{ J}\cdot\text{kg}^{-1}$, in the early afternoon was reported, which is rare in Europe. The highest CAPE values, exceeding $5,000\text{ J}\cdot\text{kg}^{-1}$, were recorded by rawinsonde on September 13, 2008 (LICT Trapani, Italy), with $6,216\text{ J}\cdot\text{kg}^{-1}$, and on August 23, 2011 (Vienna, Austria), with $5,753\text{ J}\cdot\text{kg}^{-1}$ (Taszarek et al. 2021b).

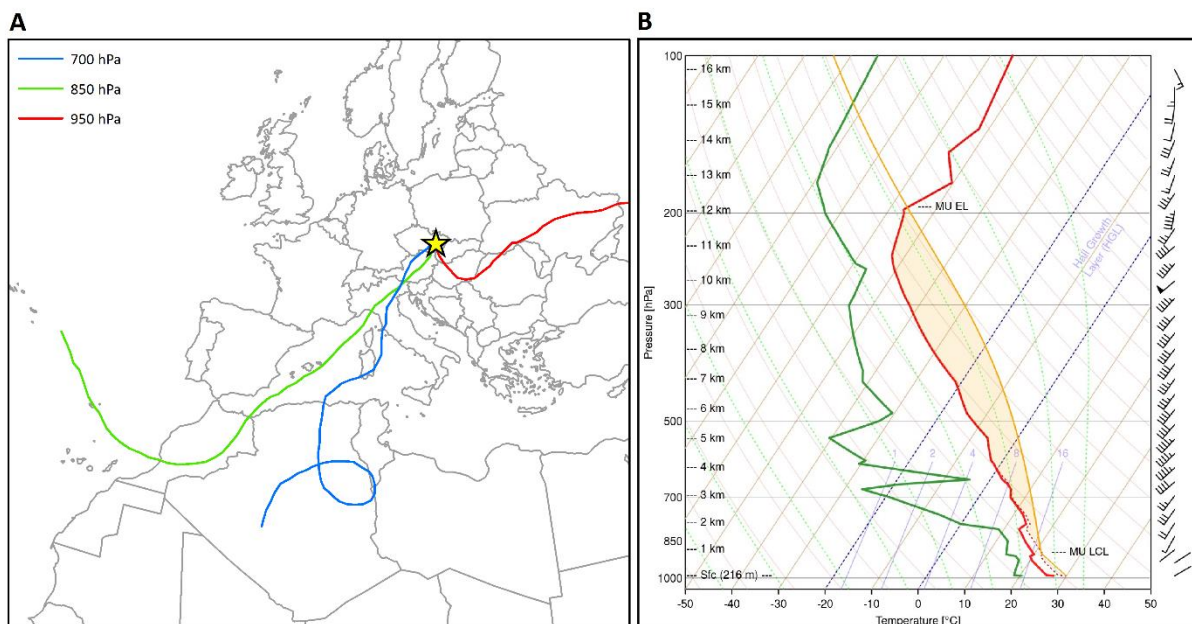


Fig. 3. A – Backward trajectories ending at 1200 UTC on June 24, 2021 (based on the Global Forecast System). The star symbol denotes the location for which model sounding is presented in part B. B – Vertical profile of temperature (red line), dewpoint temperature (blue line) for Prostejov ($49^{\circ}31'$, $17^{\circ}05'$) derived from the thundeR rawinsonde package for R programming language. Orange line denotes the most unstable parcel. Profile indicates the environment just ahead of the approaching convective line.

Near-ground measurements taken on 1200 UTC showed a markedly increased wind speed from 1-3 km AGL, indicating favorable kinematic conditions for thunderstorms in the later hours (Fig. 4A). The rapid increase in wind speed was visible in the higher parts of the troposphere. Strong, vertical ascending movements often develop overshooting tops, indicating the formation of extensive supercell thunderstorms with hailstorms and tornadoes. A model ERA5 hybrid-sigma level sounding from 1800 UTC, displaying the environment while the tornado passed through the town of Hodonín, indicated a well-developed clockwise-curved hodograph (Fig. 4B). This characteristic profile is conducive to the formation of supercells and severe thunderstorms (Bunkers et al. 2000; Coffey et al. 2020). Declining wind speed at an altitude of 9-12 km AGL suggests a progressive slow disintegration of this particular cell.

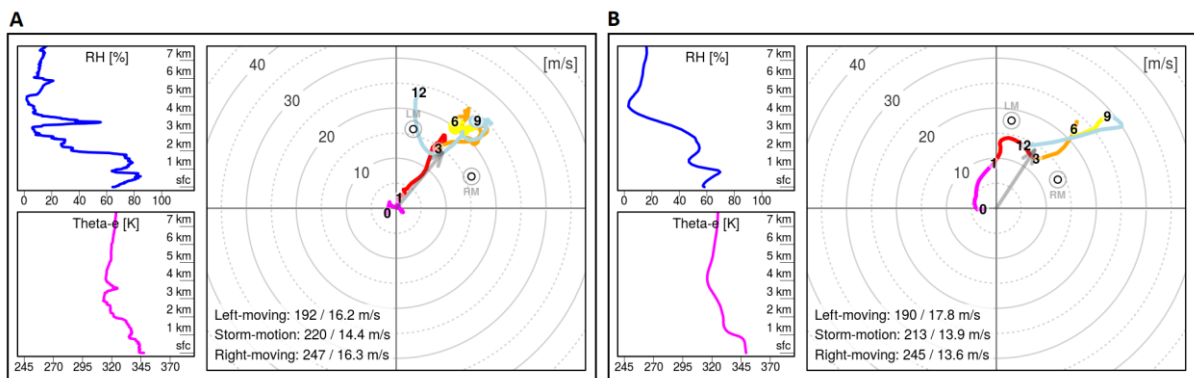


Fig. 4. A – Vertical wind profile for Prostejov (49°31', 17°05') with relative humidity and Theta-e for 1200 UTC, derived from sounding. B – Vertical wind profile for Hodonín (48°50', 17°00') with relative humidity and Theta-e for 1800 UTC, derived from the ERA5 hybrid-sigma level.

High convection energy values were also supported by the wind shear profile at 0-6 km above the earth's surface, reaching $30 \text{ m}\cdot\text{s}^{-1}$. Regarding the wind shear in the layer closer to the earth's surface, these values were lower than those at 0-6 km and increased over time, finally reaching $15 \text{ m}\cdot\text{s}^{-1}$ at 1800 UTC (Fig. 5).

The increase in the values of the indicators over time can also be observed on the example of the lifted condensation level (LCL). Often referred to as the condensation level, this indicator is the height above the earth's surface at which water vapor in the raised test particle of air condenses. Until the LCL level is reached, the rising molecule cools down dry adiabatically, whereas above the LCL, it cools down moist-adiabatic. Numerous but disorganized storms are often observed at low LCLs because convective inhibition (CIN) is low and the lower troposphere relatively moist. On the other hand, at high LCLs (above 2,000 m), there may be a large CIN, especially when isothermal or temperature inversion occurs in the lower troposphere. During previous observations, it was found that LCLs with a height of 500-1,000 m have a positive effect on the development of tornadoes (Belo-Pereira et al. 2017). During the tornado up-rising near Hodonín, the LCL reached a value of around 1,300 m. Importantly, the (SRH) index, which determines the potential for rotation within the ascending current in the storm cloud (mesocyclone), remained at $150 \text{ m}^2\cdot\text{s}^{-2}$ for several hours preceding the upcoming tornado, which, as previous studies have shown, favors the formation of strong whirlwinds (Thompson et al. 2007) (Fig. 5). On the night of June

23 to June 24, a mesoscale convective system (MCS) with a bow echo built in the squall line passed through the territory of the Czech Republic, causing damage by strong winds in the area of Central Bohemia. In the morning hours, the MCS headed towards Poland and moved north-east. The morning storms and the remaining moisture outflow created favorable conditions for the development of subsequent supercell storms in the Czech Republic and Poland on the same day. A similar situation took place on August 10 and 11, 2017, when two extremely strong thunderstorms developed, passing through a large area of Poland, with high electrical activity, strong wind gusts, and severe hail (Taszarek et al. 2019; Sulik, Kejna 2020; Figurski et al. 2021). Convection initiated around 1200 UTC in Austria was possible due to the large thermal gradient in the upper and lower tropospheric layers. Over the Czech Republic, the temperature gradient at a height of 500 hPa was 10°C , and at a height of 850 hPa, the air was heated to a temperature of 24°C , with a mixing ratio in the profile at 0-500 m from 8 to $15\text{ g}\cdot\text{kg}^{-1}$ (Fig. 6).

The expanding system of several storm cells merged into one storm cluster around 1700 UTC and entered the Czech Republic around 1720 UTC, becoming a supercell. Such a supercell is a well-organized storm structure which can exist for several hours and move during its entire life cycle for several hundred kilometers at a speed of about 90 km/h or even faster (Sulik, Kejna 2020). Throughout the life cycle of a supercell, highly dangerous storms may occur within its range. The core of the storm is a swirling ascending current (called a mesocyclone). Rotation in the ascending current allows the supercell to soar higher and more rapidly than a normal storm cell (Fig. 7A). A supercell can be considered a very low-pressure system; its size does not exceed 40-60 km, and the center of the low pressure is located in the mesocyclone. Some mesocyclones spin extremely strongly, and when the appropriate thermal conditions are present and the air in the lower troposphere is sufficiently humid, tornadoes may develop. Ongoing research is still unable to answer the question of why one supercell generates a tornado and another does not. The supercell that entered Czech territory was also distinguished by large hail and heavy rain. The tornadic supercell, after creating the tornado, moved north-east, absorbing smaller storm cells into its structure. June 24 was also specific in terms of heavy hail events (Fig. 7B).

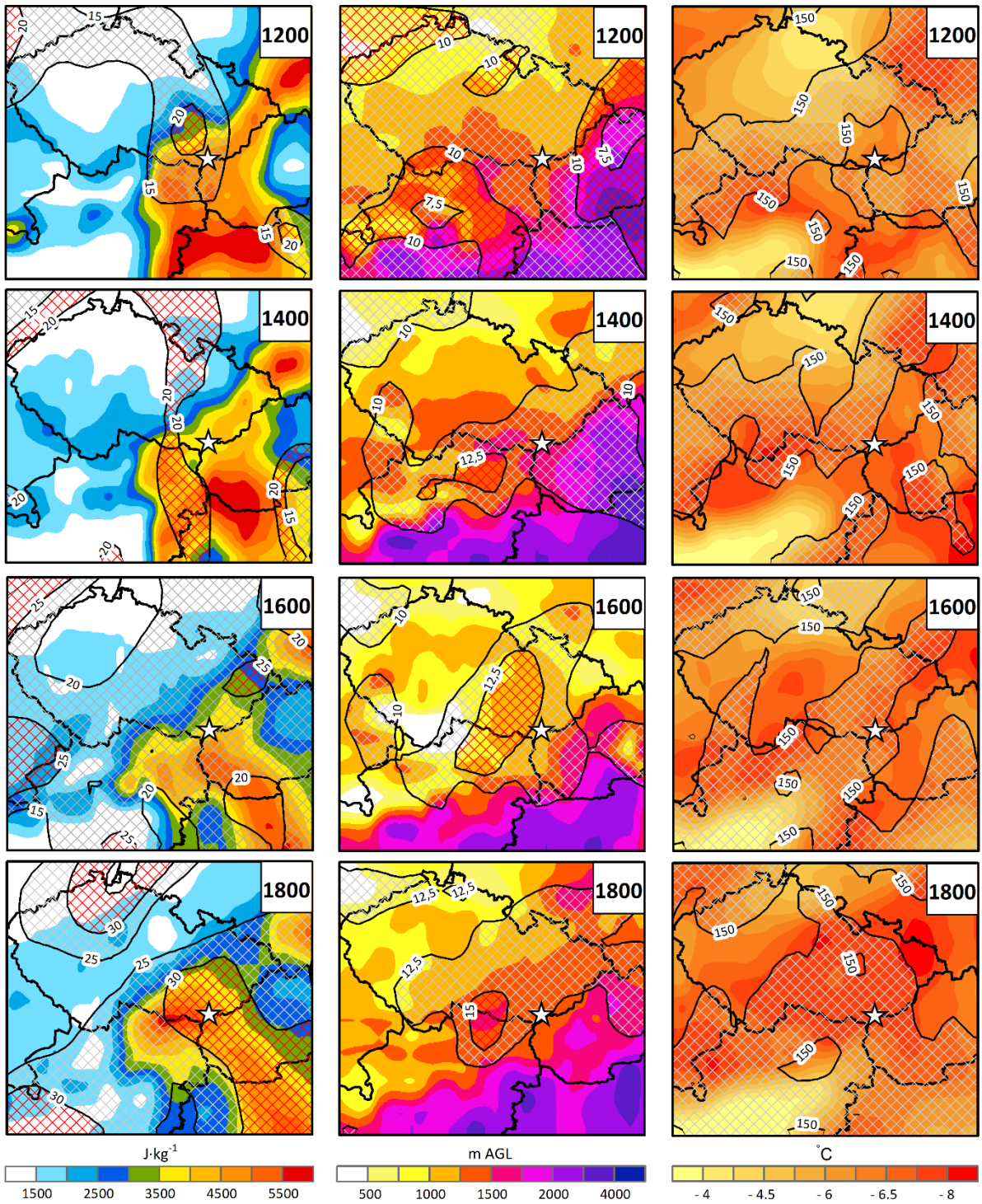


Fig. 5. (Left panel) – Surface-based CAPE [$\text{J}\cdot\text{kg}^{-1}$] (shaded) and 0-6-km AGL wind shear [$\text{m}\cdot\text{s}^{-1}$] (contours and tiles) (central panel) – Surface-based LCL [m AGL] (shaded) and 0-1-km AGL wind shear [$\text{m}\cdot\text{s}^{-1}$] (contours and tiles) (right panel) – Lifted index [$^{\circ}\text{C}$] (shaded) and 0-3-km AGL SRH [$\text{m}^2\cdot\text{s}^{-2}$] (contours and tiles) (based on ERA5 data).

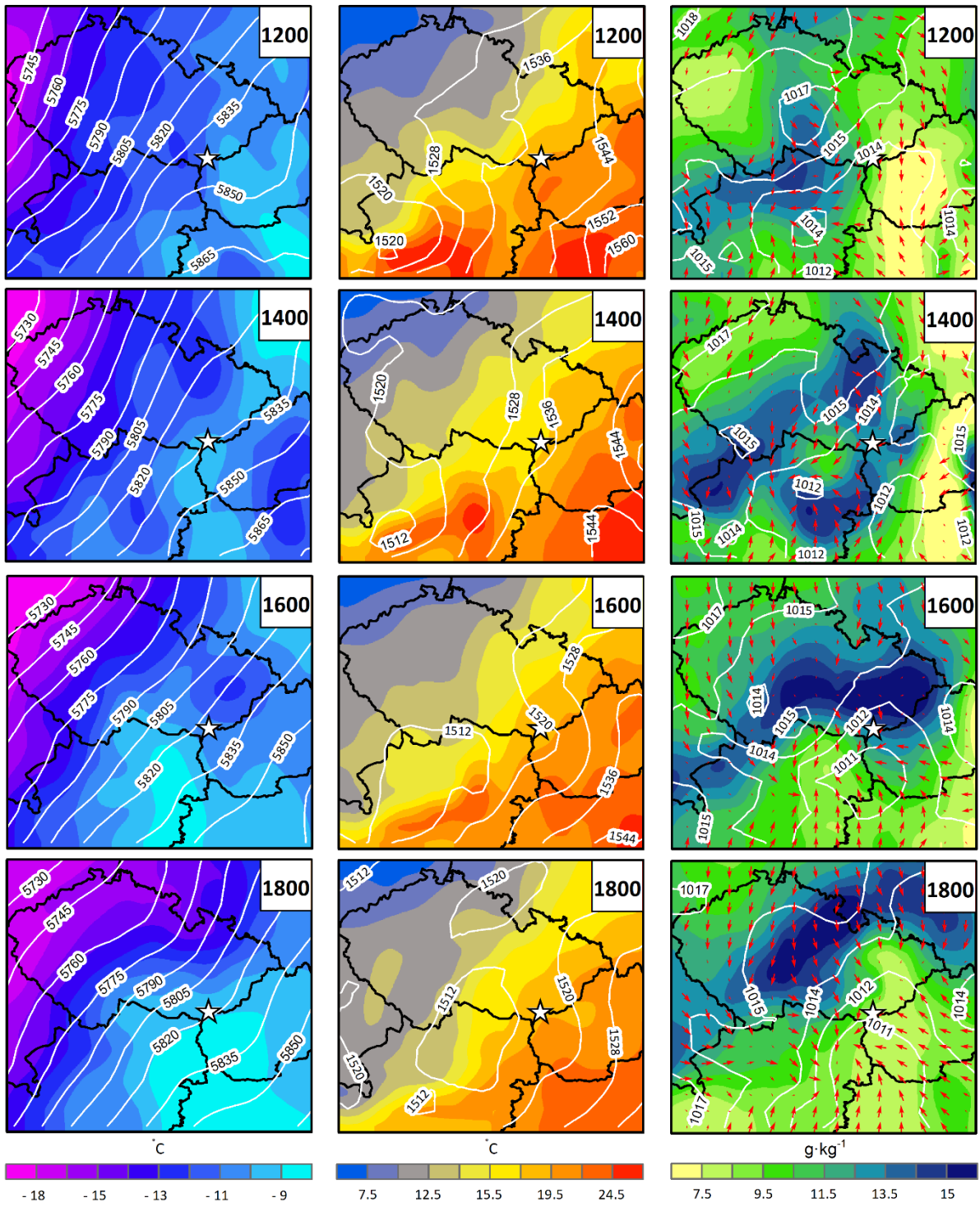


Fig. 6. (Left panel) – Temperature [°C] (shaded) and geopotential height [gpm] (contours) at 500 hPa (central panel) – Temperature [°C] (shaded) and geopotential height [gpm] (contours) at 850 hPa (right panel) – 0-500-m AGL ML mixing ratio [g·kg⁻¹] (shaded) and MSLP [hPa] (contours) (based on ERA5 data).

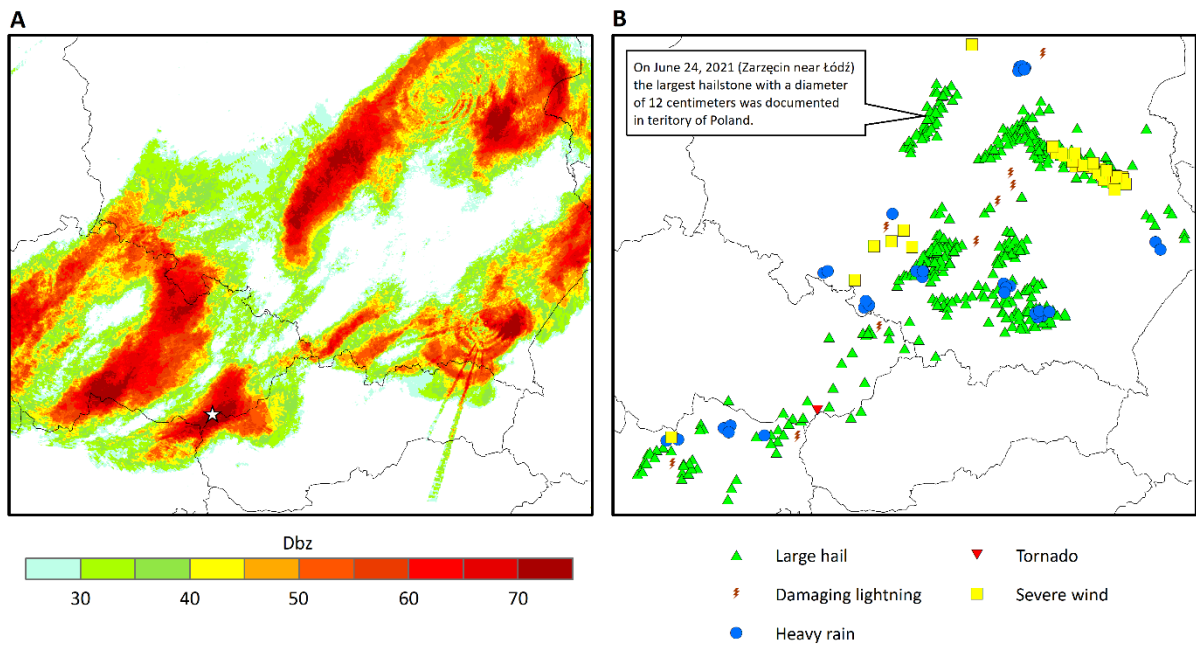


Fig. 7. A – Maximum reflectivity between 1700 and 2000 UTC with 10-minute steps (based on POLRAD data). B – Severe weather reports on June 24, 2021 (based on the European Severe Weather Database). Star symbol denotes tornado location.

On that day, the largest hailstone (with a diameter of 12 cm) that ever fell in Poland was documented in Zarzęcin near the Łódź City (central Poland). Based on satellite data from Sentinel-2 and the damage caused by the tornado, it was possible to reconstruct the tornado path (Fig. 8A). For the first time, the tornado hit the ground near the town Hrušky. At this point, the tornado was only taking its mature stage, so the damage was not as violent as in other places on the further path of the tornado. The traces of further activity showed that, for a while, the main core of the mesocyclone lost its connection with the ground and regained it several times after a few meters, descending to the ground near the village of Moravská Nová Ves. It remained in contact with it until leaving the town of Hodonín, destroying Mikulčice and Lužice on the way. Around 1745 UTC, the tornado reached the city of Hodonín, where it caused the greatest damage (Fig. 8B).

The damage done on the tornado route was assessed via force EF3 on the Fujita scale. This means that at the tornado crossing point, the wind hit at a speed of 218-266 km/h. The EF scale is nothing more than an updated scale for assessing the force of a tornado, proposed by Ted Fujita in 1973. The designation EF3 (former F2) denotes severe damage characterized by the significant destruction of solid structures such as residential buildings and shopping malls. Trees are usually badly broken, cars overturned and moved elsewhere, and poorly constructed buildings are completely destroyed (Fujita 1973). At its widest point, the tornado was about 70 meters wide (Fig. 9).

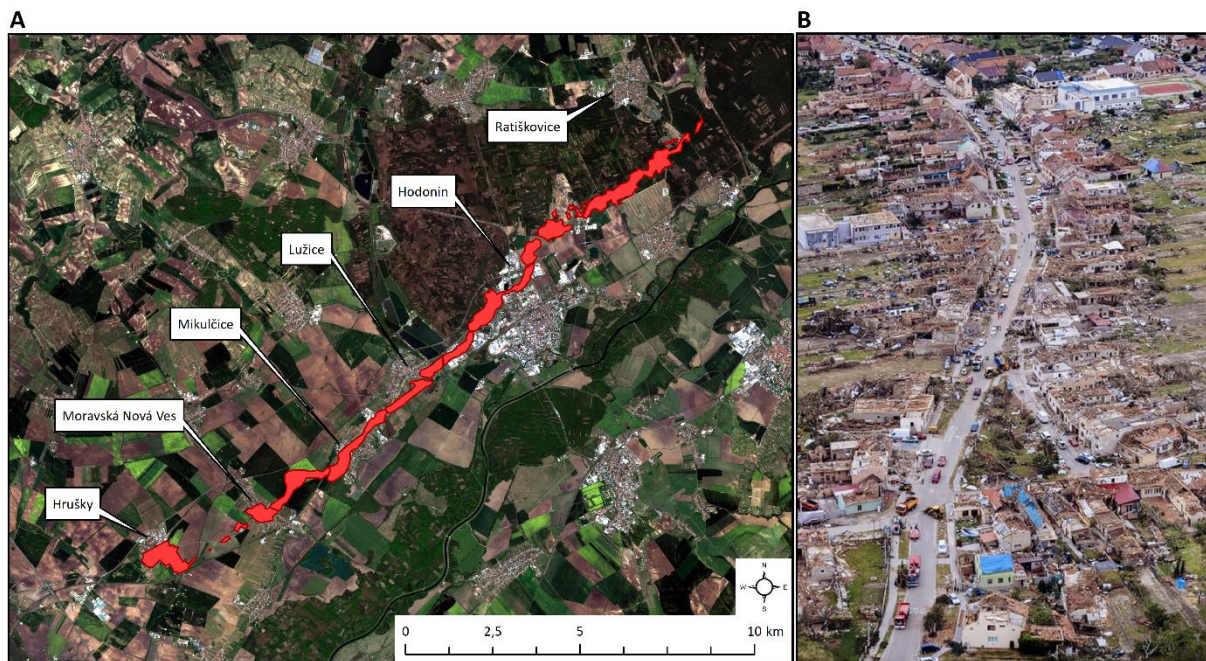


Fig. 8. A – Tornado track on June 24, 2021. B – Aftermath of the violent tornado in the town Hodonín. Photography: Severe Weather Europe.



Fig. 9. Tornado observed at around 1740 UTC near the town of Hodonín. Photography: D. Herka.

When leaving Hodonín, the tornado continued toward north-east, where it entered areas less inhabited by people. It destroyed hectares of forests, and its trail ended near Ratiškovice.

4. Conclusion

June 24, 2021, saw one of the most severe weather events in Europe. Against the background of a changing climate, such events will become more frequent in the near future. For example, each additional 0.5°C causes a marked increase in the intensity and frequency of heat waves and heavy rainfall. With a 1.5°C warming, the frequency of extreme events, also severe thunderstorms evolving into tornadoes, will increase (IPCC 2021). In this context, particular attention should be paid to the phenomena that are taking place, their strength, and their impacts on human health and life as well as material. On June 24, 2021, several serious thunderstorm incidents took place in Central Europe, with losses estimated at several billions of euros. The tornado that occurred in the Czech Republic was created mainly due to the hot and unstable mass of air of tropical origin. Favorable kinematic conditions in the form of CAPE values around 5,000 J·kg⁻¹ and an SRH around 150 m²·s⁻² allowed the storm cloud to rise to a height of 12 km (Equilibrium Level, strong vertical wind) to later take the form of a mesocyclone storm supercell, which generated a tornado with the force of EF3/T5 on the Fujita/TORRO scale. On that day, high precipitable water levels in the troposphere >50 PW and a strong vertical wind profile at the level of 0-6 km AGL of 30 m·s⁻¹ also contributed to various incidents, with hailstones reaching a diameter of more than 2 centimeters. In a climatological study on tornadoes in the Czech Republic, the authors indicate that the strongest tornadoes in this area in the entire history of this country had the maximum force of F3 and F2 (Brázdil et al. 2020). It can therefore be concluded that the tornado of June 24, 2021, was one of the most powerful incidents in history. As a result of the devastating tornado passing through the centers of some Czech towns, 6 people lost their lives, about 200 were seriously injured, and several hundred houses and cars were completely destroyed. Further studies on strong thunderstorms in Europe are necessary for their better understanding and prediction by specialists.

References

- Antonescu B., Schultz D.M., Lomas F., Kühne T., 2016, Tornadoes in Europe: Synthesis of the observational datasets, *Monthly Weather Review*, 144 (7), 2445-2480, DOI: 10.1175/MWR-D-15-0298.1.
- Belo-Pereira M., Andrade C., Pinto P., 2017, A long-lived tornado on 7 December 2010 in mainland Portugal, *Atmospheric Research*, 185, 202-215, DOI: 10.1016/j.atmosres.2016.11.002.
- Brázdil R., Chromá K., Púčik T., Černoch Z., Dobrovolný P., Dolák L., Kotyza O., Řezníčková L., Taszarek M., 2020, The climatology of significant tornadoes in the Czech Republic, *Atmosphere*, 11 (7), 689, DOI: 10.3390/Atmos11070689.
- Bunkers M.J., Klimowski B.A., Zeidler J.W., Thompson R.L., Weisman M.L., 2000, Predicting supercell motion using a new hodograph technique, *Weather and Forecasting*, 15 (1), 61-79, DOI: 10.1175/1520-0434(2000)015<0061:PSMUAN>2.0.CO;2.
- Coffer B.E., Taszarek M., Parker M.D., 2020, Near-Ground wind profiles of tornadic and nontornadic environments in the United States and Europe from ERA5 reanalyses, *Weather and Forecasting*, 35 (6), 2621-2638, DOI: 10.1175/WAF-D-20-0153.1.
- Corine Land Cover, 2018, available online <https://land.copernicus.eu/pan-european/corine-land-cover/clc2018> (data access 23.05.2022).
- Dotzek N., Groenemeijer P., Feuerstein B., Holzer A.M., 2009, Overview of ESSL's severe convective storms research using the European Severe Weather Database ESWD, *Atmospheric Research*, 93 (1-3), 575-586, DOI: 10.1016/J.Atmosres.2008.10.020.

- Figurski M.J., Nykiel G., Jaczewski A., Baldysz Z., Wdowikowski M., 2021, The impact of initial and boundary conditions on severe weather simulations using a high-resolution WRF model. Case study of the derecho event in Poland on 11 August 2017, *Meteorology Hydrology and Water Management*, DOI: 10.26491/mhwm/143877.
- Fujita T.T., 1973, Tornadoes around the World, *Weatherwise*, 26 (2), 56-62, DOI: 10.1080/00431672.1973.9931633.
- Glickman T.S. (ed.), 2000, *Glossary of Meteorology*, 2nd edition, American Meteorological Society, 850 pp.
- Grieser J., Haines P., 2020, Tornado risk climatology in Europe, *Atmosphere*, 11 (7), 768, DOI: 10.3390/atmos11070768.
- Groenemeijer P.H., Dotzek N., Stel F., Brooks H., Doswell C., Elsom D., Giaiotti D., Gilbert A., Holzer A., Meaden T., Salek M., Teittinen J., Behrendt J., 2004, ESWD – A standardized, flexible data format for severe weather reports. Preprints, 3rd European Conference on Severe Storms, León, 9-12 November 2004.
- Groenemeijer P.H., Kühne T., 2014, A climatology of tornadoes in Europe: Results from the European Severe Weather Database, *Monthly Weather Review*, 142 (12), 4775-4790, DOI: 10.1175/Mwr-D-14-00107.1.
- Hersbach H., Bell B., Berrisford P., Biavati G., Horányi A., Muñoz Sabater J., Nicolas J., Peubey C., Radu R., Rozum I., Schepers D., Simmons A., Soci C., Dee D., Thépaut J.-N., 2018, ERA5 hourly data on pressure levels from 1979 to present, Copernicus Climate Change Service (C3s), Climate Data Store (Cds), DOI: 10.24381/Cds.Bd0915c6.
- IPCC, 2021, *Climate Change 2021: The Physical Science Basis. Contribution Of Working Group I To The Sixth Assessment Report Of The Intergovernmental Panel On Climate Change*, V. Masson-Delmotte, P. Zhai, A. Pirani, S.L. Connors, C. Péan, S. Berger, N. Caud, Y. Chen, L. Goldfarb, M.I. Gomis, M. Huang, K. Leitzell, E. Lonnoy, J.B.R. Matthews, T.K. Maycock, T. Waterfield, O. Yelekçi, R. Yu, B. Zhou (eds.), Cambridge University Press, in press.
- Meaden G.T., 1976, Tornadoes in Britain: Their intensities and distribution in the time and space, *Journal of Meteorology*, 1, 242-251.
- Mishra P.K., 2017, Origin of air masses and their classification, DOI: 10.13140/Rg.2.2.16956.59528.
- Peterson R.E., 1982, Tornadic activity in Europe – the last half-century, Preprints, 12th Conference on Severe Local Storms, San Antonio, Texas, 63-66.
- R Core Team, 2014, R: A language and environment for statistical computing, R Foundation For Statistical Computing, Vienna, Austria, available online <http://www.r-project.org/> (data access 23.05.2022).
- Sulik S., 2021, Formation factors of the most electrically active thunderstorm days over Poland (2002-2020), *Weather and Climate Extremes*, 34, DOI: 10.1016/j.wace.2021.100386.
- Sulik S., Kejna M., 2020, The origin and course of severe thunderstorm outbreaks in Poland on 10 and 11 August, 2017, *Bulletin Of Geography. Physical Geography Series*, 18, 25-39, DOI: 10.2478/bgeo-2020-0003.
- Taszarek M., Allen J.T., Brooks H.E., Pilguy N., Czernecki B., 2021a, Differing trends in United States and European severe thunderstorm environments in a warming climate, *Bulletin of the American Meteorology Society*, 102 (2), 296-322, DOI: 10.1175/bams-d-20-0004.1.
- Taszarek M., Brooks H.E., 2015, Tornado climatology of Poland, *Monthly Weather Review*, 143 (3), 702-717, DOI: 10.1175/mwr-d-14-00185.1.
- Taszarek M., Brooks H.E., Czernecki B., Szuster P., Fortuniak K., 2018, Climatological aspects of convective parameters over Europe: A comparison of ERA-Interim and sounding data, *Journal of Climate*, 31 (11), 4281-4308, DOI: 10.1175/jcli-d-17-0596.1.
- Taszarek M., Pilguy N., Allen J., Gensini V., Brooks H.E., Szuster P., 2021b, Comparison of convective parameters derived from ERA5 and MERRA-2 with rawinsonde data over Europe and North America, *Journal of Climate*, 34 (8), 3211-3237, DOI: 10.1175/jcli-d-20-0484.1.
- Taszarek M., Pilguy N., Orlikowski J., Surowiecki A., Walczakiewicz S., Pilorz W., Piasecki K., Pajurek Ł., Pórolniczak M., 2019, Derecho evolving from a mesocyclone - A study of 11 August 2017 severe weather outbreak in Poland: Event analysis and high-resolution simulation, *Monthly Weather Review*, 147 (6), 2283-2306, DOI: 10.1175/MWR-D-18-0330.1.
- Thompson R.L., Mead C.M., Edwards R., 2007, Effective storm-relative helicity and bulk shear in supercell thunderstorm environments, *Weather and Forecasting*, 22 (1), 102-115, DOI: 10.1175/Waf969.1.

An overview of groundwater resources evolution in North Africa: sustainability assessment of the CI aquifer under natural and anthropogenic constraints

Houda Besser

Research Unit of Geo-systems, Geo-resources and Geo-environments (UR3G), Department of Earth Sciences,
Faculty of Sciences of Gabes

Laifa Dhaouadi

Regional Center for Research in Oasis Agriculture

Abstract

Given the complex links to the major economic activities and climate variability, water is becoming the most fiercely contested resource, challenging human survival and food security especially in arid hot dry regions, such as in the Middle East and North Africa areas (MENA). In the Kebili and Tozeur regions in southern Tunisia, groundwater resources undergo abusive exploitation mostly for agricultural activities. The lack of efficient management and adequate conservation strategies to ensure sustainable exploitation has resulted in gradual irreversible ecological and geological effects. Thus, this review paper provides a useful background synthesis for the critical assessment of the recursive dynamic substantial increase in freshwater in these regions, using a general equilibrium model of hydrodynamic and chemical changes of aquifers based on several water scarcity indices and economic-ecological factors.

The collected data highlight the good correlation between the reviewed studies and the observed and (or) measured disturbance of the natural functioning of the deep confined aquifers, manifested by the gradual severity of the resulted environmental issues, the permanent irreversible depression of the water table, aquifer decompression, land subsidence in the Douz area, and contamination by petroleum flows, with 4 g/L of asphalt and 12 to 90 µg/L of cadmium in northern Kebili. Based on the assembled evidence, water scarcity has heavily influenced the equilibrium of these resources, and the adopted conservation plans have been insufficient to ensure economic incentives for environmental natural resources conservation (the annual average loss of fertile land is 1.25 ha).

A detailed equilibrium analysis, relying on evaluating the water productivity-water exploitation ratio, is undoubtedly necessary for improving the integration among different decision makers. Moreover, a re-examination of the resulting impacts of the previously implemented strategies for reliable database development is the key to the successful handling of this transitory fragile situation.

Keywords

Subsidence, oil contamination, resource protection, water productivity, economic security.

Submitted 10 December 2021, revised 8 April 2022, accepted 31 May 2022

DOI: 10.26491/mhwm/150572

1. Introduction

Groundwater represents a continental archive that stores the multiple interactions among the different environmental components. This function can be used in environmental studies to obtain information about environmental changes, climate data comparison, and the paleo-climate (Zhang et al. 2017). Despite their vital importance, these resources are facing severe deterioration in many countries all over the world relative to the impacts of increasing exploitation and climate variability. The continuous decrease in the resilience of these systems, known as the slow component of the hydrological cycle with long-term responses

(Russo, Lall 2017), generally leads to irreversible ecological impacts, frequently resulting in serious disasters and important economic losses (Swezey 1996; Edmunds et al. 2003; OSS 2003; Molden et al. 2010; Hamed et al. 2014a-b; Zhang et al. 2017).

Given the crucial role of groundwater in maintaining ecological balance, especially in hot and dry areas, the sustainability of groundwater resources in response to the continuous socio-economic development and intensifying climate variability has gained traction in recent years (GIEC 2007; Waiyaki et al. 2012). However, water conservation is an extremely complex process, difficult to evaluate and manage, mainly regarding deep multi-layered aquifers. It requires a quantitative and qualitative assessment of potential productivity, degradation issues, and management plans given institutional, political, engineering, technical, and financial drivers based on a sound analysis of ecological consequences requirements, economic growth needs, and social stabilization.

The evaluation of the efficiency of the adopted management actions involves, consequently, all the factors and conditions that may influence the performance of the water-dependent system during the entire exploitation process, from the real water requirements to the calculated water productivity ratio and the measured gains (Barker et al. 2003). This evaluation is generally associated with high uncertainty given the heterogeneous properties of the deep aquifers, which have hampered the comprehensive understanding of the hydrodynamic behavior evolution and the accurate identification of contamination sources and pollutant transport flows (Ayers, Westcot 1985; Edmunds et al. 2003; Kumar 2012; Konar et al. 2012; Russo, Lall 2017).

Numerous studies have reviewed the increasing risks from groundwater overdevelopment, focusing on the environmental risks associated with expanding groundwater exploitation, namely groundwater quality deterioration, associated ecological impacts, environmental degradation, and natural resource pollution (Hamed et al. 2014a-b; Mokadem et al. 2016; Zhang et al. 2017; Besser, Hamed 2019). Based on the results, prediction of the responses of these fragile resources to the emerging issues is related to natural conditions (background geochemical and climate) and anthropogenic perturbations (land use, exploitation, contamination), and the feasible remediation measures are constrained by several challenges. Once these aquifers are contaminated, remediation seems to be a challenging task given the cumulative hidden impacts that may induce long-term changes, depending on the inherent aquifer properties and the specific contaminant characteristics.

In southwestern Tunisia, as a large part of the Middle East and North Africa areas (MENA), the overexploitation of deep groundwater has attracted considerable attention (Guendouz et al. 1997; Edmunds et al. 2003; Kamel 2013; Hamed et al. 2014a-b; Hamed 2015; Mokadem et al. 2016; Besser et al. 2017, 2018, 2019, 2021; Besser, Hamed 2019; Dhaouadi et al. 2020, 2021). These works have highlighted various pieces of evidence of groundwater degradation leading to the gradual intensity of several socio-economic implications. The study area of the Tozeur and Kebili regions, characterized by harsh climatic conditions with less than 100 mm of precipitation (INM 2019), solely relies on groundwater resources to meet the

increasing demands, of which more than 82% is devoted to the agricultural sector (CRDA 2020). The hydrogeological system of the region is represented by the multi-layered SASS (Système Aquifère du Sahara Septentrional) aquifer system, consisting of two principal aquifers according to the lithologic variation, geological age, the distribution of aquifers and aquitards and hydrodynamic conditions: the Complex Terminal (CT) (Salinity ranging from 1.7 to 5.3 g/L) located in the Cretaceous and the Early tertiary porous deposits of the Continental Intercalaire (CI) in the thick Mesozoic-Early Tertiary sediments (temperatures from 35 to 78°C and salinity from 2.5 to 5.8 g/L) (Agoun 2005; Ben Brahim et al. 2012; Kamel 2013; Mokadem et al. 2016; Besser et al. 2017). The intensifying exploitation of these semi-confined to confined reservoirs, despite the low renewability potential under the present-day conditions (lack of surface water, scarce and irregular precipitations), induces a series of environmental issues that seem to be progressively irreversible (Kamel 2013; Hamed et al. 2014a-b; Besser, Hamed 2019, 2021).

Correspondingly, various actions of remediation have been adopted during the last two decades, such as international and national projects (PDES, APIOS, CES), sensibilization frameworks, periodic training programs for farmers via conferences, numerous formation sessions completed by field surveys with the association of local and regional institutions (CRDA, CRRAO, IRA), investment reinforcement, financial and administrative support with eco-benefits for water and soil savers, national valorization of the individual innovative alternative of environmental conservation, and several pilot stations for new water-saving techniques (Dhaouadi et al. 2021). However, the overexploitation of these natural resources has continuously increased from 393.3 Mm³ in 2010 to 418.64 Mm³ in 2019 for only 242.2 Mm³ of available resources in the Kebili region (from 162.38% to 172.84% of the exploitation ratio in 9 years) and from 176.5 Mm³ to 197.23 Mm³ for the same period in Tozeur area, where the available resources are of 208.4 Mm³ (an increase of 1.29% of the exploitation ratio per year). This has resulted in more severe environmental issues frequently measured and (or) observed during the last years (Hamed et al. 2014a-b; Besser et al. 2019, 2021).

Besides their ecological impacts, the inefficiency and inadequacy of environmental protection measures, taken until the present, threaten the economic income and the food security of the residents depending exclusively on agriculture for their livelihood. Thus, and regarding the complex open and partially known proprieties of these reservoirs; considering the frequent water stress repercussions and the lack of continuous large-scale data, a re-evaluation of the management strategies aiming for the rational exploitation of these low renewable resources and an accurate assessment of the ecological risks as well as the value of the rehabilitation measures is required based on several environmental, pedagogical, hydrogeological and petroleum studies conducted in the study area, coupled with field surveys.

In this context, this paper presents a careful review of the historical data in southern Tunisia about the amplitude of the emerging ecological concern resulting from the inadequate management of groundwater resources within the largest aquifer system of the Continental (CI) Intercalaire aquifer. It aims (1) to discuss the gradual potential and measured risks associated with groundwater exploitation and quality degra-

dation, (2) to outline the principal political, socio-economic, and institutional drivers of efficient monitoring systems to early predict further degradation, and (3) to present a synthesis of the relevant factors and processes governing fruitful exploitation and optimal productivity concerning the Eco-Eco dimensions, opening expanding research areas.

2. Groundwater vulnerability

Groundwater resources exhibit different vulnerability degrees depending on several natural and anthropogenic factors. Natural groundwater vulnerability relies on the recharge conditions and the impacts of the climate variability (Randall, Mulla 2001; Foster et al. 2002; Gurdak et al. 2007). Thus, the deep confined hydrogeological systems are considered particularly vulnerable to different forms of degradation and depletion regarding their low renewability and the insufficient amount of freshwater dilution, even if recharge flows are available (Wu, Hunkeler 2013; Freitas et al. 2015). The evaluation of this vulnerability, despite the various estimation methods and the increasing accuracy of the performed analyses, is ranking high, along with great uncertainties mainly related to the anisotropy of aquifer properties (intrinsic vulnerability), the great spatio-temporal variability of the most influencing factors, and the causal relationship between the natural system characteristics and the evolutionary external environment (risks, challenges, land use, land management, climatic oscillations, human exploitation) (Rickwood, Carr 2009; Hamed 2015; Besser, Hamed 2019; Burri et al. 2019).

In the study area, based on the review of the collected monitoring data and previously published research, the vulnerability of groundwater resources was evaluated via the usable amount or the exploitation ratio, which may not provide sufficiently accurate information about the evolution of the equilibrium balance of the natural ecosystem. Generally, the usable amount of groundwater represents the amount of groundwater that can be continuously exploited without any environmental issues. It defines the limits of the recharge-discharge ratio concerning the aptitude of the natural system to regain balance. However, for most countries globally, the question is no longer about the equilibrium status but about the limits of reversible-irreversible effects which cannot accurately be evaluated as the resilience of the natural system is inadequately qualitatively described and indirectly quantitatively assessed via indirect effects generally observed *a posteriori*. Additionally, given the multiple influencing factors for multi-layered, and the huge extent of the CI aquifer system understanding the hydrodynamic and geochemical transition of the system represents a huge participatory task that needs the agglomeration of large data sets of different water-controlling factors and water-dependent sectors to gain information about the intrinsic evolution of the system in response to natural and anthropogenic stimulation. This assessment is afflicted with additive constraints when the investigated resources are semi-confined transboundary low renewable resources under present-day conditions and with a slow response, such as the continental Intercalaire aquifer.

Historically, the abstraction from the CI aquifer has begun in the late 1970s (OSS 2003); prior to this time, the surface manifestations of underground water have played a fundamental role in human settlements and social development (Foggaras, and Mkael systems). This exploitation is variable at a regional scale

(Algeria 6.1 Bm³, Tunisia 0.72 Bm³, and Libya 0.95 Bm³; Fig. 1), depending upon accessibility (Edmunds et al. 1997, 2003; OSS 2003). Such variability may be explained by the different productive horizons in exploitation (geological structure, structural configuration of the multi-layered aquifer of CI) (Baba Ould 2005; OSS 2014; Petersen et al. 2014); despite this regional variability in the exploitation ratio from 78% to 216%, overall, the CI resources in the study area are in a state of overexploitation (CRDA 2017; Besser et al. 2019).

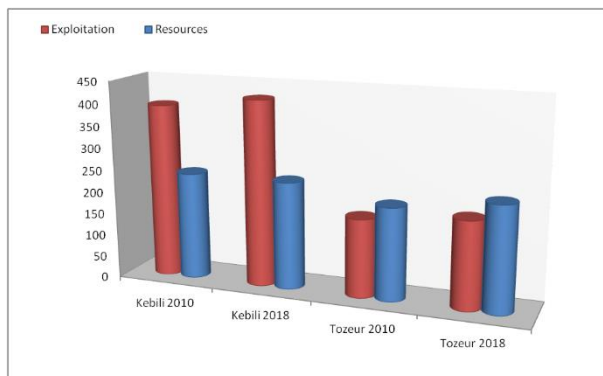


Fig. 1. Groundwater exploitation in the study area.

Besides the differences in exploitation among the three countries, the vulnerability of the hydrogeological system shows a local variability from 180% in the Tozeur area to more than 270% in the Kebili region, highlighting different degrees of resilience and, consequently, various corresponding risks. The degree of vulnerability of the aquifer, in this case, is evaluated according to various features, namely the presence of systematic control, exploitation rate, recharge conditions, climate impacts, water-dependent economy evolution, institutional and regulatory conditions. Nevertheless, for SW Tunisia, the lack of rigorous aquifer protection policies has led to progressively observed incidents related to the regional head decline and a permanent quality degradation. These effects are generally difficult to remediate considering the huge reservoir of the aquifer, the long residence times of CI water, and the physical inaccessibility to these deep confined resources.

The agglomeration of the results highlights the high level of vulnerability for decades, whereas the exploitation is continuously resulting in various environmental challenges discussed in the following sections.

3. Exploitation concerns about water table lowering

Frequent water shortage has resulted in the sharp growth of the exploitation of groundwater for different usages, consequently exceeding the carrying capacity of groundwater, especially in hot-dry areas with low annual rainfall, such as SW Tunisia, where the percentage of the humid period does not exceed 10% (Ferchichi 1996). This continuous abstraction to meet the agricultural demands (70% of the total regional demand for water) in southern Tunisia causes declining groundwater levels and aquifer replenishment (FAO 2020). Under natural conditions, the cycling period of deep groundwater is more than a thousand million

years (Edmunds et al. 2003); the deep groundwater resources that have been exploited are made mainly of paleo waters, which were recharged thousands or tens of thousands of years ago.

The water table evolution of the CI aquifer indicates that the groundwater level fell sharply, and the depression cones have been developed quickly due to continuous overexploitation (Edmunds et al. 1997; Ben Brahim et al. 2012; Hamed et al. 2014a). The water withdrawal amount shows a remarkable spatial distribution that exhibits a good correlation with the availability of complimentary water resources and the expansion of agricultural lands. The average water table decrease is 2 to 3 m/yr (OSS 2014), reaching 10 m locally in some regions of the Kebili field, where the situation becomes more critical with two or three water wells implemented in less than 100 m, such as in the case of Esteftimi (Besser et al. 2017). The cumulative impacts of these neighboring boreholes induced large depression cones and modified the local flow directions (Besser et al. 2019). According to previous studies, the hydrodynamic behavior of the CI groundwater system, regarding the complex lithologic properties of the multi-layered system and the multi-directional tectonic features, has become difficult to predict as the preferential pathways can be modified in response to the continuous exploitation, leading to a series of environmental problems such as inversion drainage from the Chotts aquifer downward to the deep reservoirs as well as for the shallow new-formed aquifer beneath the oasis agro-systems (Omar et al. 2019).

Based on the guidelines and the threshold of international water legislation, the evolution of the CI water table defines seriously overexploited areas with a restricted amount of overexploitation for those requiring urgent remediation and areas with increasing attention for those needing continuous examination. This classification in SW Tunisia considers the quasi total area of Tozeur and Kebili as a zone protected from further exploitation and the creation of new water wells. Unfortunately, the number of private water wells has exceeded 10,000 in 2020 (CRDA 2020). Given the growing use of solar power systems, the abstraction is no longer determined either with measures or estimations. Thus, these efforts should be completed with severe governmental and institutional control.

Groundwater withdrawal will impact all water-dependent ecosystems (requiring surface expression or water availability) with different geomorphologic features and flow mechanisms (Foster, Perry 2010; Eamus et al. 2015). In the studied area, the frequent inaccessibility to irrigation water has led to the expansion of private illegal water wells which, in turn, have induced uncontrolled exploitation adversely affected land productivity. In fact, the important quantities of delivered irrigation water for cultivated crops are largely above the recommended requirements leading to progressive waterlogging of poor water quality unsuitable for agriculture purposes. This quality, which represents a huge challenge, often attracts less consideration until the potential repercussions define irreversible impacts (Fig. 2).

The major issue constraining rehabilitation plans is related to the variable progressive responses of groundwater resources to increasing exploitation and continuous depletion on the anisotropic distribution

of physical proprieties of the hydrogeological system, aquifer dimensions, and boundary conditions (Konikow, Leake 2014; Besser et al. 2019), requiring a continental-scale mapping framework and expert knowledge to complete a shared task via a participative interdisciplinary approach.

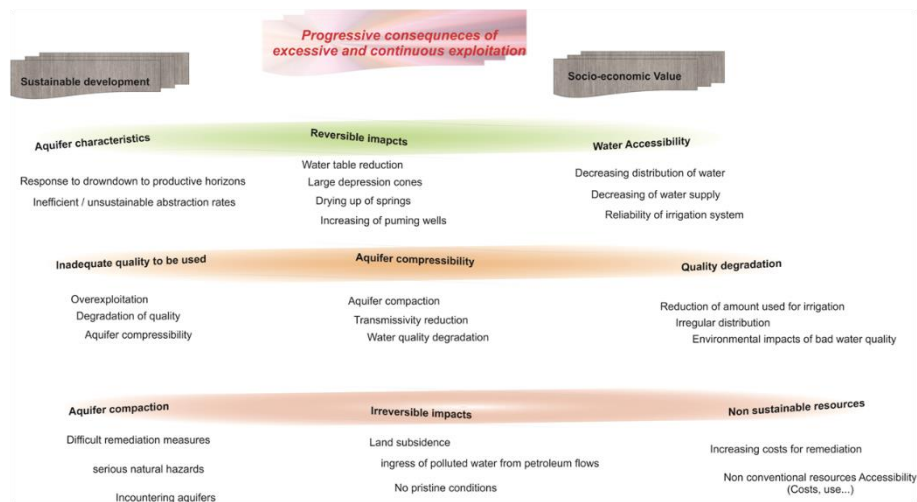


Fig. 2. Socio-economic and environmental drivers of groundwater exploitation.

4. Concerns about quality deterioration

Groundwater abstraction and pumping can alter natural flows and modify the small-scale water balance (hydrogeological cycle), increasing groundwater desiccation (Custodio 2005), defined by the process of groundwater rebound upon mining and pumping cessation, with likely implications for groundwater quality (Henton 1981). Pumping and continuous abstraction from deep aquifers have undoubtedly various impacts on groundwater recharge and flow movements and increase system vulnerability to incurable effects. The spatial distribution of this vulnerability mainly depends on the intrinsic aquifer characteristics, reservoir geometry, anthropogenic development, and field features (Khan et al. 2016; Russo, Lall 2017). In the case of fossil groundwater, such as the CI aquifer system, this evaluation includes the assessment of water chemistry evolution, concerning the paleoclimatic oscillations and the exploitation conditions. For the transboundary systems, such as the SASS multi-layered aquifer, local geological and tectonic features are to be considered, as well as the sedimentary-structural proprieties of the large-scale basins, which define the physical characterization of the aquifer, control the hydrodynamic behavior of groundwater, and, consequently, influence the different processes governing the distribution of water composition. However, the heterogeneity of the natural environment, coupled with the partially known aquifer characterization at a large basin, can make a straightforward characterization of many systems nearly impossible (Hakoun et al. 2017). This situation defines a growing challenge for remediation and rehabilitation efforts, despite the multiple studies and management plans related to the complexity of the system and the adequacy and accuracy of the collected data concerning water quality degradation, which remains generally elusive (Famiglietti 2014).

Table 1 shows a summary of the overall assessment of the measured and (or) observed quality problems of the CI aquifer. Increasing salinization and alkalization issues have been reported for more than 82% of

the total analyzed points. The major challenge for the continuous use of these waters is mainly related to the unclear trend of water quality and chemical composition evolution. Additionally, recent works have indicated that an important percentage of groundwater resources in the study area is enriched with trace elements (Besser, Hamed 2019).

Table 1. Improvements in water productivity.

Use		Criteria	Policy measures/ legislation	Analytical Soundness	Data availability/ cost	Institutional control	Decision of Stakeholders	
Consumptive fraction	Beneficial		Conservative measure of smart agriculture			Effective irrigation technique		
	Non beneficial		Eco-agriculture					
Non consumptive reusable fraction	Beneficial		Integrated management of water			Reduction of unproductive losses		
	Non beneficial		Water harvesting					

The changes in groundwater quality are caused by the dual impacts of humans and the intrinsic factors of the hydraulic system, namely mixing and hydraulic continuity (Sheng et al. 2020). A significant decline in groundwater level changes the stress state of the groundwater system and accelerates vertical and horizontal groundwater migration, possibly resulting in the migration of poor-quality groundwaters from deeper reservoirs and (or) from the Chotts brackish aquifer. Additionally, significant correlations have been found among soil degradation, desertification, vegetation ecosystem destruction, and the excessive development and use of groundwater. Besser et al. (2021) indicated that during the last 20 years, the quality of CI water was not suitable for irrigation purposes, which has resulted in fertility losses. These findings are confirmed by field investigations done by Dhaouadi et al. (2021) and justified by the GIS-based models developed by Besser and Hamed (2021). The distribution of the most sensitive areas for potential land degradation is consistent with the spatial evolution of groundwater abstraction (Sepehr et al. 2007; Maroufpoor et al. 2018). Adequate soil moisture is the basic condition required for healthy vegetation growth without physiological stresses or oasis shrinking (Peng et al. 2014; Sheng et al. 2020; Besser et al. 2017). Hence, the long-term decline in groundwater levels has further led to a reduction in crop yield quality, as well as the degradation of wind break and sand fixation oases and forests, among other serious ecological problems in the region (Zammouri et al. 2007; Besser et al. 2017, 2021).

5. Concerns about land subsidence

Land subsidence caused by the over exploitation of groundwater has become an increasingly serious challenge in many arid and semi-arid regions (Sheng et al. 2020). Previous studies (Hamed et al. 2014a-b; Cao et al. 2016; Zhang et al. 2017) have demonstrated that there is an important causality link between land subsidence and groundwater level decrease, especially in the hot dry areas of China and the MENA regions. In these water-deficient areas, extensive groundwater pumping induces a progressive compaction of

sediments after water subtracting from porous horizons, leading to land subsidence (Han et al. 2014; Sheng et al. 2020). The subsequent land use changes and the cumulative impacts of anthropogenic activities via gradual alteration of the equilibrium of the hydrogeological system (decompression, geometry) induce natural subsidence, which is enhanced in human-induced sensitive areas. The rehabilitation of this form of degradation is generally difficult, time-consuming, and expensive as it requires an accurate evolution of the subsidence rate and the exploitation amount for determining the required pressure to regain pristine conditions in view of the subterranean architecture (Figs. 3 and 4).

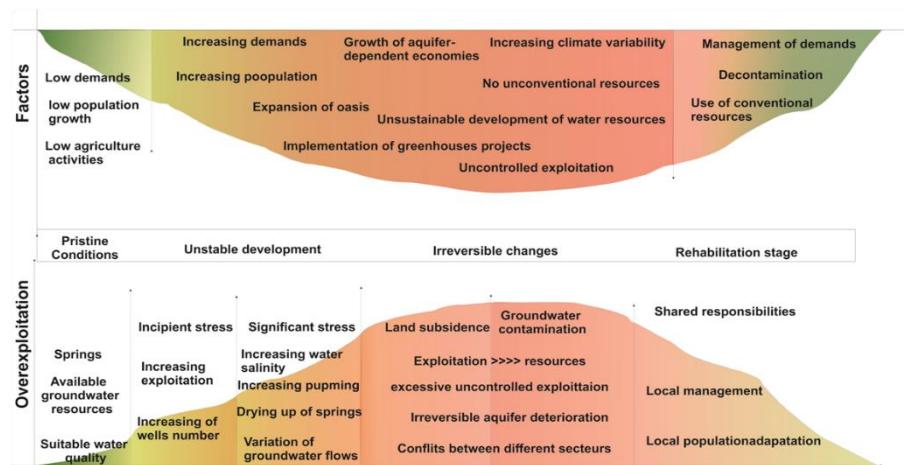


Fig. 3. Progressive groundwater quality degradation in the study area.



Fig. 4. Observed degradation issues: A. Land subsidence (Hamed et al. 2014a); B. Petroleum contamination (Besser, Hamed 2019).

According to a previous study in the same area, the sediments of a fluvio-deltaic complex, such as the mega sequence of the Lower Cretaceous, are susceptible to high compressibility and significant natural subsoil compaction and aeration (Syvitski et al. 2009). These properties define the high intrinsic vulnerability to the various effects of human activities, namely excessive pumping and the continuous exploitation of deep aquifers (Kamel 2013; Hamed 2015; Zhang et al. 2017).

Land subsidence is defined by the ultimate consequence resulting from the agglomeration of the cumulative impacts exceeding the recommended limits for natural equilibrium regeneration. It is a sluggish process with slow progressive evolution in response to several time-dependent factors and processes mainly related to gradual land use changes (Hamed et al. 2014a-b). Overexploitation induces a progressive overpressure dissipation from clay-rich sediments, which start to compact according to a time-dependent secondary consolidation. This slow evolution highlights the importance of the resilience of natural systems to consecutive uncontrolled stimulations up to the ultimate tolerance limits (Fig. 3)

Correspondingly, the overexploitation of groundwater in the study area was amplified by an extensive area of land subsidence in 2013 at the Douz region (Kebili-SW Tunisia), related to a local piezometric drop of about 2.5 m (Hamed et al. 2014a). This subsidence indicated that the exploitation has exceeded the regenerative capacity of the aquifer and that the porosity caused by the continuous abstraction from the CI aquifer resulted in an unrecoverable compaction of the permeable horizons, which cannot support the charge of the overlain sediments, consequently inducing a fall of the upper sedimentary column (Hamed et al. 2014a-b).

6. Concerns about water contamination

Aquifer intrinsic vulnerability to different contamination types and sources is amplified by the increasing risks for groundwater quality deterioration relative to the anthropogenic environment. The complex links between the natural dynamics of the successive processes of the hydrogeological cycle can be significantly modified by man-induced physical alterations, water resources exploitation, and industrial or chemical pollution. Deep aquifers are generally considered, regarding their depth and limited outcrop at the recharge areas, less prone to these types of contamination (Essefi et al. 2013; Besser, Hamed 2019). These properties, which may ensure a relative protection of these reservoirs, represent, at the same time, a real challenge for remediation as once the aquifer is contaminated, it seems difficult to reliably evaluate the amplitude of contamination, the diffusion of pollution, the pollutant inflow into the aquifer, and the groundwater quality deterioration (Conant et al. 2004; Chapman, Parker 2005; Freitas et al. 2015; Moeck et al. 2017; Burri et al. 2019).

Despite the various types of investigation and the various methods commonly used to examine a likely incident, only a fraction of the flow and some transport pathways can be identified (Göppert, Goldscheider 2008; Robert et al. 2012). The effects of anthropogenic practices (land development, natural resources exploitation) on groundwater in terms of pollutant diffusion, multi-point sources, inflow movement, and transport modeling are various, revealing increasing risks from reversible impacts to incurable effects. These likely consequences are discussed in a number of scientific papers to underscore the myriad of issues that can arise when anthropogenic controls are present on top of natural controls (Gonçalves et al. 2007; Hakoun et al. 2017; Burri et al. 2019) (Fig. 3).

The query about the magnitude of the released concentrations of the pollutants into the aquifers and the potential recovery of the background safe contents, as well as the time required to reset the pristine conditions, is complex. These issues require detailed studies based on modeling the response of the aquifers, developed through accurate analysis of the different scenarios of system evolution. The uncertainty, related to the unpredictable response of the aquifer due to the anisotropic characteristics of the subterranean basin, is constraining the management of deep aquifer resources (Edmunds et al. 2003; Baba Ould 2005; Kamel 2013; Besser, Hamed 2021). Thus, to adjust certain physical and chemical properties of these deep reservoirs, a hierarchical list of the contaminants is required, containing the description of the sites altered by multiple pollutants and the areas requiring rapid clean-up actions.

In the study area, despite the serious degradation measured and observed for CI waters, the exploitation has been continuous, largely threatening these critical resources. Hamed (2015) and Besser and Hamed (2021) have indicated a progressively emerging issue related to the contamination of the CI aquifer by continuous oil/gas flow, which may be considered the ultimate impact of groundwater mismanagement (Besser et al. 2017; Besser, Hamed 2019). The contamination was observed at the canals distributing hot waters as well as along the atmospheric cooling systems, forming a unique hydrocarbon seepage mixed with groundwater resources in the MENA region. This contamination is confirmed by the results of the analyses via the GC-MS technique, which indicate the presence of different pollutants such as octacosane, 1,2-benzenedicarboxylic acid, dodecyl ester, hexadecanoic acid, trimethylsilyl ester, cyclooctasiloxane, and hexadecamethyl. The concentrations of asphalt exceeded 4 g/L in CI water, and the total petroleum amount reached 16 mg/kg for agricultural lands in the contaminated zone (Besser et al. 2019; Besser, Hamed 2019).

Different hypotheses have been put forward to evaluate the migration pathways by which petroleum enters aquifers, based on the tectonic evolution of the region, the local structural and geological features of the region, and the hydrodynamic and hydrogeological properties of the water-bearing system. The paleogeological and tectonic history of the region is characterized by numerous active tectonic and sedimentary phases. Faults and fractures created by the successive tectonic processes and hydraulically induced fractures related to lateral and vertical changes of the aquifer geometry and lithology may act as permeable conduits controlling pathways of fluid migration. These preferential pathways have been investigated in several geophysical studies (Hlailiem 1999; Said et al. 2011; Zouaghi et al. 2011; Soua 2014), confirming the presence of numerous local-scale faults in the contaminated field that may play a major role in the distribution of pressure and upward-moving fluids. These multidimensional faults create complex subsurface drainage systems, ensuring hydraulic continuity between the different water-bearing strata. These conduits ensure the migration of petroleum under huge pressure from deeper reservoirs (Mejri et al. 2006; Akrouf et al. 2012), especially in the context of the great charge difference in comparison with the upper, overexploited aquifer.

Irrespective of the multiple ways by which the pollutants enter the aquifers, the continuous contamination and the diffusion of pollutant flows are consistent with the increasing exploitation of the aquifer (Figs. 3

and 4). This pollution is irreversible considering the partially known properties of the aquifer and the unstable properties of petroleum products.

7. Synthesis

This literature review of the likely consequences of natural resources exploitation highlights the strong causal links between anthroposocial drivers and the processes of land degradation. This explicit evaluation is of paramount importance to provide insights into the political and institutional constraints for appropriate natural resources conservation. This study, conducted in southern Tunisia, outlines the necessity of a quantitative multi-criteria index of risk evaluation of groundwater exploitation that summarizes the partially known features of the open and the complex subterranean system. It proves that the responses of the groundwater circulation system to the external environmental perturbations range from relative disequilibrium strengths to various incurable changes with progressive intensity and severity, requiring an environmental sensitivity baseline study.

This review is urgently required for the CI aquifer in southern Tunisia, a huge groundwater system of crucial ecological and economic importance currently facing various degradation issues. The following question remains: What are the actions and measures to provide for the next step to at least conserve the current disequilibrium of the balanced ecological vs. socio economic values of these resources?

In the last decades, different approaches have been adopted in southern Tunisia to mitigate the impacts of the continuous exploitation of CI groundwater resources. More than 10 national and international projects have been developed, different techniques of irrigation have been used, along with renewable energy system implementation, the creation of new irrigated parcels, experiences and pilot stations, and the development of a wastewater station. However, the environmental issues have grown with the continuous agricultural expansion. This unbalance highlights the low effectiveness of the chosen approach and the lack of rigorous control to attend the optimal adhesion to the planned strategies. Such inadequate management results in more serious issues.

Currently, as the situation has reached a critical status that requires effective and urgent actions, the remediation should be defined by a careful design of hierarchical actions comprising projects, programs, plans, policies, and individual initiatives ensuring full integration or relevant biophysical, economic, social, and political considerations; this would facilitate wider scenarios of protection and exploitation (Table 1).

Sivapalan et al. (2012) and Di Baldassarre et al. (2013) indicated that the ambiguous aspects of the political strategies on the economic efficiency of water resources use define a new research field related to socio-hydrology, the self-organizing managing efforts along with collective actions. In the study area, despite the crucial importance of groundwater for social and economic development, socio-ecological studies coupled with the findings of socio-environmental modeling, socio-hydrology, human-natural system modeling, and behavioral economics (Camerer et al. 2004; Filatova et al. 2015; Liu et al. 2016), have not yet been applied (Fig. 5).

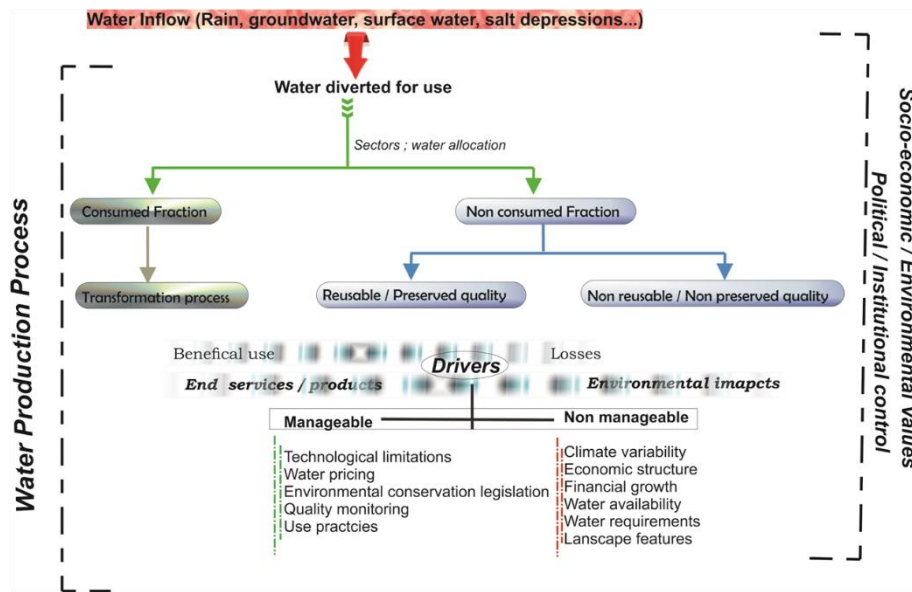


Fig. 5. Water productivity evaluation criteria.

7.1. Economic efficiency vs. environmental security

Agricultural water productivity as a broad concept is expressed in terms of the water benefit output by the water volume input (Bossio et al. 2010). This encompasses biophysical, environmental, social, and economic aspects for the nexus exploitation-production-sustainability. The assessment of this productivity requires the review of the involved values at different scales (plant field, farm, irrigation network, basin, agro-economic zone) and for different stakeholders (farmers, system managers, policy makers) (Amede et al. 2009; Descheemaeker et al. 2009; Gebreselassie et al. 2009; Haileslassie et al. 2009; Peden et al. 2009; Bossio et al. 2010). The concept of water productivity further includes a variety of options of water use related to scales of irrigated fields, systems of agricultural development, cultural practices, and water access security (Maxwell, Wiebe 1999).

Correspondingly, to increase water productivity in the presence of important water allocations, the three important terms, namely waster use efficiency (water productivity), water scarcity (water availability, cycle resilience, storage), and water requirements, should be identified regarding the water-dependent sector and the corresponding economic value before embarking on assessing the global economic equilibrium. The premise of sustainable water management relies on the flexible adaptation of these global notions at small-scale proprieties of the ecosystem, referring to a number of physical, chemical, and biological changes in natural resources and landscapes. The key factor governing the success or failure of these actions refers to obtaining reliable information about the obvious quantifiable effects and reducing the ambiguity concerning the insidious impacts frequently detected *a posteriori* (Barker et al. 2003; Bossio et al. 2010; Liu et al. 2016).

Regarding agro-based countries such as Tunisia, where water exploitation increases with high and low water productivity, several cautions should be attributed to differentiate between the highest short-term crop water productivity and the optimal water productivity, taking into account the ratio of the consumed water

to the lost fraction, the requirements of the irrigated crops, the harvest index, and the runoff released into the environment.

The irrigation technique is one of the most important factors conditioning water productivity and water use efficiency. In southwestern Tunisia, agricultural performance has gained crucial importance in management plans (Hatfield et al. 2001; Stocking 2003; Bossio et al. 2010). The comparative analysis of the efficiency of irrigation with respect to water productivity in monetary terms indicates that the micro-techniques increase economic productivity while optimizing water use according to the requirements of the cultivated crops (Dhaouadi et al. 2020, 2021). These techniques have, in turn, crucial importance for sustaining land conservation and soil fertility; they inhibit the development of different forms of land degradation (CEC, salinization, acidification, nutrient depletion). However, different conditions may constrain the appropriate adoption of these techniques in the study area due to the lack of adequate large datasets for rainfall, evapotranspiration, and soil properties (Oweis, Hachum 2003).

The economic analysis in southern Tunisia is also constrained by the non-continuous monitoring data concerning livestock, non-conventional water resources, and soil properties modification. This intermittent data collection and the non-reliable information from participants inhibit a clear assessment of a number of profitability indices, namely benefit-cost ratio, non-productive value, and internal rate of return, which are of crucial importance for the evaluation of water use efficiency and, consequently, water conservation plans (Figs. 5, 6). The lack of efficient communication among social, scientific, and institutional committees needs to be considered.



Fig. 6. Impacts of groundwater quality on agricultural activities (Besser, Hamed 2019).

7.2. Rehabilitation measures

Despite the various papers discussing the evolution of groundwater chemistry in response to natural factors and anthropogenic perturbations in southern Tunisia, such discussion is generally restricted to the first two categories explained in Table 2. Rehabilitation measures, however, require a dynamically comprehensive analysis to provide a scientific decision-making basis for social and economic development (Barker et al. 2003; Oweis, Hachum 2003).

The successful management depends on a participatory approach in which farmers play the pivotal role to regain confidence and to create a reliable database, the baseline step for further management efforts (Gigar-Reverdin, Gihad 1991; Sileshi et al. 2003; McGregor 2004a). Additionally, institutional organizations

re-organize accessibility to water and soil resources to obtain a clear image of the degradation drivers at local scale. These governmental participants should encourage the investment into degraded land and contaminated sites with more financial, technical, and administrative support. The participatory methods emphasize training and building capacity for voluntary engagement in conservation efforts within social and political drivers. The valorization of the indigenous knowledge of farmers and their individual initiative represents, in addition, a relevant alternative to enhance water resources conservation based on the cultural heritage of farmers. Pricing irrigation water based on water efficiency, irrigation water transfer; runoff water harvesting systems, the importance of the cultivated types, and the adoption of water-soil saving techniques (Table 2) further constitutes an important alternative to mitigate the emerging issues of water degradation.

Table 2. Environmental conservation approach.

Comprehensive risk situation of groundwater exploitation and use				
Groundwater system conditions		Groundwater exploitation and use		Groundwater environmental problems
Hydraulic conductivity Groundwater quantity exploitable Aquifer thickness Groundwater depth Aquitard thickness		Groundwater exploitation Artificial recharge degree of exploitation		Decrease of piezometric level Degradation of water quality Land subsidence Groundwater pollution
Rational groundwater evaluation				
Risk assessment	Integrated planning	Reasonable demand management	Reasonable aquifer management	Reasonable resources management
	Socio-economic value Ecological value climatic uncertainty	Increase of efficiency of water use Agricultural development (modern techniques, land use management)	Aquifer artificial recharge Decrease of pumping wells	Use of treated wastewater
Political regulatory constraints				
Water pricing reform		Water resources tax		New implementation
Function of negative impacts and conditions of use		Efficiency and effectiveness Hierarchical conditions		Acceptability Benefits (ecological, economic)

The renewable energy systems can, in turn, be used to purify the treated wastewater to reduce the costs. Solar and wind energy can also be applied for the managed aquifer recharge, especially in the contaminated field, to restore the pressure of the groundwater in the deeper aquifer and inhibit the migration of petroleum from Jurassic and Paleozoic reservoirs. Obviously, the first step to inhibit further diffusion of the contamination is increasing the groundwater recharge to presume the equilibrium conditions. Some geologic storage structures in the region of interest for underground reservoir construction may reduce depression cones and ground subsidence. This may resolve the problem of groundwater pollution diffusion by regulating groundwater pressure. The implementation of inter-basin water transfer structures represents an effective method for achieving groundwater recharge, alleviating water scarcity during water shortage periods in spring and summer (Figs. 6 and 7).

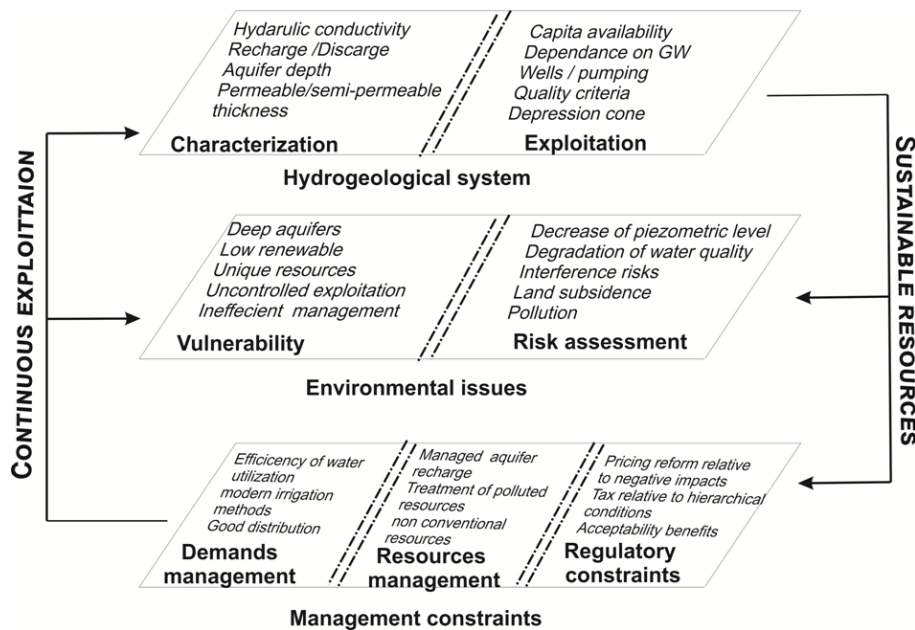


Fig. 7. Rehabilitation measures.

Pretty et al. (2006), Noble et al. (2006), and Bossio et al. (2010) have indicated that the rehabilitation of degraded sites using resource conserving techniques may achieve sustainable outcomes, especially for smallholder agricultural systems, with increasing yields and lower investments (Figs. 6 and 7). Thus, a detailed characterization of the study area should be conducted at local scale to implement a flexible management plan.

Additionally, the used irrigation technique and irrigation scheduling constraint the effectiveness of the water resources management. Thus, an evaluation of the requirements of the cultivated crops is essential to redistribute the quantity with the lowest loss of irrigation water to evaporation (“more crop less drop”). Financial and engineering support for farmers to implement new localized irrigation techniques is required.

All these alternatives should be completed with rigorous control and the continuous training of landowners (Fig. 5 and Table 2). The policy of local-level intervention represents the backbone of resource conserving and rehabilitation programs. The re-organization of institutional and political dimensions and values is of paramount importance for the long-term environmental support adoption of a green-revolution type package of complementary inputs in economies with low agriculture. The involvement of non-agricultural organisms, farmers, and water-use associations (farm advisors) derives a community-based management to ensure long-term land resources sustainability. This participatory approach strengthens the links among farmers, advisors, researchers, economists, and policy makers.

References

Agoun A., 2005, The continental intercalaire aquifer at the Kébili Geothermal Field, Southern Tunisia, [in:] Proceedings World Geothermal Congress, Antalya, Turkey, April 24-29, available online <https://www.geothermal-energy.org/pdf/IGAstandard/WGC/2005/1922.pdf> (data access 01.06.2022).

- Akrout D., Ahmadi R., Mercier E., Montacer M., 2012, Natural hydrocarbon accumulation related to formation overpressured interval; Study case is the Saharan platform (Southern Tunisia), *Arabian Journal of Geosciences*, 5, 849-857, DOI: 10.1007/s12517-011-0287-6.
- Amede T., Geheb K., Douthwaite B., 2009, Enabling the uptake of livestock-water productivity interventions in the crop-livestock systems of sub-Saharan Africa, *Rangeland Journal*, 31 (2), 223-230, DOI: 10.1071/RJ09008.
- Ayers R.S., Westcot D.W., 1985, Water quality for agriculture, FAO Irrigation and Drainage, Paper 29, Food and Agriculture Organization, Rome, available online <https://www.fao.org/3/t0234e/t0234e00.htm> (data access 10.06.2022).
- Baba Ould S.M., 2005, Recharge et paleorecharge du système aquifère du Sahara septentrional, Thèse de Doctorat en Géologie, Université De Tunis El Manar, 261 pp.
- Barker R., Dawe D., Inocencio A., 2003, Economics of water productivity in managing water for agriculture, [in:] *Water Productivity in Agriculture: Limits and Opportunities for Improvement*, J.W. Kijne, R. Barker, D. Molden (eds.). International Water Management Institute, 19-35.
- Ben Brahim F., Makni J., Bouri S., 2012, Properties of geothermal resources in Kebilli region, Southwestern Tunisia, *Environmental Earth Sciences*, 69, 885-897, DOI: 10.1007/s12665-012-1974-7.
- Besser H., Dhaouadi L., Hadji R., Hamed Y., Jemmali H., 2021, Ecologic and economic perspectives for sustainable irrigated agriculture under arid climate conditions: An analysis based on environmental indicators for southern Tunisia, *Journal of African Earth Sciences*, 177, DOI: 10.1016/j.jafrearsci.2021.104134.
- Besser H., Hamed Y., 2019, Causes and risk evaluation of oil and brine contamination in the Lower Cretaceous Continental Intercalaire aquifer in the Kebili region of southern Tunisia using chemical fingerprinting techniques, *Environmental Pollution Journal*, 253, 412-423, DOI: 10.1016/j.envpol.2019.07.020.
- Besser H., Hamed Y., 2021, Environmental impacts of land management on the sustainability of natural resources in Oriental Erg Tunisia, North Africa, *Environment, Development and Sustainability*, 23, 11677-11705, DOI: 10.1007/s10668-020-01135-9.
- Besser H., Mokadem N., Redhaouia B., Hadji R., Hamad O., Hamed Y., 2018, Groundwater mixing and geochemical assessment of low enthalpy resources in the geothermal field of Southwestern Tunisia, *Euro-Mediterranean Journal for Environmental Integration*, 3, 16, DIO: 10.1007/s41207-018-0055-z.
- Besser H., Mokadem N., Redhaouia B., Rhimi N., Khelifi F., Ayadi Y., Omar Z., Bouajila A., Hamed Y., 2017, GIS-based model evaluation of groundwater quality and estimation of soil salinization and land degradation risks in arid Mediterranean site (SW Tunisia), *Arabian Journal of Geosciences*, 10, 350, DOI: 10.1007/s12517-017-3148-0.
- Besser H., Redhaouia B., Bedoui S., Ayadi Y., Khelifi F., Hamed Y., 2019, Geochemical, isotopic and statistical monitoring of groundwater quality: assessment of the potential environmental impacts of the highly polluted water resources in Southwestern Tunisia, *Journal of African Earth Sciences*, 153, 144-155, DOI: 10.1016/j.jafrearsci.2019.03.001.
- Bossio D., Geheb K., Critchley W., 2010, Managing water by managing land: addressing land degradation to improve water productivity and rural livelihoods, *Agricultural Water Management*, 97 (4), 536-542, DOI: 10.1016/j.agwat.2008.12.001.
- Burri N.M., Weatherl R., Moeck C., Schirmer M., 2019, A review of threats to groundwater quality in the Anthropocene, *Science of the Total Environment*, 684, 136-154, DOI: 10.1016/j.scitotenv.2019.05.236.
- Camerer C.F., Ho T.-H., Chong J.-K., 2004, A cognitive hierarchy model games, *The Quarterly Journal of Economics*, 119 (3), 861-898, DOI: 10.1162/0033553041502225.
- Cao Y., Tang C., Song X., Liu C., Zhang Y., 2016, Identifying the hydrochemical characteristics of rivers and groundwater by multivariate statistical analysis in the Sanjiang Plain, China, *Applied Water Science*, 6 (2), 169-178, DOI: 10.1007/s13201-014-0215-5.
- Chapman S.W., Parker B.L., 2005, Plume persistence due to aquitard back diffusion following dense nonaqueous phase liquid source removal or isolation, *Water Resources Research*, 41 (12), DOI: 10.1029/2005WR004224.
- Chen Q., Fan G., Na W., Liu J., Cui J., Li H., 2019, Past, present, and future of groundwater remediation research: a scientometric analysis, *Interantional Journal of Environmental Research and Public Health*, 16 (20), 3975, DOI: 10.3390/ijerph16203975.

- Conant J.B., Cherry J.A., Gillham R.W., 2004, A PCE groundwater plume discharging to a river: influence of the streambed and near-river zone on contaminant distributions, *Journal of Contaminant Hydrology*, 73 (1-4), 249-279, DOI: 10.1016/j.jconhyd.2004.04.001.
- Costales A., Gerber P., Steinfeld H., 2006, *Underneath the Livestock Revolution*, Food and Agriculture Organization (FAO), Rome, Italy, available online <https://www.fao.org/3/a0255e/a0255e02.pdf> (data access 01.06.2022).
- CRDA, 2017, *Kebili en chiffres, Rapport interne*, Commissariat Régional du Développement Agricole.
- CRDA, 2018, *Kebili en chiffres, Rapport interne*, Commissariat Régional du Développement Agricole.
- CRDA, 2020, *Kebili and Tozeur en chiffres. Internal report*, Commissariat Régional du Développement Agricole.
- Custodio E., 2005, Intensive use of groundwater and sustainability, *Ground Water*, 43 (3), p. 291.
- David S., Oweis T.Y., Pasquale S., Kijne J.W., Hanjra M.A., Bindraban P.S., Bouman B.A.M., Cook S.E., Erenstein O., Farahani H., Hachum A., Hoogeveen J., Mahoo H.F., Nangia V., Peden D.G., Sikka A.K., Silva P., Turrall H., Upadhyaya A., Zwart S., 2007, Pathways for increasing agricultural water productivity, [in:] *Water for Food, Water for Life: A Comprehensive Assessment of Water Management in Agriculture*, D. Molden (ed.), Earthscan, International Water Management Institute, 279-310.
- Descheemaeker K., Raes D., Nyssen J., Poesen J., Haile M., Deckers J., 2009, Vegetation restoration on degraded hillslopes leads to groundwater recharge and increased water productivity at the landscape scale in semiarid highland areas in northern Ethiopia, *Rangeland*, 31, 237-249.
- Descheemaeker K., Raes D., Nyssen J., Poesen J., Haile M., Deckers J., 2009, Changes in water flows and water productivity upon vegetation regeneration on degraded hillslopes in northern Ethiopia: a water balance modelling exercise, *Rangeland Journal*, 31 (2), 237-249, DOI: 10.1071/RJ09010.
- Dhaouadi L., Besser H., Karbout N., Al-Omran A., Wassar F., Whba M.S., Yaohu K., Hamed Y., 2021, Irrigation water management for sustainable cultivation of date palm, *Applied Water Science*, 11, 171, DOI: 10.1007/s13201-021-01507-0.
- Dhaouadi L., Nissaf K., Besser H., Ben Maachia S., 2020, *Journal of new sciences, Agriculture and Biotechnology*, 77 (6), 4533-4542.
- Di Baldassarre G., Viglione A., Carr G., Kuil L., Salinas J.L., Blöschl G., 2013, Socio-hydrology: conceptualising human-flood interactions, *Hydrology and Earth System Sciences*, 17 (8), 3295-3303, DOI: 10.5194/hess-17-3295-2013.
- Droogers P., Aerts J., 2005, Adaptation strategies to climate change and climate variability: a comparative study between seven contrasting river basins, *Physics and Chemistry of the Earth, Parts A/B/C*, 30 (6-7), 339-346, DOI: 10.1016/j.pce.2005.06.015.
- Eamus D., Zolfaghar S., Villalobos-Vega R., Cleverly J., Huete A., 2015, Groundwater-dependent ecosystems: recent insights from satellite and field-based studies, *Hydrology and Earth System Sciences*, 19 (10), 4229-4256, DOI: 10.5194/hess-19-4229-2015.
- Edmunds W.M., Guendouz A.H., Mamou A., Moulla A., Shand P., Zouari K., 2003, Groundwater evolution in the Continental Intercalaire aquifer of southern Algeria and Tunisia: trace element and isotopic indicators, *Applied Geochemistry*, 18 (6), 805-822, DOI: 10.1016/S0883-2927(02)00189-0.
- Edmunds W.M., Shand P., Guendouz A.H., Moulla A.S., Mamou A., Zouari K., 1997, Recharge characteristics and groundwater quality of the Grand Erg Oriental basin, *British Geological Survey, final report*, 7 pp.
- Essefi E., Tagorti M.A., Tourir J., Yaich C., 2013, Hydrocarbons migration through groundwater convergence toward saline depressions: a case study, Sidi El Hani Discharge Playa, Tunisian Sahel, *International Scholarly Research Notices*, DOI: 10.1155/2013/709190.
- Famiglietti J.S., 2014, The global groundwater crisis, *Natural Climate Change*, 4, 945-948, DOI: 10.1038/nclimate2425.
- FAO, 2020, *Transformer les systèmes alimentaires pour une alimentation saine et abordable*, Food Agriculture Organization, available online <https://www.fao.org/publications/sofi/2020/fr/> (data access 01.06.2022).
- Ferchichi A., 1996, *Etude climatique en Tunisie présaharienne*, *Medit*, 7 (3), 46-53.
- Filatova T., Polhill J.G., van Ewijk S., 2015, Regime shifts in coupled socio-environmental systems: Review of modelling challenges and approaches, *Environmental Modelling and Software*, 75, 333-347, DOI: 10.1016/j.envsoft.2015.04.003.

- Foster S., Hirata R., Gomes D., D'Elia M., Paris M., 2002, Groundwater Quality Protection: A Guide for Water Utilities, Municipal Authorities, and Environment Agencies, World Bank Group, available online <https://openknowledge.worldbank.org/handle/10986/13843> (data access 01.06.2022).
- Foster S.S.D., Perry C.J., 2010, Improving groundwater resource accounting in irrigated areas: a prerequisite for promoting sustainable use, *Hydrogeology Journal*, 18, 291-294, DOI: 10.1007/s10040-009-0560-x.
- Fraiture C., Wichelns D., Rockström J., Kemp-Benedict E., Eriyagama N., Gordon L.J., Hanjra M.A., Hoogeveen J., Huber-Lee A., Karlberg L., 2007, Looking ahead to 2050: scenarios of alternative investment approaches, [in:] *Water for Food, Water for Life: A Comprehensive Assessment of Water Management in Agriculture*, D. Molden (ed.), Earthscan, International Water Management Institute, 91-145.
- Freitas J.G., Rivett M.O., Roche R.S., Durrant M., Walker C., Tellam J.H., 2015, Heterogeneous hyporheic zone dechlorination of a TCE groundwater plume discharging to an urban river reach, *Science of the Total Environment*, 505, 236-252, DOI: 10.1016/j.scitotenv.2014.09.083.
- Gebreselassie S., Peden D.G., Haileslassie A., Mpairwe D.R., 2009, Factors affecting livestock water productivity: animal scale analysis using previous cattle feeding trials in Ethiopia, *Rangeland Journal*, 31 (2), 251-258, DOI: 10.1071/RJ09011.
- GIEC, 2007, Bilan 2007 des changements climatiques. Contribution des Groupes de travail I, II et III au quatrième Rapport d'évaluation du Groupe d'experts intergouvernemental sur l'évolution du climat, GIEC, Genève, Suisse, 103 pp.
- Gigar-Reverdin S., Gihad E.A., 1991, Water metabolism and intake in goats, [in:] *Goat Nutrition*, P. Morand-Fehr (ed.), Pudoc: Wageningen, Germany, 37-45.
- Gonçalves J.M., Pereira L.S., Fang S.X., Dong B., 2007, Modelling and multicriteria analysis of water saving scenarios for an irrigation district in the upper Yellow River Basin, *Agricultural Water Management*, 94 (1-3), 93-108, DOI: 10.1016/j.agwat.2007.08.011.
- Göppert N., Goldscheider N., 2008, Solute and colloid transport in karst conduits under low- and high-flow conditions, *Groundwater*, 46 (1), 61-68, DOI: 10.1111/j.1745-6584.2007.00373.x.
- Guendouz A., Moulla A.S., Edmunds W., Shand P., Poole J., Zouari K., Mamou A., 1997, Paleoclimatic information contained in groundwater of the grand erg oriental. N. Africa, [in:] *Proceedings of Symposium*, International Atomic Energy Agency, Vienna, 349.
- Gurdak J.J., Hanson R.T., McMahon P.B., Bruce B.W., McCray J.E., Thyne G.D., Reedy R.C., 2007, Climate variability controls on unsaturated water and chemical movement, High Plains aquifer, USA, *Vadose Zone Journal*, 6 (3), 533-547, DOI: 10.2136/vzj2006.0087.
- Haileslassie A., Peden D., Gebreselassie S., Amede T., Descheemaeker K., 2009, Livestock water productivity in mixed crop-livestock farming systems of the Blue Nile basin: assessing variability and prospects for improvement, *Agricultural Systems*, 102 (1-3), 33-40, DOI: 10.1016/j.agsy.2009.06.006.
- Hakoun V., Orban P., Dassargues A., Brouyère S., 2017, Factors controlling spatial and temporal patterns of multiple pesticide compounds in groundwater (Hesbaye chalk aquifer, Belgium), *Environmental Pollution*, 223, 185-199, DOI: 10.1016/j.envpol.2017.01.012.
- Hamed Y., 2015, Les ressources hydriques en Tunisie et impact des changements climatiques. Editions europeennes universitaires, Université de Gabès, Tunis, 380 pp.
- Hamed Y., Ahmadi R., Demdoun A., Bouri S., Gargouri I., Dhia H.B., Al-Gamal S.A., Laouar R., Choura A., 2014a, Use of geochemical, isotopic, and age tracer data to develop models of groundwater flow: a case study of Gafsa mining basin-Southern Tunisia, *Journal of African Earth Sciences*, 100, 418-436, DOI: 10.1016/j.jafrearsci.2014.07.012.
- Hamed Y., Ahmadi R., Hadji R., Mokadem N., Ben Dhia H., Ali W., 2014b, Groundwater evolution of the continental intercalaire aquifer of southern Tunisia and a part of southern Algeria: use of geochemical and isotopic indicators, *Desalination and Water Treatment*, 52 (10-12), 1990-1996, DOI: 10.1080/19443994.2013.806221.
- Han D., Tong X., Currell M.J., Cao G., Jin M., Tong C., 2014, Evaluation of the impact of an uncontrolled landfill on surrounding groundwater quality, Zhoukou, China, *Journal of Geochemical Exploration*, 136, 24-39, DOI: 10.1016/j.gexplo.2013.09.008.

- Hatfield J.L., Sauer T.J., Prueger J.H., 2001, Managing soils to achieve greater water use efficiency: a review, *Agronomy Journal*, 93 (2), 271-280, DOI: 10.2134/agronj2001.932271x.
- Henton M.P., 1981, The problem of water table rebound after mining activity and its effect on ground and surface water quality, *Studies in Environmental Science*, 17, 111-116, DOI: 10.1016/S0166-1116(08)71891-0.
- Hlaïem A., 1999, Halokinesis and structural evolution of the major features in Eastern and Southern Tunisian Atlas, *Tectonophysics*, 306 (1), 79-95, DOI: 10.1016/S0040-1951(99)00045-1.
- INM, 2019, Observatoire des variations mensuelles des paramètres climatiques en Tunisie méridionale, *Annuaire des Climats*, 140 pp.
- Kamel S., 2013, Salinisation origin and hydrogeochemical behaviour of the Djerid oasis water table aquifer (Southern Tunisia), *Arabian Journal of Geosciences*, 6, 2103-2117, DOI: 10.1007/s12517-011-0502-5.
- Khan M.R., Koneshloo M., Knappett P.S.K., Ahmed K.M., Bostick B.C., Mailloux B.J., Mozumder R.H., Zahid A., Harvey C.F., van Geen A., Michael H.A., 2016, Megacity pumping and preferential flow threaten groundwater quality, *Nature Communications*, 7, DOI: 10.1038/ncomms12833.
- Kijne J.W., Barker R., Molden D. (eds.), 2003, *Water Productivity in Agriculture*, CABI, Wallingford, 368 pp.
- Konar M., Dalin C., Hanasaki N., Rinaldo A., Rodriguez-Iturbe I., 2012, Temporal dynamics of blue and green virtual water trade networks, *Water Resources Research*, 48 (7), DOI: 10.1029/2012WR011959.
- Konikow L., Leake S., 2014, Depletion and capture: revisiting “the source of water derived from wells”, *Groundwater*, 52 (S1), 100-111, DOI: 10.1111/gwat.12204.
- Kumar C.P., 2012, Assessment of groundwater potential, *International Journal of Engineering and Science*, 1 (1), 64-79.
- Liu J., Hertel T.W., Taheripour F., 2016, Analyzing future water scarcity in computable equilibrium models, *Water Economics and Policy*, 2 (4), DOI: 10.1142/S2382624X16500065.
- Long S.P., Ainsworth E.A., Leakey A.D.B., Nösberger J., Ort D.R., 2006, Food for thought. Lower-than-expected crop yield stimulation with rising CO₂ concentrations, *Science*, 312 (5782), 1918-1921, DOI: 10.1126/science.1114722.
- Luquet D., Vidal A., Smith M., Dauzat J., 2005, More crop per drop: how to make it acceptable for farmers?, *Agricultural Water Management*, 76 (2), 108-119, DOI: 10.1016/j.agwat.2005.01.011.
- Maroufpoor S., Fard A.F., Shiri J., 2018, Evaluation and zoning the desertification destructive effects using IMPDA model and clustering (case study: Normashir and Rahmatabad plain), *Iranian Journal of Ecohydrology*, 5 (1), 123-134, DOI: 10.22059/IJE.2017.231963.568.
- Maxwell D., Wiebe K., 1999, Land tenure and food security: exploring dynamic linkages, *Development and Change*, 30 (4), 825-849, DOI: 10.1111/1467-7660.00139.
- McGregor B.A., 2004a, Water quality and provision for goats, A report for the Rural Industries Research and Development Corporation, RIRDC Publication No 04-036, available online <https://www.agrifutures.com.au/wp-content/uploads/publications/04-036.pdf> (data access 09.06.2022).
- McGregor D., 2004b, Coming full circle: indigenous knowledge, environment, and our future, *The American Indian Quarterly*, 28 (3-4), 385-410, DOI: 10.1353/aiq.2004.0101.
- Mejri F., Burollet P.F., Ferjani A.B., 2006, Petroleum geology of Tunisia: a renewed synthesis, *Entreprise Tunisienne des Activités pétrolières (ETAP)*, Memoire, 22, 230 pp.
- Mengistu T., Teketay D., Hulten H., Yemshaw Y., 2005, The role of enclosures in the recovery of woody vegetation in degraded dryland hillsides of central and northern Ethiopia, *Journal of Arid Environments*, 60 (2), 259-281, DOI: 10.1016/j.jaridenv.2004.03.014.
- Moeck C., Affolter A., Radny D., Dressmann H., Auckenthaler A., Huggenberger P., Schirmer M., 2017, Improved water resource management for a highly complex environment using three-dimensional groundwater modelling, *Hydrogeology Journal*, 26, 133-146, DOI: 10.1007/s10040-017-1640-y.
- Mokadem N., Demdoum A., Hamed Y., Bouri S., Hadji R., Boyce A., Laouar R., Saad A., 2016, Hydrogeochemical and stable isotope data of groundwater of a multi-aquifer system: northern Gafsa basin – Central Tunisia, *Journal of African Earth Sciences*, 114, 174-191, DOI: 10.1016/j.jafrearsci.2015.11.010.

- Molden D., Oweis T., Steduto P., Bindraban P., Hanjra M.A., Kijne J., 2010, Improving agricultural water productivity: Between optimism and caution, *Agricultural Water Management*, 97 (4), 528-535, DOI: 10.1016/j.agwat.2009.03.023.
- Molle F., Mamanpoush A., Miranzadeh M., 2004, Robbing Yadullah's Water to Irrigate Saeid's Garden: Hydrology and Water Rights in a Village of Central Iran, Research Report 80, International Water Management Institute, Colombo, Sri Lanka, available online https://horizon.documentation.ird.fr/exl-doc/pleins_textes/divers15-08/010039152.pdf (data access 09.06.2022).
- Noble A.D., Bossio D.A., Penning de Vries F.W.T., Pretty J., Thiagarajan T.M., 2006, Intensifying Agricultural Sustainability: An Analysis of Impacts and Drivers in the Development of 'Bright Spots', Comprehensive Assessment of Water Management in Agriculture Research Report 13, International Water Management Institute, Colombo, DOI: 10.3910/2009.380.
- Omar Z., Bouajila A., Bouajila J., Rahmani R., Besser H., Hamed Y., 2019, Spectroscopic and chromatographic characterization of the composition of organic matter in arid salt-affected soils under different vegetation cover, Southeastern Tunisia (Gabes and Medenine), *Advances in Science, Technology and Innovation*, 309-313, DOI: 10.1007/978-3-030-01452-0_74.
- OSS, 2003, Systeme aquifere du Sahara septentrional. Gestion commune d'un bassin transfrontière, Rapport de synthèse 148, Observatoire du Sahara et du Sahel, available online https://www.riob.org/sites/default/files/IMG/pdf/I_RAPPORT_DE_SYNTHESE.pdf (data access 10.06.2022).
- OSS, 2014, Pilotes de démonstration agricole dans le bassin du SASS : vers une agriculture durable et rentable au Sahara, Observatoire du Sahara et du Sahel, 185 pp.
- Oweis T., Hachum A., 2003, Improving water productivity in the dry areas of West Asia and North Africa, [in:] *Water Productivity in Agriculture: Limits and Opportunities for Improvement*, W.J. Kijne, R. Barker, D. Molden (eds.), CABI Publishing, Wallingford, 179-197.
- Oweis T., Taimeh A., 2001, Farm water-harvesting reservoirs: Issues of planning and management in dry areas, [in:] *Integrated Land Management in Dry Areas. Proceedings of a joint UNU-CAS international workshop*, Z. Adeel (ed.), 165-182.
- Peden D., Tadesse G., Misra A.K., 2007, Water and livestock for human development, [in:] *Water for Food, Water for Life: a Comprehensive Assessment of Water Management in Agriculture*, D. Molden (ed.), Earthscan, London, 485-514.
- Peden D.G., Tadesse G., Haileslassie A., 2009, Livestock water productivity: implications for sub-Saharan Africa, *Rangeland Journal*, 31 (2), 187-193, DOI: 10.1071/RJ09002.
- Peng X., Ou W., Wang C., Wang Z., Huang Q., Jin J., Tan J., 2014, Occurrence and ecological potential of pharmaceuticals and personal care products in groundwater and reservoirs in the vicinity of municipal landfills in China, *Science of Total Environment*, 490, 889-898, DOI: 10.1016/j.scitotenv.2014.05.068.
- Pereira L.S., Cordery I., Iacovides I., 2012, Improved indicators of water use performance and productivity for sustainable water conservation and saving, *Agricultural Water Management*, 108, 39-51, DOI: 10.1016/j.agwat.2011.08.022.
- Petersen J., Deschamps P., Goncalves J., Hamelin B., Michelot J.L., Guendouz A., Zouari K., 2014, Quantifying paleorecharge in the Continental Intercalaire (CI) aquifer by a Monte-Carlo inversion approach of 36 Cl/Cl data, *Applied Geochemistry*, 50, 209-221, DOI: 10.1016/j.apgeochem.2014.04.014.
- Pretty J.N., Noble A.D., Bossio D., Dixon J., Hine R.E., Penning de Vries F.T.W., Morison J.L.L., 2006, Resource-conserving agriculture increases yields in developing countries, *Environmental Science and Technology*, 40 (4), 1114-1119, DOI: 10.1021/es051670d.
- Randall G.W., Mulla D.J., 2001, Nitrate nitrogen in surface waters as influenced by climatic conditions and agricultural practices, *Journal of Environmental Quality*, 30 (2), 337-344, DOI: 10.2134/jeq2001.302337x.
- Rickwood C.J., Carr G.M., 2009, Development and sensitivity analysis of a global drinking water quality index, *Environmental Monitoring and Assessment*, 156 (1-4), 73-90, DOI: 10.1007/s10661-008-0464-6.
- Robert T., Caterina D., Deceuster J., Kaufmann O., Nguyen F., 2012, A salt tracer test monitored with surface ERT to detect preferential flow and transport paths in fractured/karstified limestones, *Geophysics*, 77 (2), DOI: 10.1190/geo2011-0313.1.
- Rosegrant M.W., Ximing C., Cline S.A., Nakagawa N., 2002, The role of rainfed agriculture in the future of global food production, EPTD Discussion Paper No. 90, International Food Policy Research Institute (IFPRI), Washington DC, available online <https://www.ifpri.org/publication/role-rainfed-agriculture-future-global-food-production> (data access 09.06.2022).

- Russo T.A., Lall U., 2017, Depletion and response of deep groundwater to climate-induced pumping variability, *Nature Geoscience*, 10, 105-108, DOI: 10.1038/ngeo2883.
- Said A., Baby P., Chardon D., Ouali J., 2011, Structure, paleogeographic inheritance, and deformation history of the southern Atlas foreland fold and thrust belt of Tunisia, *Tectonics*, 30 (6), DOI: 10.1029/2011TC002862.
- Sepehr A., Hassanli A.M., Ekhtesasi M.R., Jamali J.B., 2007, Quantitative assessment of desertification in south of Iran using MEDALUS method, *Environmental Monitoring and Assessment*, 134 (1-3), 243-254, DOI: 10.1007/s10661-007-9613-6.
- Sheng Y., Ma S., Cao W., Wu J., 2020, Spatiotemporal changes of permafrost in the headwater area of the Yellow River under a changing climate, *Land Degradation and Development*, 31 (1), 133-152, DOI: 10.1002/ldr.3434.
- Sileshi Z., Tegegne A., Tsadik G., 2003, Improving the water productivity of livestock: an opportunity for poverty reduction, [in:] *Integrated Water and Land Management Research and Capacity Building Priorities for Ethiopia. Proceedings of a MoWR/EARO/IWMI/ILRI international workshop*, P.G. McCornick, A.B. Kamara, G. Tadesse (eds.), International Water Management Institute (IWMI), Colombo, Sri Lanka and International Livestock Research Institute (ILRI), Nairobi, Kenya.
- Singh O.P., Sharma A., Singh R., Shah T., 2004, Virtual water trade in dairy economy. Irrigation water productivity in Gujarat, *Economical and Political Weekly*, 39 (31), 3492-3497.
- Sivapalan M., Savenije H.H.G., Blöschl G., 2012, Socio-hydrology: A new science of people and water, *Hydrological Processes*, 26 (8), 1270-1276, DOI: 10.1002/hyp.8426.
- Soua M., 2014, Paleozoic oil/gas shale reservoirs in southern Tunisia: an overview, *Journal of African Earth Sciences*, 100, 450-492, DOI: 10.1016/j.jafrearsci.2014.07.009.
- Steinfeld H., Wassenaar T., Jutzi S., 2006, Livestock production systems in developing countries: status, drivers, trends, *Revue Scientifique et Technique*, 25 (2), 505-516, DOI: 10.20506/rst.25.2.1677.
- Stocking M.A., 2003, Tropical soils and food security: the next 50 years, *Science*, 302 (5649), 1356-1359, DOI: 10.1126/science.1088579.
- Swezey C.S., 1996, Structural controls on Quaternary depocentres within the Chotts Trough region of southern Tunisia, *Journal of African Earth Sciences*, 22 (3), 335-347, DOI: 10.1016/0899-5362(96)00012-7.
- Syvitski J.P.M., Kettner A.J., Overeem I., Hutton E.W.H., Hannon M.T., Brakenridge H.G.R., Day J., Vörösmarty C.J., Saito Y., Giosan L., Nicholls R.J., 2009, Sinking deltas due to human activities, *Nature Geoscience*, 2, 681-686, DOI: 10.1038/ngeo629.
- Tanner C.B., Sinclair T.R., 1983, Efficient water use in crop production: research or re-search?, [in:] *Limitations to Efficient Water Use in Crop Production*, H.M. Taylor, W.A. Jordan, T.R. Sinclair (eds.), American Society of Agronomy, Madison, Wisconsin, DOI: 10.2134/1983.limitationsto efficientwateruse.c1.
- Waiyaki E., Owiti H., Angwenyi R., Muriuki T., 2012, An assessment of the perceived socioeconomic impacts of climate change on the community of Faza Island, Lamu East District, Kenya, *Social Science Research Report Series*, 35, 83-118.
- Wu Y., Hunkeler D., 2013, Hyporheic exchange in a karst conduit and sediment system – a laboratory analog study, *Journal of Hydrology*, 501, 125-132, DOI: 10.1016/j.jhydrol.2013.07.040.
- Zammouri M., Siegfried T., El-Fahem T., Kriâa S., Kinzelbach W., 2007, Salinization of groundwater in the Nefzawa oases region, Tunisia: results of a regional scale hydrogeologic approach, *Hydrogeology Journal*, 15, 1357-1375, DOI: 10.1007/s10040-007-0185-x.
- Zhang S., Mao G., Crittenden J., Liu X., Du H., 2017, Groundwater remediation from the past to the future: A bibliometric analysis, *Water Research*, 119, 114-138, DOI: 10.1016/j.watres.2017.01.029.
- Zouaghi T., Guellala R., Lazzez M., Bédier M., Ben Youssef M., Inoubli M.H., Zargouni F., 2011, The chotts fold belt of southern Tunisia, North African margin: structural pattern, evolution and regional geodynamic implications, [in:] *New Frontiers in Tectonic Research – At the Midst of Plate Convergence*, U. Schattner (ed.), 49-72, DOI: 10.5772/20636.
- Zwart S.J., Bastiaanssen W.G.M., 2004, Review of measured crop water productivity values for irrigated wheat, rice, cotton and maize, *Agricultural Water Management*, 69 (2), 115-133.

Changes in extreme temperature indices at the Ukrainian Antarctic Akademik Vernadsky station, 1951-2020

Borys Khrystiuk , Liudmyla Gorbachova , Vitalii Shpyg 

Ukrainian Hydrometeorological Institute

Denys Pishniak

National Antarctic Scientific Center of Ukraine

Abstract

In the late 20th century, warming on the Antarctic Peninsula was most pronounced compared to other parts of Antarctica. However, air temperature showed a significant variability, which has become especially evident in recent decades. Thus, the investigation of air temperature trends on the Antarctic Peninsula is important. This study examines the extreme air temperature at the Ukrainian Antarctic Akademik Vernadsky station, located on Galindez Island, Argentine Islands Archipelago, near the Antarctic Peninsula. For 1951 to 2020, based on the daily air temperature data, the temporal trends of extreme air temperature were analyzed, using 11 extreme temperature indices. Based on linear trend analysis and the Mann-Kendall trend test, the TX_n, TN_n, TN90p, and TN90p indices showed an upward trend, whereas the FD0, ID0, TN10p, TX10p, and DTR indices showed a downward trend. Among them, annually, FD0, ID0, and TN10p significantly decreased by -0.427 days, -0.452 days, and -0.465% , respectively, whereas TX_n and TN_n increased by 0.164°C and 0.201°C , respectively. The indices TX_x and TN_n showed no statistically significant trends. The average annual difference between TX and TN (index DTR) showed a nonsignificant decreasing trend at $-0.029^{\circ}\text{C year}^{-1}$. Thus, for the period of 1951-2020, the Ukrainian Antarctic Akademik Vernadsky station was subjected to warming.

Key words

Antarctica, trend, climate change, extreme air temperature, extreme indices, RStudio Software.

Submitted 18 March 2022, revised 5 June 2022, accepted 13 June 2022

DOI: 10.26491/mhwm/150883

1. Introduction

Climate change affects all parts of the Earth. However, researchers are paying particular attention to the investigation of climate change in Antarctica, which is largely covered by glaciers. Antarctic ice sheets directly affect the global climate and ocean circulation (Kuhn et al. 2010), and an increase in the area and mass of the glacier ice contributes to lowering sea levels, intensifies atmospheric circulation, and increases planetary albedo (Lurcock, Florindo 2017; Silva et al. 2020). One of the most profound consequences of climate warming is the degradation of glacial sheets, including on the Antarctic peninsula (Vaughan, Doake 1996; Turner et al. 2002; Grischenko et al. 2005; Kuhn et al. 2010; Wouters et al. 2015; Silva et al. 2020; Diener et al. 2021). Warming on the Antarctic Peninsula has also impacts on the terrestrial flora, seasonal snow cover, lake ecology, penguin distribution, ice-shelf distribution, glacier thickness, and sea-ice duration (Vaughan et al. 2003; Turner et al. 2014, 2016).

The rate and tendencies of warming at the Antarctic Peninsula are still subject of debate (Vaughan et al. 2003; Martazinova et al. 2010; Stastna 2010; Qu et al. 2011; Schneider et al. 2012; Bromwich et al. 2013, Ding, Steig 2013; Franzke 2013; Tymofeyev 2013; Turner et al. 2016; Gonzalez, Fortuny 2018; Sato et al. 2021), and the peninsula presents physical and geographical features that distinguish it from the rest of Antarctica (King, Tuner 1997; Vaughan et al. 2003). The rugged alpine topography, a maritime climate along the west and central costa, and a continental climate along the east coast result in higher temperatures at the west coast compared to areas with similar latitudes and elevations on the east coast (Morris, Vaughan 1994). Several studies have reported stable trends in surface air temperature increase on the Antarctic Peninsula. For example, Vaughan et al. (2003) demonstrated that the Antarctic Peninsula has warmed at $3.7 \pm 1.6^{\circ}\text{C century}^{-1}$, which is several times the rate of global warming and different to most of the other station records from the Antarctic continent. However, Bromwich et al. (2013) reported a linear increase in annual temperature between 1958 and 2010 by $2.4 \pm 1.2^{\circ}\text{C}$, establishing central West Antarctica as one of the fastest-warming regions globally. Stastna (2010) reported about three distinct regions with different trends of warming on the Antarctic Peninsula. Franzke (2013) and Turner et al. (2014, 2016, 2020, 2021) reported extremely high rates of surface air temperature changes on the Antarctic Peninsula. Moreover, according to Turner et al. (2016), Gonzalez and Fortuny (2018), and Sato et al. (2021), on the Antarctic Peninsula, the surface air temperature varies significantly, which has been especially evident in recent decades. Thus, current research is aimed at understanding such variable trends and the factors that determine them (Clem et al. 2019; Bozkurt et al. 2020; Turner et al. 2020; Bozkurt et al. 2021).

This study examines the extreme air temperatures in the Ukrainian Antarctic Akademik Vernadsky station, located on the western side of the Antarctic Peninsula. Historical observations of this station have been used in various studies that investigated the trends of average and extreme temperatures. For example, Turner et al. (2005) reported that the Antarctic Peninsula has experienced a major warming over the last 50 years and that on the Akademik Vernadsky station, the surface air temperature increased at a rate of $0.56^{\circ}\text{C decade}^{-1}$ over the year and $1.09^{\circ}\text{C decade}^{-1}$ during the winter. Martazinova et al. (2010) reported that according to the data of the Akademik Vernadsky station, the increase in the mean annual air temperature exceeded 2°C for the observation period 1947-2007. According to Franzke (2013), the Akademik Vernadsky station has been experiencing a significant warming trend of about $0.6^{\circ}\text{C decade}^{-1}$ over the last few decades. Tymofeyev (2013) reported the greatest warming, with a linear trend coefficient of $0.53^{\circ}\text{C}/10$ years, at the Akademik Vernadsky station. At the same time, modern warming is separated by a period of relative cooling in the beginning and middle 1970s. Turner et al. (2020) reported that 13 of the 17 stations have experienced a positive trend in annual mean temperature over the full length of their record (until 2018), with the largest being observed at the Akademik Vernadsky station ($0.46 \pm 0.15^{\circ}\text{C decade}^{-1}$). One of the latest in-depth studies analyzing the formation conditions and trends of maximum and minimum air temperature in Antarctica is the paper Turner et al. (2021). However, both in this paper and in others, the climate extremes indices were not used. These indices have been developed by the expert team of the World Meteorological Organization (Zhang, Yang 2004; Tashebo et al. 2021) and contribute

to a better understanding and analysis of the trends of climate change, particularly the temperature and rainfall variables (Brown et al. 2010; Costa et al. 2020; Zhou et al. 2020; Tashebo et al. 2021). In this context, the objective of this paper was to investigate the extreme temperature indices change at the Ukrainian Antarctic Akademik Vernadsky station for the period 1951–2020.

2. Study area, data, and methodology

2.1. Study area

Until 1996, the Ukrainian Antarctic Akademik Vernadsky station was a British Faraday station. The station is located on Galindez Island, Argentine Islands Archipelago, near the western coast of the Antarctic Peninsula (Fig. 1) in the middle part of the peninsula (65.25°S , 64.27°W). The island is dominated by large-scale circumpolar circulation in the atmosphere and ocean (King, Tuner 1997).

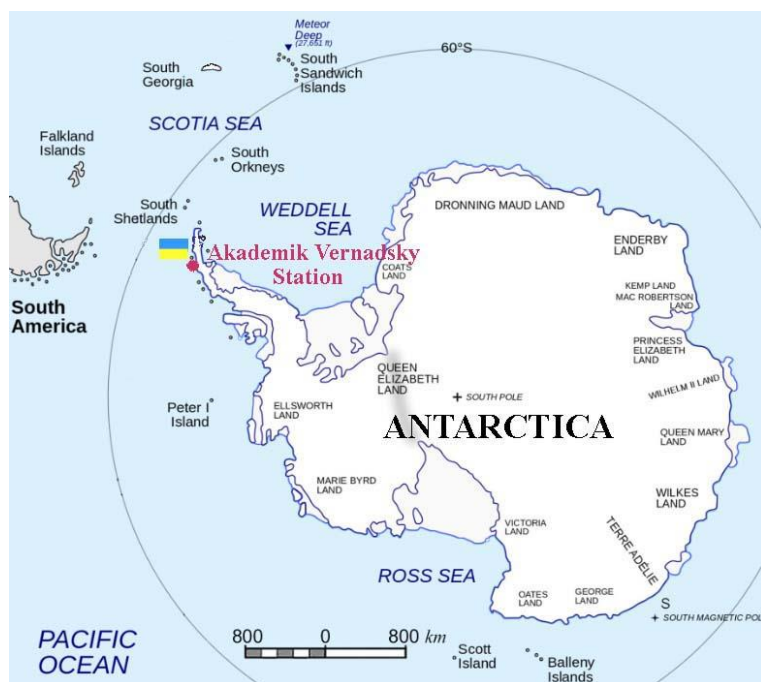


Fig. 1. Location of the Ukrainian Antarktisk Akademik Vernadsky station (background graphic from Klok, Kornus 2021).

The climate of Galindez Island is marine subarctic (King, Tuner 1997; Franzke 2013). Wind and temperatures conditions are mainly formed by the mountain system of the Antarctic Peninsula (Turner et al. 2002; King, Comiso 2003). The average plateau height is 2,000 m above sea level and the height of individual peaks reaches 2,800 m (King, Tuner 1997). This system forms the foehn wind, and the air cools over the ice cover and forms local winds. The area over the Pacific Ocean is dominated by the low-pressure systems that move eastwards towards the Antarctic Peninsula (King, Comiso 2003), causing frequent precipitation and strong winds, with frequent snowfall and snowstorms. The anticyclonic type of weather is less common. In this case, calm frosty weather is established for a long period, sometimes with fog and frost (King, Tuner 1997; King, Comiso 2003).

For the period 1951-2020, the warmest month of the year was January, with a multi-annual mean monthly temperature of +0.8°C, and the coldest month was August, with a multi-annual mean monthly temperature of -8.7°C. The highest mean monthly air temperature was +2.4°C (February) and the lowest -20.1°C (July) (Table 1).

Table 1. Multiannual mean monthly air temperature (°C) at the Akademik Vernadsky station for the period of 1951-2020.

Temperature	Mean	Highest		Lowest	
		Value	Year	Value	Year
January	0.8	2.3	1985	-1.4	1959
February	0.7	2.4	2001	-3.0	1953
March	-0.4	1.6	2001	-4.6	1953
April	-2.4	0.5	2013	-13.9	1959
May	-4.2	-0.2	2001	-13.8	1959
June	-6.2	-1.1	1998	-17.1	1958
July	-8.4	-2.6	1989, 1998	-20.1	1959
August	-8.7	-2.9	2003	-17.4	1954
September	-7.1	-2.1	1970	-14.1	1987
October	-4.5	-0.6	2010	-9.5	1994
November	-2.1	0.1	1994	-4.7	1954
December	-0.2	1.7	2009	-1.7	1958

2.2. Data

In this study, daily air temperature data for eight terms (0, 3, 6, 9, 12, 15, 18, 21 UTC) of the Akademik Vernadsky station, provided by the National Antarctic Scientific Center of Ukraine (NASC), were used; the period was 1951-2020. Data before 1996 were kindly provided by the Meteorological Information Database of the British Antarctic Survey.

When carrying out investigations, the quality of the initial data is extremely important. During the existence of the Akademik Vernadsky station, various measuring instruments and complexes were used to measure surface air temperature. Thus, regular meteorological observations of surface air temperature with the help of mercury thermometers in a psychrometric booth were started in 1947. In 1985, the Synoptic and Climatological Automatic Weather Station (SCAWS) was installed in a psychrometric booth, which was replaced by the Modular Automatic Weather Station (MAWS) in 1992. In March 2011, the MAWS system was replaced by the Ukrainian-made Mobile Meteorological Complex "Troposphere" (Mobile AWS "Troposphere"). This complex contains the temperature sensor in its own radiation protection, with artificial ventilation. In April 2020, the Mobile AWS "Troposphere" was transferred to reserve status. The main data source currently is the automatic weather station Vaisala AWS-310, which was installed 1 year earlier. This station contains the temperature sensor in its own radiation protection, with passive ventilation.

In the period from 1947 to 1950, the measurement of surface air temperature took place at different times. However, the observation data were incomplete, and data were therefore checked for missing values, gross errors, and outliers that exceeded four standard deviations from the mean for each day. The missing values were recovered by multiple regression depending on air temperature before and after the missing value; such regression dependences were established for each month of the year. The amount of missing data was insignificant (0.1% of the total data), and there were no gross errors or significant outliers in our dataset. After quality control procedures, daily minimum and maximum air temperature were calculated.

2.3. Methodology

A core set of 27 indices has been developed by the Expert Team on Climate Change Detection and Indices (ETCCDI) to standardize the definitions and analysis of extremes (Peterson et al. 2001; Klein Tank et al. 2006). Of these 27 indices, only 16 refer to air temperature, and the remaining ones refer to precipitation. Based on the analysis of the temperature regime at the Akademik Vernadsky station during the recent 70 years, 11 extreme temperature indices were chosen (Table 2) as they are most suitable to study the temporal characteristics of extreme air temperature events. The annual indices and their trend equations were obtained using the RStudio Software (version 1.4.1717) (R Core Team 2017). Percentile indices were calculated using the standard reference period of 1981-2010 to facilitate comparison of the results with those of other studies using the same reference period. The Mann-Kendall non-parametric trend test was employed to assess the statistical significance of the indices series (Mann 1945; Kendall 1975), using the RStudio Software. The statistical significance of trends was estimated depending on the τ value:

$$\tau = \frac{P-Q}{n(n-1)/2} \quad (1)$$

where P is the number of concordant pairs, Q is the number of discordant pairs, and n is the total amount of data.

Table 2. Definition of extreme air temperature indices.

Index	Name	Definition	Unit
FD0	Frost days	Annual count when TN (daily minimum) < 0°C	Days
ID0	Ice days	Annual count when TX (daily maximum) < 0°C	Days
TXx	Highest Tmax	Highest annual value of daily maximum temperature	°C
TNx	Highest Tmin	Highest annual value of daily minimum temperature	°C
TXn	Lowest Tmax	Lowest annual value of daily maximum temperature	°C
TNn	Lowest Tmin	Lowest annual value of daily minimum temperature	°C
TN10p	Cool nights	Percentage of days when TN < 10 th percentile	%
TX10p	Cool days	Percentage of days when TX < 10 th percentile	%
TN90p	Warm nights	Percentage of days when TN > 90 th percentile	%
TX90p	Warm days	Percentage of days when TX > 90 th percentile	%
DTR	Diurnal temperature range	Average annual difference between TX and TN	°C

3. Results

3.1. Cold extremes indices (ID0, FD0, TXn, TNn and TX10p, TN10p)

The number of frost days during the period of 1951-2020 varied from 149 to 254. The maximum number of frost days was observed in 1967 and 1969 (349 days) and the minimum number in 2001 (271 days). The ID0 and FD0 indices significantly decreased at -0.427 and -0.452 day year⁻¹, respectively (Table 3, Fig. 2).

Table 3. Annual trends of the extreme indices of daily air temperature for the Akademik Vernadsky station, 1951–2020.

Temperature indices	Trend equation	R ²	τ	p-value	Statistical significance of trend
FD0	$y = -0.46x + 1164$	0.18	-0.281	0.0006	yes
ID0	$y = -0.45x + 1096$	0.15	-0.249	0.0024	yes
TXx	$y = 0.016x - 23.8$	0.06	0.174	0.0352	no
TNx	$y = 0.007x - 10.0$	0.03	0.137	0.0999	no
TXn	$y = 0.16x - 347.4$	0.24	0.338	<0.0001	yes
TNn	$y = 0.20x - 425.2$	0.32	0.369	<0.0001	yes
TN10p	$y = -0.46x + 941.4$	0.44	-0.420	<0.0001	yes
TX10p	$y = -0.28x + 578.6$	0.34	-0.407	<0.0001	yes
TN90p	$y = 0.07x - 124.4$	0.13	0.272	0.0010	yes
TX90p	$y = 0.06x - 101.3$	0.15	0.276	0.0008	yes
DTR	$y = -0.029x + 62.3$	0.47	-0.469	<0.0001	yes

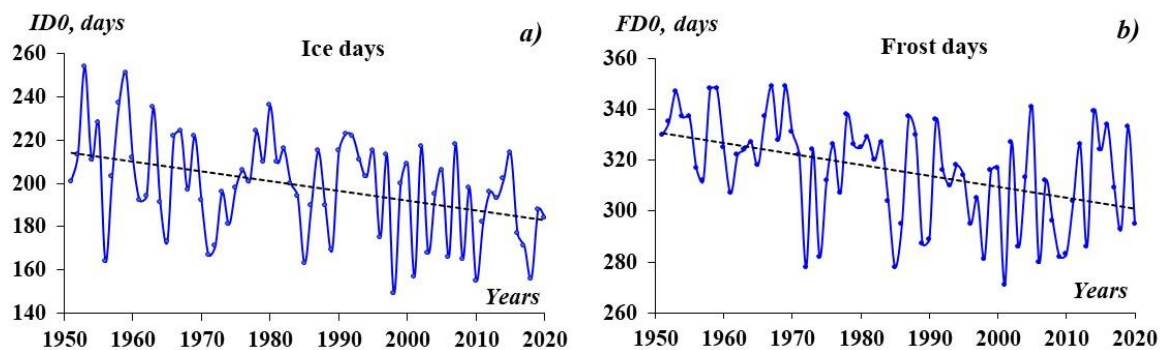


Fig. 2. Annual count when TX (daily maximum) < 0°C (a) and TN (daily minimum) < 0°C (b).

The indices TXn and TNn showed an upward trend. Annually, TXn and TNn increased by 0.164°C and 0.201°C, respectively (Table 3, Fig. 3). The lowest air temperature was observed in the winter period of 1958 (-42.4°C). In the winter of 1977, the air temperature also dropped below -40°C (-40.2°C). The warmest winter was that of 1989, when the temperature did not fall below -10.2°C at night and below -7.2°C during the day.

Annually, the TX10p and TN0p indices showed a significant decrease in cool days and cool nights by 0.46% and 0.28%, respectively (Table 3, Fig. 4). In 1959, the largest number of cold days and nights, namely 43.8% and 58.3%, respectively, was observed. In 1989, the number of cool days and nights was lowest.

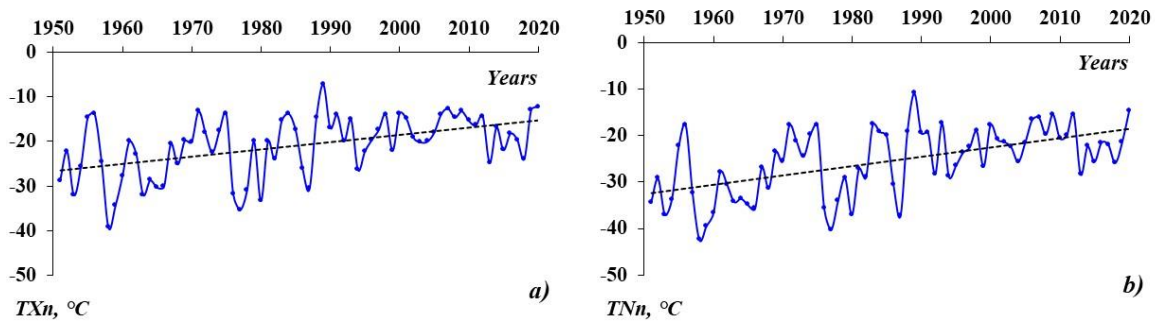


Fig. 3. Lowest annual values of daily maximum (a) and minimum (b) air temperatures.

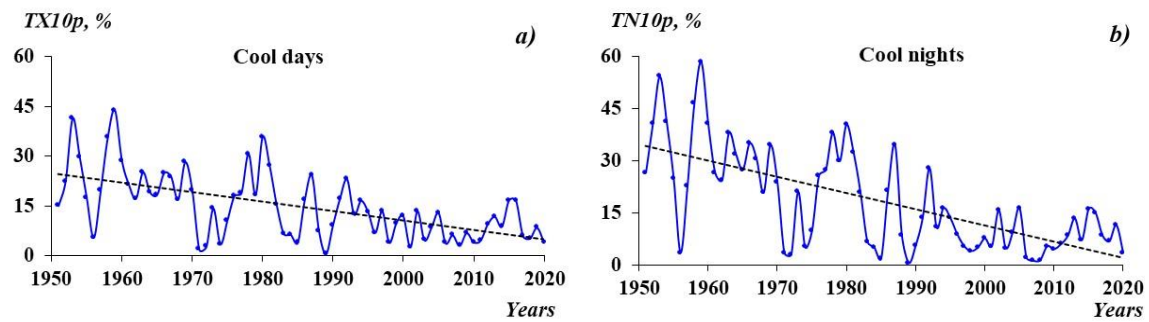


Fig. 4. Percentage of days when TX < 10th (a) and TN < 10th (b) percentile of 1981-2010.

3.2. Hot extremes indices (TXx, TNx, TX90p, and TN90p)

The TXx and TNx indices showed no statistically significant tendencies for the period of 1951-2020 (Table 3, Fig. 5). Annually, the TX90p and TN90p indices showed a small increase in warm days and nights by 0.056% and 0.067%, respectively (Table 3, Fig. 6). The highest air temperature was observed in the summer of 1985, with +10.9°C during the day and +5.1°C at night. In the summer of 1973, the daytime temperature did not exceed +4.8°C, and in the summer of 1978, the night air temperature dropped to +1.3°C. The largest number of warm days was observed in 2018 and that of warm nights in 1998, with 15.3% and 19.3%, respectively. In 2002, the number of warm days was lowest (4.2%), whereas the number of warm nights was lowest in 1958 and 1959 (2.7%).

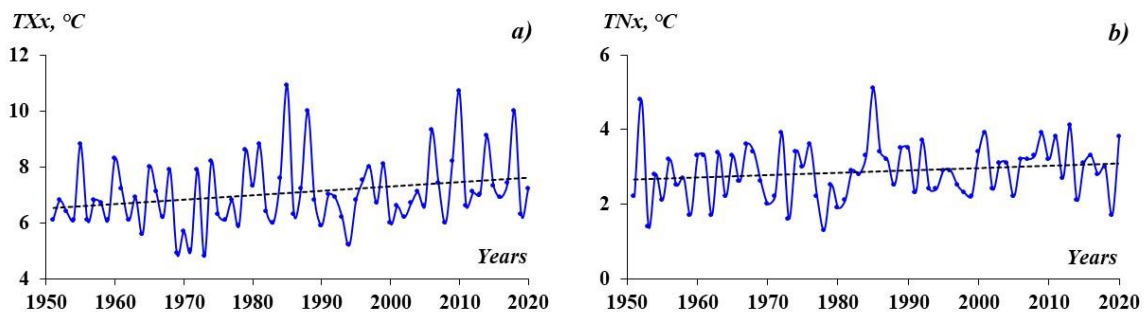


Fig. 5. Highest annual values of daily maximum (a) and minimum (b) air temperatures.

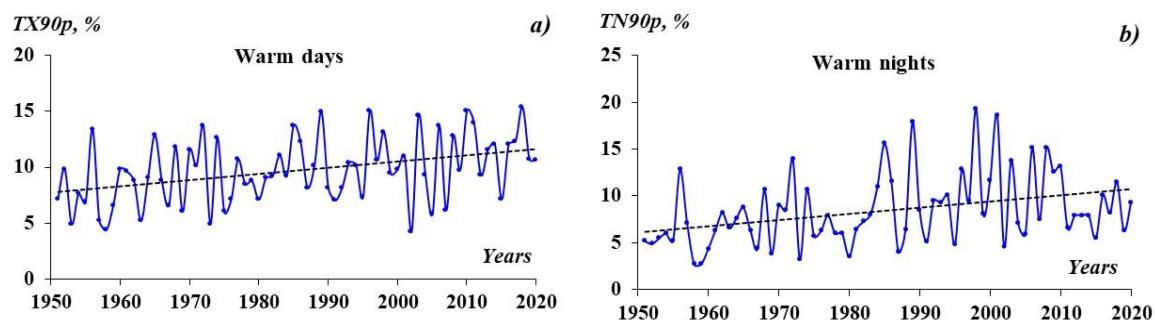


Fig. 6. Percentages of days when TX > 90th (a) and TN > 90th (b) percentile of 1981-2010.

DTR index is an average annual difference between daily maximum and minimum air temperature. DTR index shows a small negative trend ($-0.026^{\circ}\text{C}/\text{year}$) over the last 70 years (Table 3, Fig. 7). This trend is due to larger increases in average annual minimum air temperatures ($0.06^{\circ}\text{C}/\text{year}$) than average annual maximum air temperatures ($0.03^{\circ}\text{C}/\text{year}$) over the same period.

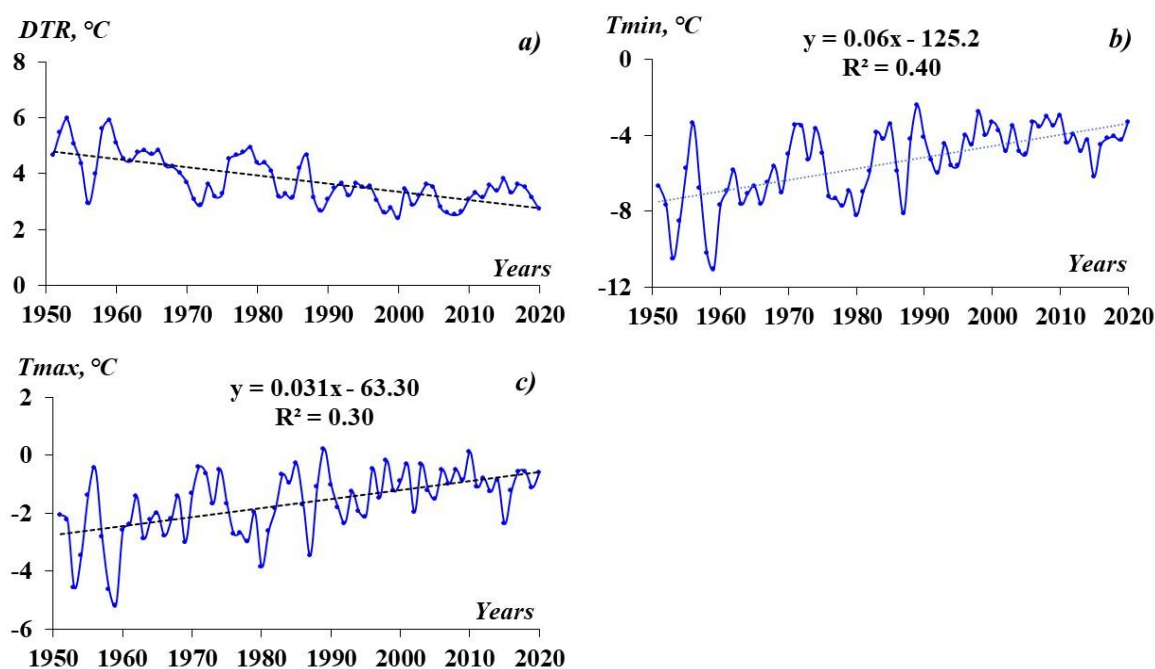


Fig. 7. Average annual difference between TX and TN (a), average annual minimum (b) and maximum (c) air temperatures.

4. Discussion

Analysis of 11 extreme air temperature indices at the Ukrainian Antarctic Akademik Vernadsky station showed the indicate unequivocal signs of heating. These results are in good agreement with those of studies using other methodological approaches (Turner et al. 2005, 2014, 2020, 2021; Franzke 2013; Gonzalez, Fortuny 2018; Bozkurt et al. 2021). Turner et al. (2005) reported the positive statistically significant trend of the mean annual air temperature at the Akademik Vernadsky station, whereas Franzke (2013) reported that for the period of February 1947 to January 2011, the Akademik Vernadsky station experienced a sig-

nificant warming trend and the magnitude of extremely cold temperatures was reduced; however, the annual maximum temperature did not increase. Some authors, such as Turner et al. (2016) and Gonzalez and Fortuny (2018), reported the decrease tendencies of the annual mean temperature on the Antarctic Peninsula in recent decades, including at the Vernadsky station. This was explained by the natural internal variability of the regional atmospheric circulation. Investigation of surface air temperature trends using the latest observational data demonstrated the presence of a persistent warming trend (Turner et al. 2020, 2021; Bozkurt et al. 2021), which is also confirmed by our research. Turner et al. (2021) researched the variability and change in the frequency of extreme daily mean temperatures in Antarctica; for the Akademik Vernadsky station, the authors observed an increase in the percentage of extreme warm days and a decrease in cold days. On the Antarctic Peninsula, the warming trend will continue in the future. According to the global climate models, forecasts suggest that the Antarctic Peninsula temperatures will increase more significantly than in other parts of Antarctica and in the world (Chyhareva et al. 2019; Stiegert et al. 2019). Chyhareva et al. (2019) reported that for the Antarctic Peninsula region for RCP4.5 and RCP8.5 scenarios on average forecast to reduce the cold period; for the Akademik Vernadsky station, this process will be three times more intensive, indicating that the region is more vulnerable to climate change. Stiegert et al. (2019) reported that with a temperature increase by 1.5°C, irreversible and dramatic changes to glacial, terrestrial, ocean, and biological systems on the Antarctic Peninsula can be expected.

5. Conclusions

Our study presents an evaluation of climate extremes indices by focusing on the analysis of daily minimum and maximum air temperatures at the Ukrainian Antarctic Akademik Vernadsky station. The results show a trend of warming for the period of 1951-2020. This is indicated by the calculated extreme air temperature indices, which showed statistically significant tendencies, namely during the recent 70 years:

- indices of ice and frost days, cool nights and days, and the diurnal temperature range significantly decreased;
- indices of warm nights and days, lowest annual values of daily maximum and minimum air temperature significantly increased.

In this study, the application of the climate indices made it possible to obtain more complete information about the tendencies of the extreme air temperature at the Ukrainian Antarctic Akademik Vernadsky station. Such results are highly important in the context of understanding the temporal variability of annual and seasonal air temperature on the Antarctic Peninsula. In general, the results of this investigation support previous findings. Further research should focus on the application of the climate indices for the investigation of the extreme temperature changes at the Akademik Vernadsky station during particular months or seasons.

Acknowledgments

This research was conducted within project № H/10-2021 "Influence of thermal regime on snow cover of the Antarctic Peninsula", funded by the State Institution "National Antarctic Scientific Center" of the Ministry of Education and Science of Ukraine.

References

- Bozkurt D., Bromwich D.H., Carrasco J., Hines K.M., Maureira J.C., Rondanelli R., 2020, Recent near-surface temperature trends in the Antarctic Peninsula from observed, reanalysis and regional climate model data, *Advances in Atmospheric Sciences*, 37, 477-493, DOI: 10.1007/s00376-020-9183-x.
- Bozkurt D., Bromwich D.H., Carrasco J., Rondanelli R., 2021, Temperature and precipitation projections for the Antarctic Peninsula over the next two decades: contrasting global and regional climate model simulations, *Climate Dynamics*, 56, 3853-3874, DOI: 10.1007/s00382-021-05667-2.
- Bromwich D.H., Nicolas J.P., Monaghan A.J., Lazzara M.A., Keller L.M., Weidner G.A., Wilson A.B., 2013, Central West Antarctica among the most rapidly warming regions on Earth, *Nature Geoscience*, 6, 139-145, DOI: 10.1038/NNGEO1671.
- Brown P.J., Bradley R.S., Keimig F.T., 2010, Changes in Extreme Climate Indices for the Northeastern United States, 1870-2005, *Journal of Climate*, 23 (24), 6555-6572, DOI: 10.1175/2010JCLI3363.1.
- Chyhareva A., Krakovska S., Pishniak D., 2019, Climate projections over the Antarctic Peninsula region to the end of the 21st century. Part 1: Cold temperature indices, *Ukrainian Antarctic Journal*, 1 (18), 47-63. DOI: 10.33275/1727-7485.1(18).2019.131.
- Clem K.R., Lintner B.R., Broccoli A.J., Miller J.R., 2019, Role of the South Pacific convergence zone in West Antarctic decadal climate variability, *Geophysical Research Letters*, 46 (12), 6900-6909, DOI: 10.1029/2019GL082108.
- Costa R.L., Baptista G.M.M., Gomes H.B., Silva F.D.S., da Rocha Júnior R.L., Salvador M.A., Herdies D.L., 2020, Analysis of climate extremes indices over northeast Brazil from 1961 to 2014, *Weather and Climate Extremes*, 28, DOI: 10.1016/j.wace.2020.100254.
- Diener T., Sasgen I., Agosta C., Fürst J.J., Braun M.H., Konrad H., Fettweis X., 2021, Acceleration of dynamic ice loss in Antarctica from satellite gravimetry, *Frontiers in Earth Science*, 9, DOI: 10.3389/feart.2021.741789.
- Ding Q., Steig E.J., 2013, Temperature change on the Antarctic Peninsula linked to the Tropical Pacific, *Journal of Climate*, 26 (19), 7570-7585, DOI: 10.1175/JCLI-D-12-00729.1.
- Franzke C., 2013, Significant reduction of cold temperature extremes at Faraday/Vernadsky station in the Antarctic Peninsula, *International Journal of Climatology*, 33 (5), 1070-1078, DOI: 10.1002/joc.3490.
- Gonzalez S., Fortuny D., 2018, How robust are the temperature trends on the Antarctic Peninsula, *Antarctic Science*, 30 (5), 322-328, DOI: 10.1017/S0954102018000251.
- Grischenko V.F., Timofeyev V.E., Klock S.V., 2005, Impacts of components of glacioclimate to climate change at the Antarctic Peninsula region, (in Ukrainian), *Ukrainian Antarctic Journal*, 3, 99-107, DOI: 10.33275/1727-7485.3.2005.574.
- Kendall M.G., 1975, *Rank Correlation Methods*, 4th edition, Charles Griffin, London, 202 pp.
- King J.C., Comiso J.C., 2003, The spatial coherence of interannual temperature variations in the Antarctic Peninsula, *Geophysical Research Letters*, 30 (2), DOI: 10.1029/2002GL015580.
- King J.C., Turner J., 1997, *Antarctic meteorology and climatology*, Cambridge University Press, DOI: 10.1017/CBO9780511524967,
- Klein Tank A.M.G., Peterson T.C., Quadir D.A., Dorji S., Zou X., Tang H., Santhosh K., Joshi U.R., Jaswal A.K., Kolli R.K., Sikder A.B., Deshpande N.R., Revadekar J.V., Yeleuova K., Vandasheva S., Faleyeva M., Gomboluudev P., Budhathoki K.P., Hussain A., Afzaal M., Chandrapala L., Anvar H., Amanmurad D., Asanova V.S., Jones P.D., New M.G., Spektorman T., 2006, Changes in daily temperature and precipitation extremes in central and south Asia, *Journal of Geophysical Research*, 111 (D16), DOI: 10.1029/2005JD006316.
- Klok S.V., Kornus A.O., 2021, Intra-annual and long-periodic components in the changes of precipitation over the Antarctic Peninsula and their possible causes, *Journal of Geology, Geography and Geoecology*, 30 (3), 490-490, DOI: 10.15421/112144.

- Kuhn M., Featherstone W., Makarynskyy O., Keller W., 2010, Deglaciation-induced spatially variable sea level change: a simple-model case study for the Greenland and Antarctic ice sheets, *The International Journal of Ocean and Climate Systems*, 1 (2), 67-84, DOI: 10.1260/1759-3131.1.2.67.
- Lurcock P., Florindo F., 2017, *Antarctic Climate History and Global Climate Changes*, Oxford University Press, DOI: 10.1093/oxfordhb/9780190699420.013.18.
- Mann H.B., 1945, Nonparametric tests against trend, *Econometrica*, 13 (3), 245-259, DOI: 10.2307/1907187.
- Martazinova V.F., Tymofeyev V.E., Ivanova Y.K., 2010, Current regional climate of the Antarctic Peninsula and Akademik Vernadsky Station, (in Russian), *Ukrainian Antarctic Journal*, 9, 231-248. DOI: 10.33275/1727-7485.9.2010.411.
- Morris E.M., Vaughan D.G., 1994, Snow surface temperatures in West Antarctica, *Antarctic Science*, 6 (4), 529-535, DOI: 10.1017/S0954102094000787.
- Peterson T.C., Folland C., Gruza G., Hogg W., Mokssit A., Plummer N., 2001, Report on the Activities of the Working Group on Climate Change Detection and Related Rapporteurs 1998-2001, WMO, Rep. WCDMP-47, WMO-TD 1071, Geneva, Switzerland, available online <http://etccdi.pacificclimate.org/docs/wgccd.2001.pdf> (data access 13.06.2022).
- Qu X., Hall A., Boe J., 2011, Why does the Antarctic Peninsula warm in climate simulations?, *Climate Dynamics*, 38 (5-6), 913-927, DOI: 10.1007/s00382-011-1092-3.
- R Core Team, 2017, R: A language and environment for statistical computing, R Foundation for Statistical Computing, Vienna, Austria, <https://www.r-project.org/>.<https://www.r-project.org/>.
- Sato K., Inoue J., Simmonds I., Rudeva I., 2021, Antarctic Peninsula warm winters influenced by Tasman Sea temperatures, *Nature Communications*, 12, DOI: 10.1038/s41467-021-21773-5.
- Schneider D.P., Deser C., Okumura Y., 2012, An assessment and interpretation of the observed warming of West Antarctica in the austral spring, *Climate Dynamics*, 38, 323-347, DOI: 10.1007/s00382-010-0985-x.
- Silva A.B., Arigony-Neto J., Braun M.H., Espinoza J.M.A., Costi J., Jaña R., 2020, Spatial and temporal analysis of changes in the glaciers of the Antarctic Peninsula, *Global and Planetary Change*, 184, DOI: 10.1016/j.gloplacha.2019.103079.
- Stastna V., 2010, Spatio-temporal changes in surface air temperature in the region of the northern Antarctic Peninsula and south Shetland islands during 1950-2003, *Polar Science*, 4 (1), 18-33, DOI: 10.1016/j.polar.2010.02.001.
- Stiebert M., Atkinson A., Banwell A., Brandon M., Convey P., Davies B., Downie R., Edwards T., Hubbard B., Marshall G., Rogelj J., Rumble J., Stroeve J., Vaughan D., 2019, The Antarctic Peninsula under a 1.5°C global warming scenario, *Frontiers in Environmental Science*, 7, DOI: 10.3389/fenvs.2019.00102.
- Tashebo G.B., Mekonn E.F., Eshete A.A., 2021, Trends in daily temperature and precipitation extremes over Dire-Dawa, 1980-2018, *Journal of Environment and Earth Science*, 11 (9), 31-37, DOI: 10.7176/JEES/11-9-03.
- Turner J., Barrand N.E., Bracegirdle T.J., Convey P., Hodgson D.A., Jarvis M., Jenkins A., Marshall G., Meredith M.P., Roscoe H., Shanklin J., French J., Goosse H., Guglielmin M., Gutt J., Jacobs S., Kennicutt II M.C., Masson-Delmotte V., Mayewski P., Navarro F., Robinson S., Scambos T., Sparrow M., Summerhayes C., Speer K., Klepikov A., 2014, Antarctic climate change and the environment: an update, *Polar Record*, 50 (3), 237-259. DOI: 10.1017/S0032247413000296.
- Turner J., Colwell S.R., Marshall G.J., Lachlan-Cope T.A., Carleton A.M., Jones P.D., Lagun V., Reid P.A., Lagovkina S., 2005, Antarctic climate change during the last 50 years, *International Journal of Climatology*, 25 (8), 1147-1148, DOI: 10.1002/joc.1130.
- Turner J., Lachlan-Cope T.A., Marshall G.J., Morris E.M., Mulvaney R., Winter W., 2002, Spatial variability of Antarctic Peninsula net surface mass balance, *Journal of Geophysical Research*, 107 (D13), DOI: 10.1029/2001JD000755.
- Turner J., Lu H., King J., Marshall G.J., Phillips T., Bannister D., Colwell S., 2021, Extreme temperatures in the Antarctic, *Journal of Climate*, 34 (7), 2653-2668, DOI: 10.1175/JCLI-D-20-0538.1.
- Turner J., Lu H., White I., King J.C., Phillips T., Hosking J.S., Bracegirdle T.J., Marshall G.J., Mulvaney R., Deb P., 2016, Absence of 21st century warming on Antarctic Peninsula consistent with natural variability, *Nature*, 535, 411-415, DOI: 10.1038/nature18645.
- Turner J., Marshall G.J., Clem K., Colwell S., Phillips T., Lu H., 2020, Antarctic temperature variability and change from station data, *International Journal of Climatology*, 40 (6), 2986-3007, DOI: 10.1002/joc.6378.

- Tymofeyev V.E., 2013, Multi-years' changes in the air temperature at the Antarctic Peninsula and the possible reasons, (in Ukrainian), Proceedings of Ukrainian Hydrometeorological Institute, 264, 9-17.
- Vaughan D., Marshall G.J., Connolley W.M., Parkinson C., Mulvaney R., Hodgson D.A., King J.C., Pudsey C.J., Turner J., 2003, Recent rapid regional climate warming on the Antarctic Peninsula, *Climatic Change*, 60, 243-274, DOI: 10.1023/A:1026021217991.
- Vaughan D.G., Doake C.S.M., 1996, Recent atmospheric warming and retreat of ice shelves of the Antarctic Peninsula, *Nature*, 379, 328-331, DOI: 10.1038/379328a0.
- Wouters B., Martin-Español A., Helm V., Flament T., Van Wessem J.M., Ligtenberg S.R.M., Van Den Broeke M.R., Bamber J.L., 2015, Dynamic thinning of glaciers on the Southern Antarctic Peninsula, *Science*, 348 (6237), 899-903, DOI: 10.1126/science.aaa5727.
- Zhang X., Yang F., 2004, RCLimDex (1.0) User Manual, Climate Research Branch, Environment Canada, Ontario, available online <https://acmad.net/rcc/procedure/RCLimDexUserManual.pdf> (data access 13.06.2022).
- Zhou J., Huang J., Zhao X., Lei L., Shi W., Wang L., Wei W., Liu C., Zhu G., Yang X., 2020, Changes of extreme temperature and its influencing factors in Shiyang River Basin, Northwest China, *Atmosphere*, 11 (11), DOI: 10.3390/atmos11111171.